University of Natural Resources and Life Sciences, Vienna

Impact of cavitation, high shear stress and air/liquid interfaces on protein aggregation

Dissertation zur Erlangung des Doktorgrades an der

Universität für Bodenkultur Wien

Department für Biotechnologie

Institut für angewandte Mikrobiologie

Vorstand: Reingard Grabherr, Univ.Prof. Dipl.-Ing. Dr.rer.nat.

Betreuer: Alois Jungbauer, Univ.Prof. Dipl.-Ing. Dr.nat.techn.

Eingereicht von Mark Dürkop, Dipl.-Ing.

Wien, April 2018

Danksagung

Ich möchte mich eingangs bei einigen Personen bedanken, ohne deren Input das Verfassen der nachfolgenden Arbeit nicht möglich gewesen wäre. Um einen chronologischen Aufbau zu gewährleisten, will ich mit meinem Großvater Walter beginnen. Er hat mein Interesse an der Technik und den Naturwissenschaften von meinen ersten Schritten an gefördert wie kein anderer. „Wie funktioniert das Opa?“ war eine sehr häufige Frage meinerseits. Meiner Mutter Irene möchte ich danken, weil sie immer an mich geglaubt hat, und es mir dadurch ermöglicht hat, viele Dinge zu probieren. Sowohl in meiner schulischen Laufbahn, als auch in Bezug auf Freizeitgestaltung, wurden mir alle Türen geöffnet. Man weiß nie, was man im Leben gut oder gar nicht kann, bevor man es nicht ausprobiert hat. Meiner Frau Alexandra möchte ich für die letzten 12 Jahre danken, in denen sie mich unterstützt und ermutigt hat, meinen eigenen Weg zu gehen. Es ist wunderschön dich an meiner Seite zu haben und die Höhen und Tiefen unseres Lebens gemeinsam zu beschreiten! “Hand in Hand ein Leben lang“. Meinem Doktorvater Alois Jungbauer möchte ich dafür danken, dass er mir einerseits das Vertrauen geschenkt hat ein Teil seiner Arbeitsgruppe sein zu dürfen, und andererseits, mir immer die Zeit und Ressourcen eingeräumt hat, die nötig waren, um diese Arbeit kreativ und gewissenhaft umzusetzen. Meiner treuen Technikerin Eva Berger möchte ich an dieser Stelle ein ebenso großes Dankeschön aussprechen. Ohne sie wäre es niemals möglich gewesen, die benötigte Zeit in experimentelle und in-silico Methodenentwicklung zu investieren, ohne dabei den zeitlichen Rahmen der Arbeit zu sprengen. Der gesamten Arbeitsgruppe möchte ich für die angeregten und unterhaltsamen on- und off-topic Diskussionen beim Mittagessen, in den legendären Kaffeepausen sowie in der Freizeit danken. Ein ganz spezieller Dank sei hier meinen Kollegen, den „5th floor gangsters“ ausgesprochen. Es war mir eine Ehre mit euch zu forschen und stundenlang angeregt zu diskutieren!

Herzlichen Dank, dass ihr alle ein Stück des Weges mit mir gegangen seid!

Im Speziellen möchte ich diese Arbeit meiner Tochter Laura widmen. Obwohl sie erst seit zehn Monaten auf der Welt ist, saugt sie neue Eindrücke und generell das Leben auf, wie ein Staubsauger. Liebe Laura, falls du diese These einmal mit Interesse lesen solltest, und verstehst worum es geht, bin ich noch mehr stolz auf dich, als ich das nicht ohnehin schon bin. Dann freue ich mich sehr, dass auch ich, ähnlich wie mein Großvater bei mir, dein Interesse an den Naturwissenschaften wecken konnte.

Abstract

Shear stress is commonly made responsible for protein aggregation but the reports remain contradictory. Furthermore, the effect of cavitation occurring at very high shear rates in gear pumps, process pipes or valves was not addressed so far. Cavitation occurs when the local static pressure falls below the vapor pressure of the liquid resulting in boiling at ambient temperatures. Gas bubbles are formed providing vapor/liquid interfaces. When the gas bubbles collapse, hydroxyl radicals are formed. It has been hypothesized that these radicals damage proteins. Hence, cavitation is a potential cause for protein aggregation. Hydrodynamic cavitation only occurs when the velocity gradient in a system is very steep. Consequently, the protein is exposed to high shear rates, vapor/liquid interfaces and hydroxyl radicals simultaneously.

In this thesis a method was designed to generate cavitation using a micro-orifice. In order to dissect the influence of shear stress, vapor/liquid interface and hydroxyl radicals, each stress factor was addressed independently. To suppress cavitation inside the micro-orifice a flow restrictor was built to raise the downstream pressure. To mimic the effects of vapor-liquid interfaces on protein aggregation a foaming method was designed. The generation rate of hydroxyl radicals occurring from cavitation was tested by a fluorometric assays. The stress factors were tested with nine proteins (alpha-Lactalbumin, two antibodies, fibroblast growth factor 2, granulocyte colony stimulating factor, green fluorescent protein, hemoglobin, human serum albumin, lysozyme) covering a wide range of protein sizes, isoelectric points, and conformational stabilities. The velocity field, shear rates, and appearance of cavitation was calculated by computational fluid dynamic (CFD) simulation and experimentally validated.

The maximum shear rate in the micro-orifice at highest flowrates was calculated to be 10^8 s^{-1}. Although the shear rate was among the highest ever reported in literature, not a single protein showed increased aggregation behavior when cavitation was suppressed. However, hydrodynamic cavitation was identified as possible reason for protein aggregation. Three of the nine tested proteins aggregated under cavitational flow. The aggregation behavior could be correlated to the increase in surface area by vapor/liquid interfaces occurring from cavitation bubble growth. The concentration of hydroxyl radicals generated by vapor bubble collapse was found to be insignificant as a cause for protein aggregation. This work conclusively shows that isolated shear stress is not an issue when processing proteins but cavitation should be prevented at any time.

Zusammenfassung

Obwohl hohe Scherraten in der Vergangenheit oft mit Proteinaggregation in Zusammenhang gebracht wurden, gibt es Arbeiten in denen keine Korrelation gefunden werden konnte. Der Einfluss von Kavitation, welche bei sehr hohen Scherraten in Pumpen oder Ventilen auftreten kann, wurde hingegen noch nicht beschrieben. Kavitation entsteht wenn der lokale statische Druck unter den Dampfdruck der Flüssigkeit fällt. Dabei entstehen Gasblasen bereits bei Raumtemperatur. Wenn der lokale Druck wieder zunimmt, werden die Blasen instabil und implodieren. Hierbei entstehen Hydroxyl-radikale, von welchen man annimmt, dass sie in der Lage sind, Proteine zu zerstören. Aufgrund der hohen benötigten Strömungsgeschwindigkeiten tritt Kavitation nur zusammen mit hohen Scherraten auf. Dadurch werden Proteine hohen Scherraten, Hydroxyl-radikalen und Phasengrenzflächen gleichzeitig ausgesetzt.

Im Zuge dieser Arbeit wurden Kavitation, extrem hohe Scherraten und Phasengrenzflächen unabhängig voneinander betrachtet, um ihren jeweiligen Einfluss auf Proteine zu verstehen. Kavitation wurde mithilfe einer Mikromessblende erzeugt. Durch den Einsatz eines Druckerhöhers konnte Kavitation unterdrückt werden und hohe Scherraten isoliert betrachtet werden. Der Einfluss der Kavitationsphasengrenzfläche wurde mithilfe eines Proteinschaumversuches imitiert. Die Hydroxyl-radikalbildungsrate konnte mittels einer Fluoreszenzanalytik aufgeklärt werden. Es wurde eine große Anzahl strukturell unterschiedlicher Proteine getestet (Alpha-Lactalbumin, zwei Antikörper, Fibroblast growth factor 2, Granulocyte Colony Stimulating Factor, Green Fluorescenct Protein, Hämoglobin, Humanes Serum Albumin und Lysozym). Die Scherraten, welche in der Messblende erzeugt werden konnten, wurden mittels einer validierten Computersimulation, berechnet.

Es konnte gezeigt werden, dass die vorliegende maximale Scherrate, bei maximalem Fluss (10^8 s^{-1}), eine der höchsten jemals an Proteinen getesteten Scherrate war. Dennoch wurde bei keinem der ausgewählten Proteine erhöhte Aggregation festgestellt. Im Gegensatz dazu, führte Kavitation bei drei von neun Proteinen zur Aggregation. Darüber hinaus konnte gezeigt werden, dass die entstehenden Grenzflächen, welche durch Kavitationsblasen entstehen, für die Aggregation verantwortlich waren, und nicht Hydroxyl-radikale, wie bisher vermutet. Diese Arbeit demonstriert eindrucksvoll, dass Scherstress, auch auf sehr hohem Niveau, keinen Einfluss auf Proteinaggregation hat. Im Gegensatz dazu sollte die Entstehung von Kavitation in Bioprozessen zu jeder Zeit verhindert werden.

Table of content

1 Introduction 1
1.1 Proteins 1
1.2 Production of proteins 3
1.3 Protein stability 4
1.4 Temperature and chemically induced unfolding of proteins 5
1.5 Mechanically induced unfolding of proteins 6
1.6 Effect of shear stress on protein integrity 7
1.7 Calculation of shear rates 9
1.8 Unfolding force 11
1.9 Computational fluid dynamics 12
1.10 Cavitation 13
1.11 Hydroxyl radicals 15
1.12 Protein adsorption to surfaces 17
1.13 Analysis of protein aggregates 18
2 Objectives 21
3 Results 22
4 Outlook 31
5 List of Publications 31
6 Abbreviations 32
7 Symbols 32
8 List of figures 33
9 References 35
10 Publications 39

1 Introduction

1.1 Proteins

Generally, the demand for innovative drugs and sustainable medical treatment is high. By 2015 almost 400 recombinant produced proteins were approved as biopharmaceuticals by the authorities. Furthermore, 1300 other candidates were in the pipelines of pharmaceutical companies were 50 % of these potentially new drugs were in pre-clinical and 33 % in the stage of clinical trials [1]. Due to the increase in antibody production which requires complex glycosylation more and more recombinant proteins are produced in mammalian cells. The ratio between productions in mammalian cell to not-mammalian changed from 37:63 in 1989 to 70:30 until 2014 [2]. In 2016 11 out of the top 15 best-selling drugs worldwide were either proteins, peptides or recombinant vaccine-conjugates (Figure 1) [3]. Together, these 11 drugs came in with sales of 81.8 b$. For the antibody Humira®, which is used to treat rheumatoid arthritis the sales growth from 2007 to 2016 was 900% (1.6b$ to 16.1) [3, 4].

Although the outlook for biopharmaceuticals is promising there is a drawback. Until a certain pharmaceutical is approved by the regulatories it has to pass a pre-clinical and three clinical stages in which it must be shown to be safe for use and superior compared to the existing standards. It was shown that from 2005 to 2009 out of an average of 24 newly developed drugs only a single one passed all trials and was finally approved by the FDA [5]. Therefore, it was estimated that the averaged costs for an approved biopharmaceutical is $615 million, $626 million, and $1.2 billion for the preclinical period, the clinical period, and in total, respectively [6]. Additionally, the bigger the market of a certain drug, the higher the probability competitor market entry once patent protection runs out. These generic substitutes of the originator drug are called biosimilars. Compared to chemical generics, biologically produced drugs can only be produced “similar” but not in an identical way. Due to the reduced R&D costs biosimilars are of immense interest [7].

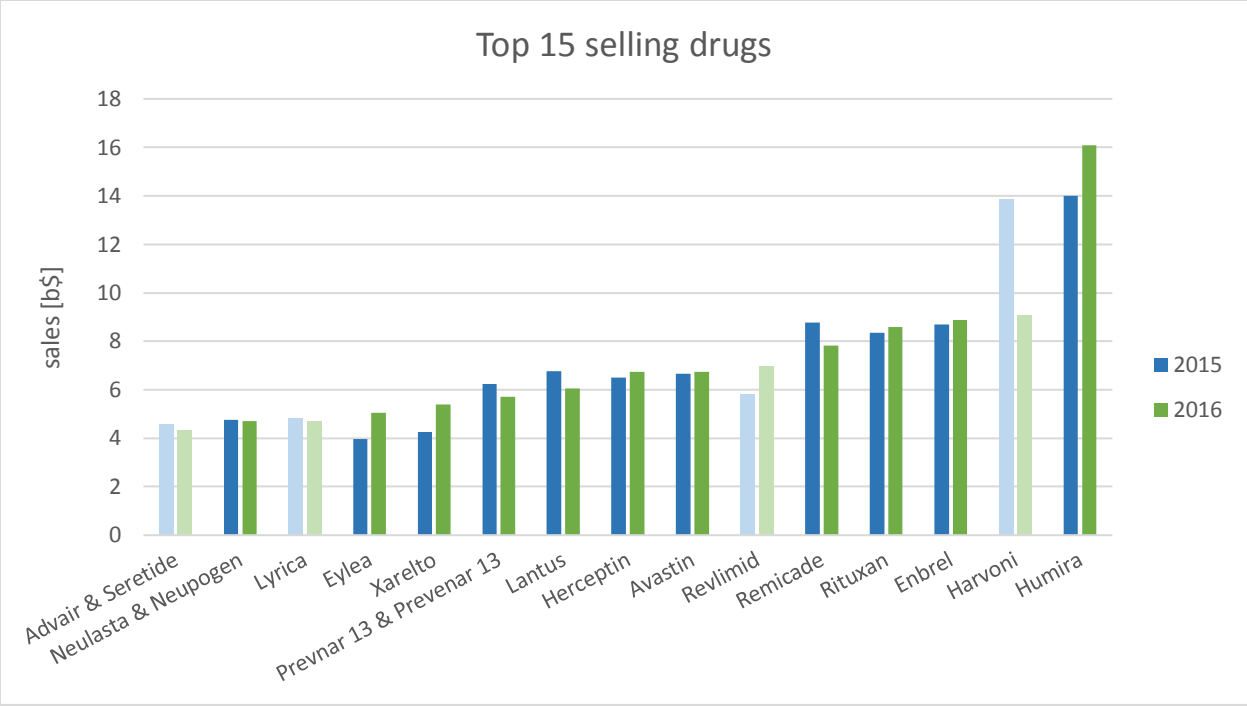

Figure 1: Top selling drugs of 2015 and 2016 in billion US Dollar. Recombinant obtained drugs are opaque while chemically produced compounds are transparently colored [3].

In April 2006, Omnitrope® (Novartis Pharma GmbH), a recombinant human growth hormone, was the first biosimilar gaining access to the European market [8] after approval. The first biosimilar antibody to be approved by the EMA was infliximab (Celltrion, Inc. and Hospira, Inc) targeting tumor necrose factor alpha, in 2013 [7]. In 2015, Zarxio® (filgrastim-sndz Novartis Pharma GmbH) became the first biosimilar product to receive approval from the FDA [9]. Manufactured by Novartis, Zarxio is a biosimilar to Amgen's Neupogen® which is a granulocyte colony stimulating factor (GCSF). Although, it was already approved in the European Union since 2009 it took almost 6 years to enter the US market. As described above the market for Neupogen is huge hence the potential conflict between different companies even bigger. First biosimilars of Humira with sales of 16 b$ in 2016 are expected to enter the market by the end of 2018 when the patent protection expires [10].

1.2 Production of proteins

As mentioned before there is a huge cost pressure for the development of biopharmaceuticals nowadays. Hence, a lot of effort is spent to bring a certain biopharmaceutical to the market as quickly as possible in order to prolong the period in which the drug can be exclusively produced under patent protection. However, the process understanding and the definition of critical control parameters (CCPs) is therefore often underdeveloped, with dramatic effects on manufacturing efficiency [11]. In general the production of a certain biopharmaceutical is divided into up- and downstream (Figure 2). In the upstream the protein is produced in a genetically modified host like microbials, yeast or mammalian cell cultures. While in the downstream the target protein is separated from host materials. This purification process is required to remove process related impurities such as host cell proteins (HCP), viruses, DNA or endotoxins. These impurities can cause patients side effects and must therefore be removed to meet authority requirements [12]. Also product related impurities with higher or lower molecular weight must be separated to ensure high potency per delivered drug dosage. The separation of undesired side products is based on the different physical properties of these impurities like size or charge. With each purification step at least one class of such impurities is addressed to be removed [13, 14].

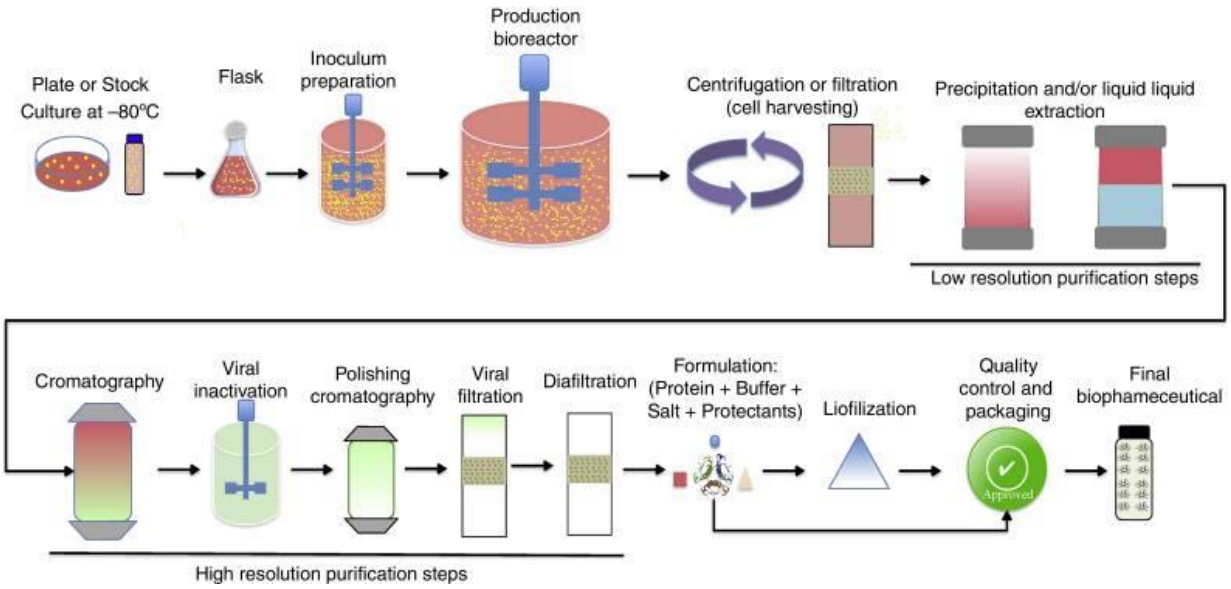

Figure 2: Schematic description of a possible bioprocess which includes the production of the biopharmaceutical with a host inside a bioreactor and the followed separation and purification [15].

However, during or after fermentation the target protein is separated from the encapsulated environment of the host cell. This exposes the protein to physical stressors such as air/liquid, liquid/solid interfaces, shear stress, changes in pH, temperature or chemotropic chemicals. As will be described in the following chapters, all these properties are at least surmised to reduce protein activity at a certain level. Currently, process understanding and the prediction of how a certain protein behaves in a certain situation is still not accessible for industries [11]. Due to the increase in the complexity of target proteins and the high pressure on the pharmaceutical market, novel manufacturing approaches have to be found. The quality by design (QbD) concept promotes early understanding of the interplay between product quality and the manufacturing process. This emphasizes including quality through the process, not testing it in [11]. Hence process understanding and QbD are increasing in importance due to market pressure.

1.3 Protein stability

Although proteins are over 1000 times bigger than chemical pharmaceuticals they still have a highly ordered structure. This three-dimensional fold is characterized by the secondary, tertiary and quaternary structure [16, 17]. However, this three-dimensional folded state fluctuates with a limited number of preferred conformations. The conformation of a protein that possesses the least overall energy is also the most stable one and described as the native state. At this state the bioactivity of the drug is highest. Although there are some purification methods like precipitation and flocculation where this confirmation is reversibly altered for a short period of time to ensure selective purification, the native conformation must be given for the final biopharmaceutical.

Several different interactions are responsible for the present folding state. There are electrostatic interactions, hydrophobic interactions, hydrogen bonding, van der Waals forces and intrinsic propensities. However, among those hydrophobic interactions were identified to be the most dominant force . Here hydrophobic amino acids of proteins do not favor to interact with polar water molecules surrounding the protein. Hence this uncharged and nonpolar residues tend to be located in the inside of the protein shielded from water whereas polar side chains are oriented towards water. Furthermore, it was suggested that the lack of hydrogen bond between nonpolar molecules and water, rather than favorable interactions between nonpolar groups themselves, is a major factor contributing to the structural stability of proteins and nucleic acids [18]. In biopharmaceutical industries protein aggregation must be prevented at any time because these

aggregates reduce the process yields therefore increasing the manufacturing cost per dose. Second, and even more import, protein aggregates must not be found in the final product because of immunogenic risk of the patients [19].

1.4 Temperature and chemically induced unfolding of proteins

A good thermodynamical description of protein folding is the free energy of unfolding ΔG_{unf} (Equation 1). It is a function of enthalpy (ΔH_{unf}), temperature (T) and entropy (ΔS_{unf}) changes. For proteins under moderate temperatures both enthalpy and entropy are negative. Here, the decrease in enthalpy overcomes the decrease in entropy. An unfolded protein has a higher free energy than a folded protein. Hence, protein folding occurs spontaneously to reach the native state which has the least free energy.

$$\Delta G_{unf} = \Delta H_{unf} - T\Delta S_{unf} \quad (1)$$

However, at higher temperatures the entropic term is more weighted favoring unfolding of proteins. With the assumption of a two stage reversible aggregation process (folded ↔ unfolded) and a given ΔG_{unf} at a certain temperature the percentage of unfolded protein can directly be calculated (Equation 2), with R as the gas constant and U and F as fractions of unfolded and folded protein. In other words, at the midpoint temperature of unfolding (T_m) the ratio of unfolded to folded protein is 1:1 resulting in a ΔG_{unf} of zero.

$$\Delta G_{unf} = -RTln\frac{[U]}{[F]} \quad (2)$$

Similar to temperature induced unfolding, chemical agents such as chaotropic salts can also induce unfolding of proteins. When a protein population unfolds, its fluorescence and circular dichroism spectra change. When the ratio of unfolded to folded protein at several unfolding agent concentrations is measured, a linear extrapolation can be set up to predict the free energy at a concentration of zero unfolding agent ΔG_0 [20]. Similar experiments can be performed to describe protein stability towards changes in pH [21].

1.5 Mechanically induced unfolding of proteins

The unfolding of proteins due to temperature, chemicals or pH can be described thermodynamically. However, a lot of effort was spent to compare thermodynamical parameters with mechanical strength to define which features of the underlying energy landscape modulate the force response of a protein. With this knowledge the behavior of a defined protein towards a certain force can be predicted and such knowledge would be useful for tailor-made proteins in the future. Unfortunately, no correlation was found between the thermodynamic stability of a domain and the force at which it is likely to unfold [22-24]. It was found that the unfolding force at which a certain protein unfolds depends on the amount to which it is extended indicating that unfolding is a kinetic and not a thermodynamic process [25]. Hence, the unfolding force is expected to depend on the activation energy that must be overcome to undergo the transition from the folded to the unfolded state. As a consequence a lot of effort was spent to determine the force which is required to unfold proteins mechanically. One promising approach is to immobilize proteins onto a surface and to use an atomic force microscope (AFM) to unfold proteins (Figure 3). The tip of the AFM is pushed into the immobilized proteins and upon binding it is possible to both measure the unfolding force as well as the elongation distance when the tip is pulled back. Many studies have been conducted in this field and the unfolding force for different proteins was correlated to the secondary structure. While α-helical dominated proteins tent to unfold around or even below 20 pN [25, 26] β-strand dominated proteins being known to have a higher mechanical stability unfold approximately one order of magnitude higher between 180 to 220 pN [25, 27]. In theory it should be possible to use this knowledge of force required to unfold certain proteins and translate it to the force obtained by shear stress. If it is possible to correlate shear rates with unfolding forces, the threshold for shear induced protein unfolding can be drawn.

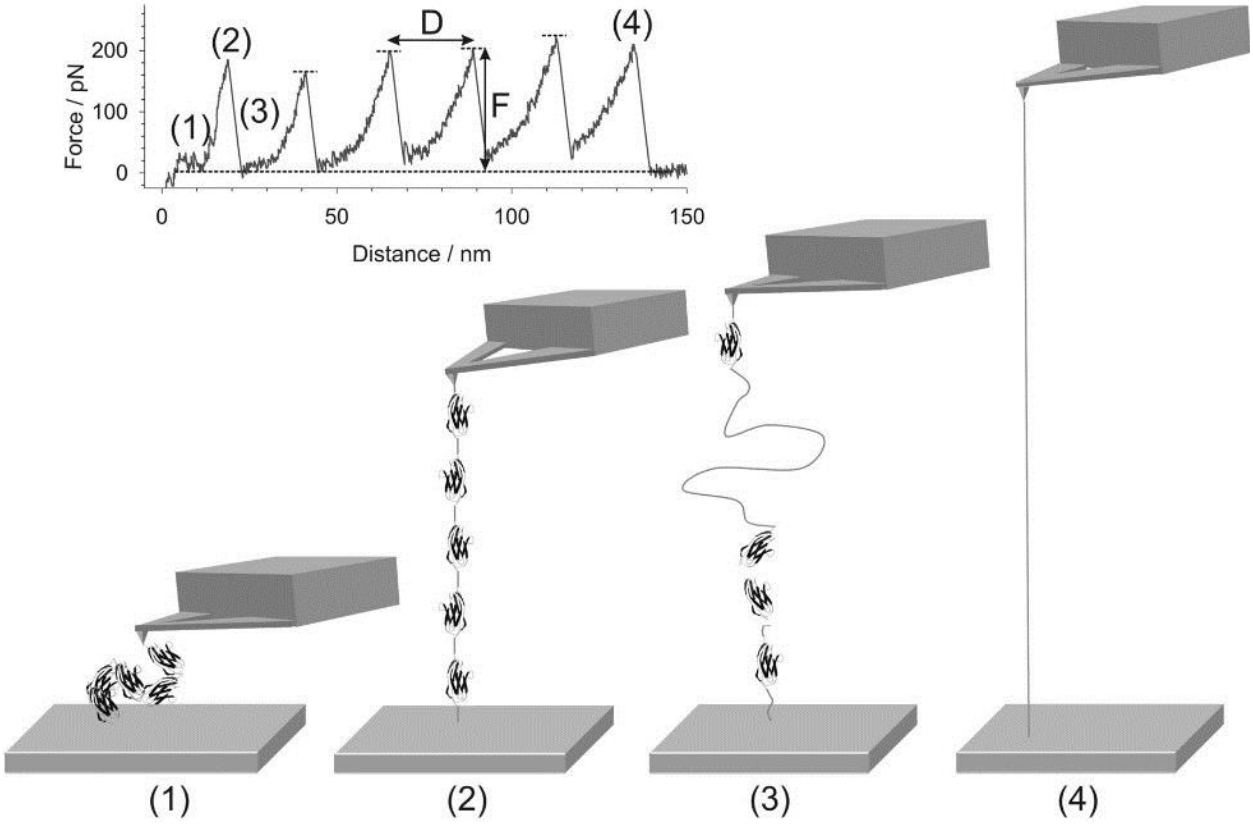

Figure 3: Schematic diagram of a mechanical unfolding experiment and the force-extension profile for different unfolding states. Protein binding (1), linearization of the protein (2), unfolding of a single domain (3), unfolding of all domains (4). With the force (F) and the elongation distance (D) given for each step in the insert [25].

1.6 Effect of shear stress on protein integrity

Shear stress can be seen as a mechanical force acting on proteins to unfold them. Already in the 1980's, Charm and Wong [28] reported the effect of shear stress on proteins. They used the catalytic activity of enzymes to address the influence of shear on the structural integrity of proteins. Catalase, carboxypeptidase and rennet were stressed either in a narrow gap coaxial viscometer or pumped through a narrow capillary. They found inactivation of rennet, catalase and carboxypeptidase already at shear rates of 9.15, 91.5 and 290 s^{-1}, respectively. In a follow up publication Charm and Lai [29] described how shear stress inactivated catalase during ultrafiltration at shear rates > 10000 s^{-1}. However, rennet did not show reduced catalytical activity under the same conditions. This behavior was attributed to the recovery of tertiary structure and activity after the end of ultrafiltration. They further showed that when the product of the shear

rate ($\boldsymbol{\gamma}$) times incubation time (t) exceeded 10^4 ($\boldsymbol{\gamma}$ t), inactivation of rennet occurred irreversibly. Tirrell and Middleman [30] found urease enzyme inactivation in a hydrodynamic flow already at shear rates of 48 s^{-1}. The impact of a turbulent flow regime inside a capillary on protein aggregation behavior of heparin, fibrinogen and interferon was also addressed by Charm and Wong [28]. Their findings suggested that the turbulent flow regime induces protein aggregation even faster than laminar conditions.

Contrary to the above cited publications, other reports showed no correlation between shear stress and protein aggregation. Thomas, Nienow [31] showed that there was no inactivation of alcohol dehydrogenase sheared at 30 °C in a coaxial cylinder viscometer at 683 s^{-1} for 5 hours. In the same year Thomas and Dunnill [32] further highlighted a lack of shear damage using urease and catalase when stressed in a capillary with shear rates of up to 10^6 s^{-1}. They concluded that isolated shear alone was not enough to damage proteins and that other effects such as air/liquid interfaces inactivation must occur together with the shear stress. In concentric cylindrical viscometer study alcohol dehydrogenase was stressed with $2.6x10^4$ s^{-1} without noticing any loss in activity after 1 h ($\boldsymbol{\gamma}$ t = 9.4 x 10^7) [33]. Jaspe and Hagen [34] also did not find evidence for the inactivation or the unfolding of cytochrome c in a silicon capillary tube with shear rates of up to 2 x 10^5 s^{-1}. Additionally, they derived a bead based theoretical model to predict shear rates for protein unfolding. According to their calculations a protein with 100 amino acids would require shear rates of ~10^7 s^{-1} to unfold. This in turn would require a very high driving force inside the capillary and laminar flow conditions would not be given under this conditions. Also a detailed study on highly concentrated monoclonal immunoglobulin G1 did not yield protein aggregation at shear rates of up to 2.5 x 10^5 s^{-1} [35]. The authors also concluded that the entrapment of air-bubbles, adsorption to solid surfaces, the contamination by certain particulates or pump cavitation stresses are much more important than isolated shear. They calculated the required shear force to unfold an antibody with a different theoretical approach to be 5 x 10^7 s^{-1} in a 3 mPas solution. Although the conclusion that isolated shear stress in the magnitude below 10^7 s^{-1} has no negative effect on protein integrity has been reached by most researchers, there remain dissenting voices. A setup which can describe isolated shear rates without the entrapment of air and the test of several structurally different proteins is missing.

1.7 Calculation of shear rates

When proteins are exposed to a velocity gradient like in a valve, a tube or close to an impeller tip, the differences in velocity result in a shear gradient (Figure 4). This shear gradient ($\boldsymbol{\gamma}$) is calculated by taking into account the difference in flow velocity (Δv) between two layers and the distance between those (Δd).

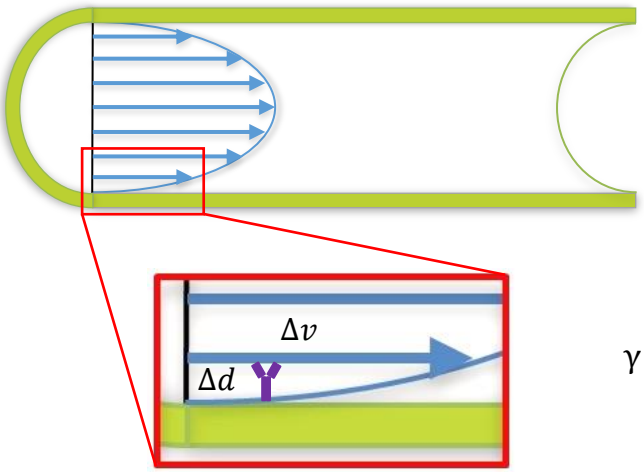

$$\gamma = \frac{\Delta v}{\Delta d}$$

Figure 4: Schematic drawing of a tube with a laminar flow profile. Shear rates can be calculated for each velocity layer. An antibody is schematically drawn into the shear field (purple).

The shear rate is a local function with its maximum close to the wall and its minimum at the center of the tube. For an impeller the highest shear rate is close to the tip and the shear rates decrease with distance to the impeller. Shear induced damage to proteins might be caused by changes to their secondary and/or tertiary structures through unfolding. Also a disruption of the quaternary structure of multi subunit proteins is reasonable. Due to the irreversible stretching inside the shear field the protein might unfold resulting in a loss of enzymatic activity or protein aggregation.

The maximum shear rate in a tube can be derived by taking into account the mass flow (Q) and the radius of the tube (r) (Equation 3) [36]. Also the average shear rate under laminar flow can directly be calculated due to the parabolic flow profile (Equation 4) [34].

$$\gamma_{max} = \frac{4Q}{\pi r^3} \tag{3}$$

$$\gamma_{avarage} = \frac{\partial P}{\partial z}\frac{R}{3\eta} = \frac{8Q}{3\pi r^3} \tag{4}$$

In turbulent flow the steepness of the velocity gradient depends on the velocity and the geometry of the system. Therefore, the shear rates cannot be directly derived (Figure 5).

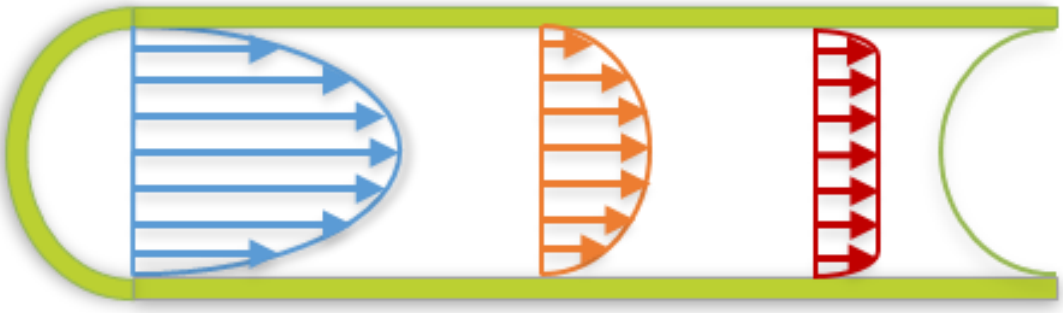

Figure 5: Flow profiles in a tube: laminar flow (blue), transition (orange), turbulent flow (red)

To estimate the current flow regime inside a tube, the Reynolds Equation (Equation 5) is used, where ρ is the density of the liquid, v the linear flow velocity, d the diameter of the tube, and μ the dynamic viscosity.

$$Re = \frac{\rho v d}{\mu} \tag{5}$$

Below 2300 the flow regime is assumed to be laminar, above there is turbulent flow. To describe the shear profile in turbulent flow and therefore to be able to calculate shear rates computational fluid dynamics simulations (CFD) can be used.

1.8 Unfolding force

As previously mentioned for a laminar flow profile shear rates can be calculated rather simply. However, on their own they cannot answer the question which force is required to unfold a certain protein by shear. In recent years a lot of research was performed on atomic force microscopy (AFM) to answer this question [25, 27, 37-39]. To calculate the shear force (F) (Equation 6) which is necessary to unfold a protein by shear one has to take into account the local shear rate ($\boldsymbol{\gamma}$), the dynamic fluid viscosity (μ) and the surface area of a protein on which this force acts (A) [40].

$$F = \gamma \mu A \tag{6}$$

While the viscosity and the area on which the shear acts does not change inside the observation point, the shear rate is a local function. It is expected to be highest the wall. The closer it is measured to the center of the tube, the lower the number becomes. The area on which this force acts is related to the structure of the target. Assuming proteins to be spherical particles the square radius of the target is proportional to the area on which the shear pressure (γμ) acts. Therefore, the size of the structure which is stressed is even more important than the magnitude of shear. Since particles can rotate in solution the amount of shear which is used to stretch and rotate the protein is difficult to define. However, with this simple description it is possible to correlate shear rates directly with mechanical unfolding forces when the ratio between protein rotation and elongation is defined.

1.9 Computational fluid dynamics

The flow profile under turbulent conditions is difficult to predict a-priori, but computational fluid dynamics (CFD) can be used to overcome this limitation. CFD Simulation, also known as CFD modeling is an engineering based scientific process module which runs on Computational Fluid Dynamics theory and is applied for resolving different fluid flow related problems. It is able to describe flow velocity, density, temperature, and chemical concentrations for any area where flow is present. It's a numerical method based on Navier-Stokes Equations for the calculation of nonlinear differential equations relating to fluid flow. Therefore, a certain geometry must be built virtually in computer aided design (CAD) and filled with defined finite volumes, called a mesh. After implementing border conditions for the setup the simulation is run (Figure 6).

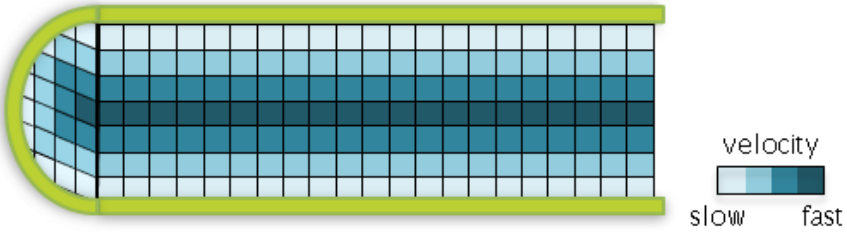

Figure 6: Schematic description of an CFD simulation for the description of velocity inside a tube. A cubic mesh was chosen to describe the velocity profile.

While the Navier-Stokes Equations were available from the mid of the 19th century, the usage of CFD is highly computationally demanding. Early work on numerical solution was published in the mid of the 20th century with the advent of computers [41-44]. With increased computational capacity and decreased cost per flop CFD became more popular. Nowadays CFD simulation is used across various fields in order to achieve flawless product design by combining computational tools and the theory of fluid dynamics. CFD enables scientists and engineers to perform numerical experiments in a virtual flow laboratory without the need of an actual experiment. However, predicted solutions are more reliable when the input variables or border conditions are matched with experimental data [45, 46]. As mentioned, compared to laminar flow the description of local velocity, vortices or shear rates cannot be predicted by simple equations for turbulent flow. Hence a lot of effort was spent to describe flow profiles under turbulent conditions with CFD [41, 47-53] to overcome this limitation and to make CFD applicable for very challenging prediction problems.

1.10 Cavitation

Bee, Stevenson [35] suggested that at extremely high shear rates the phenomenon of cavitation might occur. If cavitation has a negative influence on proteins but is not considered then the effect of cavitation can be misattributed to shear stress. Cavitation is a phenomenon in which the local static pressure falls below the vapor pressure of the liquid, resulting in localized boiling. The occurrence of cavitation can be described by both the Bernoulli equation and the Cavitation number. For Bernoulli, the sum of flow velocity (v), the local pressure (p) divided by the liquid density (μ) and the gravitational acceleration (g) times the difference in height (z) is constant in a certain streamline for incompressible fluids (Equation 7).

$$\frac{v^2}{2} + \frac{p}{\rho} + gz = constant \tag{7}$$

Assuming that the fluid is only transported horizontally the equation can be reduced to Equation 8.

$$\frac{v^2}{2} + \frac{p}{\rho} = constant \tag{8}$$

If a certain fluid is pumped through a constriction such as a nozzle, the flow velocity increases under the assumption of equal mass transport. As a result the local pressure has to decrease according to Bernoulli. If it falls below the vapor pressure of the liquid, cavitation occurs (Figure 7). To predict cavitation in a certain flow path the cavitation number can also be used (Equation 9).

$$Ca = \frac{2(\mathrm{p}-\mathrm{p}_v)}{\rho * v^2} \tag{9}$$

The equation relates the local static pressure in a liquid (p) to the vapor pressure of the liquid (p_v), the density (ρ), and the flow velocity (v). Below a value of 0.2 to 1.5 for the Ca, cavitation can be expected [54]. When the pressure recovers downstream of the orifice, the vapor filled bubbles collapse under enormous pressure and temperatures [55], forming microjets and hydroxyl radicals [56]. In material science the destructive nature of this phenomenon is well known [57-59]. For protein integrity the occurrence of vapor/liquid interfaces from bubble growth as well as the formation of hydroxyl radicals was not clearly addressed yet.

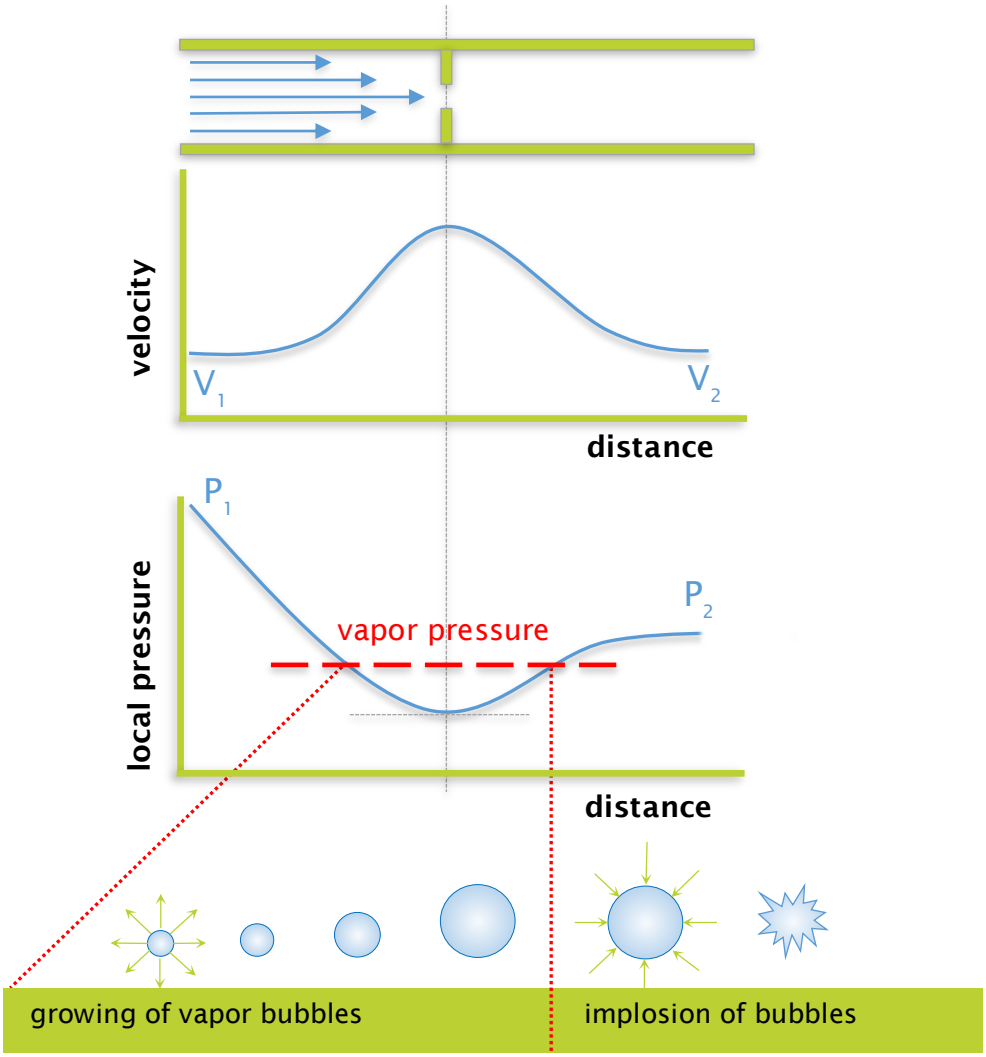

Figure 7: Schematic drawing of the occurrence of cavitation generated by an orifice inside a tube. A steep increase in velocity leads to a decrease in local pressure below the vapor pressure.

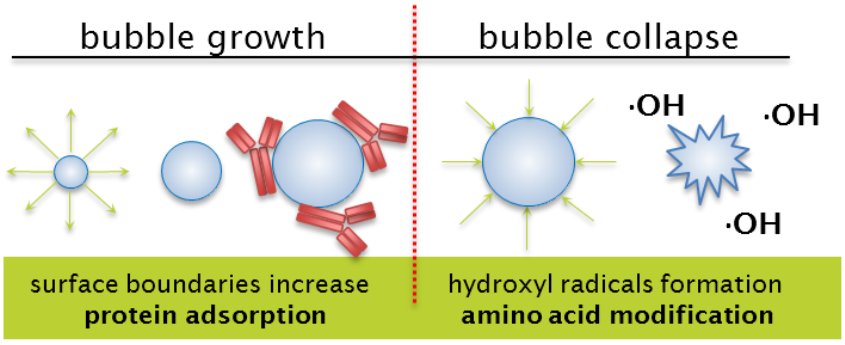

Figure 8: Expected effect of cavitation on proteins.

1.11 Hydroxyl radicals

As previously mentioned, hydroxyl radicals are formed when vapor filled cavities generated by cavitation collapse under pressures higher than the vapor pressure of the liquid. This results in implosion of these cavities. The destructive nature of these hydroxyl radicals generated by X-ray radiolysis of water or Fenton's reaction on antibodies and amino acid side chains was reported previously [60-64]. In the catalytic Fenton's reaction one ferrous iron ion (Fe^{2+}) reacts with peroxide to form ferric iron ion (Fe^{3+}), one hydroxyl radical and one hydroxyl ion (Formula 1). In the backward reaction ferric iron reacts with peroxide to form ferrous iron, a hydroperoxyl radical and one H^+ (Formula 2). In the backward reaction ferric iron is reduced to ferrous iron. Hence, only a little amount of ferric iron is needed to generate large amounts of radicals as long as peroxide and an acidic pH is present [65, 66].

$$Fe^{2+}\ H_2O_2 \rightarrow Fe^{3+} + OH^{\circ} + OH^{-} \quad \text{(F1)}$$

$$Fe^{3+}\ H_2O_2 \rightarrow Fe^{2+} + OOH^{\circ} + H^{+} \quad \text{(F2)}$$

It was possible to describe the relative reactivity of the 20 amino acids with hydroxyl radicals as followed: Cys >Met > Trp > Tyr > Phe > Cystine >His > Leu ~ Ile > Arg ~ Lys~ Val > Ser ~ Thr ~ Pro > Gln ~Glu > Asp ~ Asn > Ala > Gly [64]. In a publication by Randolph *et al.*, protein filled vials were dropped from varying heights to induce cavitation [67]. Protein aggregation increased with the drop height. On the other hand, consistent evidence for oxidative damage of the protein, measured by mass spectrometry, was not found. They still considered that hydroxyl radicals were the only possible driving force for protein aggregation under cavitational conditions. Another study in which the combined effect of cavitation and agitation was described did also not find evidence for hydroxyl radical mediated protein aggregation [68]. However, no correlation between protein aggregation and hydroxyl radical concentration generated by cavitation has been found so far.

Another source of cavitation and hydroxyl radicals is ultra-sonication [56]. In this method, ultrasound waves are transmitted through the medium, compressing and stretching the molecular spacing of the medium. Thus, the average distance between the molecules varies as they oscillate about their mean position. When the distance between water molecules is extremely large, the local pressure undercuts the vapor pressure of the liquid and cavitation occurs [69]. At high intensities Hydroxyl radicals occurring from ultra-sonication were already

associated with DNA degradation [70]. The threshold at which hydroxyl radical concentration is high enough to alter protein integrity was not addressed so far.

To measure hydroxyl radical concentrations in solution several methods can be used. Guaiacol can be used to detect these radicals from solutions [71] but it is cross sensitive to light [72]. Also with the amino acid Tryptophan the effects of hydroxyl radicals onto proteins could be mimicked very easily. However, Tryptophan is cross sensitive to other radical species such as singlet O_2 [73], making a specific assay difficult. Dimethyl sulfoxide (DMSO) has potential for hydroxyl radical scavenging but experiments suggest that DMSO oxidation may be achievable by mechanisms unrelated to hydroxyl radicals [74, 75]. Also aromatic hydroxylation was used to measure hydroxyl radicals in vitro. One prominent compound is 2-hydroxybenzoat which is solely sensitive to hydroxyl radicals. However, from this radical reaction 3 different products are formed: 2,5-dihydroxybenzoate 2,3-dihydroxybenzoate and catechol [76, 77]. These products must be separated by HPLC to calculate the amount of hydroxyl radicals. Hence, this method cannot be used to directly measure hydroxyl radicals from solution. The most prominent chemical to specifically sense hydroxyl radicals from solution without any cross sensitivity is terephthalic acid (TPA). Here one hydroxyl radicals specifically reacts with the meta-position of the acid to form fluorescent active compound hydroxyl terephthalic acid (hTPA) (

Figure 9). Compared to other chemical hydroxyl radicals dosimeters, hTPA is heat and light resistant [78] and its emits a high fluorescents signal (425 nm) when excited at 315 nm [79]. This enables direct measurement from the sample solution. Over the past decades this method was validated and used for radical detection in many studies [78-82].

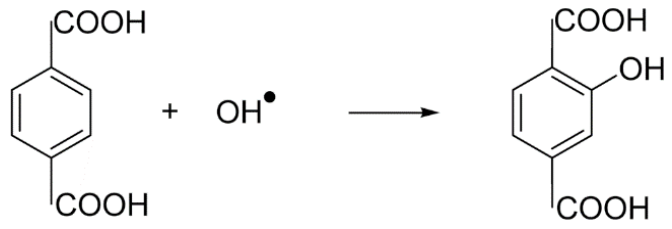

Figure 9: Reaction of terephthalic acid with hydroxyl radicals to form hydroxyl terephthalic acid.

Recent protein studies investigated the effect of hydrodynamic cavitation by dropping protein filled vials [67, 68]. Protein aggregation was found in both experiments but the mass

spectrometry data on hydroxyl radical mediated amino acid modification was inconsistent. Also the concentration of hydroxyl radicals occurring from this experiment was not determined. Till today, it remains unclear if the amount of hydroxyl radicals generated by hydrodynamic cavitation is high enough to reasonable influence protein integrity. Hence has to be proofen that hydroxyl radicals can indeed be seen as the driving force for the described protein aggregation or if the increase in surface area was responsible (Figure 8). However, cavitation mediated increase in surface area was not subject of a study so far. Furthermore, the effect of hydrodynamic cavitation as expected from pipe reductions or valves was not subject of a single protein study.

1.12 Protein adsorption to surfaces

Surface induced aggregation is regarded as critical for the processing of proteins. When proteins are exposed to air/liquid interfaces the proteins directly attach to these interfaces. This binding is most probably driven by hydrophobic interactions, due to the higher hydrophobic property of air compared to water molecules [83]. Upon contact with the surface the protein monomer undergoes conformational changes. Proteins degrading at air/liquid interfaces often produce fibre like aggregates. It increases the contact area with the surface and therefore unfolds. The behavior of Hemoglobin, Insulin, Gliadin, Ovalbumin, serum albumin towards surfaces and the negative impact of protein surface-interactions onto protein integrity was already described in the mid of the last century [84, 85]. However, it remains unclear whether these unfolded monomers attach to other unfolded monomers at the surface or if they attach when being released to the solution [86]. The use of surfactant can prevent this phenomenon. It is believed that the surfactant covers the air/liquid interface in a thin layer. This blocks the access of the protein to the air/liquid interfaces protecting it from aggregation [87]. On the other hand, the general use of surfactants to overcome surface mediated protein aggregation is not recommended due to several reasons. It can accelerate protein aggregation as shown in several studies [83, 88] due to a strong binding to the protein which inducing aggregation. Also the oxidation of surfactants is reasonable and might result in the formation of hydro-peroxides which can in turn lead to an oxidation of the final product [89]. A Recent study suggested that the surface tension directly unfolds proteins [35]. Water without the addition of proteins, salt or surfactants shows a surface tension of 70 mN/m. If this force acts over a distance between two

to three nanometer, the resulting force would be 140 to 210 pN. This force is of the same dimension which is required to unfold proteins with AFM.

However, it was considered that in many early stage shear stress studies the effect of air entrapment was overseen and the resulting effect of air/liquid interfaces was misattributed to shear stress [90, 91]. When cavitation occurs, the increase in surface area due to vapor bubble growth was not considered as possible protein aggregation source so far. Here vapor/liquid interfaces built up as long as the local pressure stays below the vapor pressure of the liquid. The destabilization of vapor/liquid interfaces can be achieved by the use of surfactant. The surfactant reduces the surface tension of vapor cavities, leading to destabilization of the cavities and therefore an early break up resulting in a reduced interfacial area [92]. So far, all cavitation associated protein aggregation studies focused on effect of hydroxyl radicals [67, 68, 70] but missed to address vapor/liquid interfaces. If the effect of cavitation is addressed in a detailed protein study it is important to use methods which are able to describe the effects of cavitation, shear and surface interactions independent from each other.

1.13 Analysis of protein aggregates

To analyze protein structure alterations obtained from cavitation, shear or air/liquid interfaces several methods can be taken into account to address proteins in the supernatant, and insoluble aggregated protein. When analyzing the secondary structure of a protein in the supernatant curricular dichroism (CD) is a well-established routine analytic. CD is defined as the unequal absorption of right-handed and left-handed circular polarized light. When asymmetric molecules like proteins interact with both types of polarized light, they absorb left and right-handed polarized light to different extent. It was found that often a reason for the formation of insoluble aggregates was the presents of increased numbers of β-sheets [93, 94]. Similarly, a two-phase sequential dynamic change in the secondary structure was described when lysozyme adsorbed on solid substrates [95]. The first phase involved fast conversion of α-helix to random/turns. This happened within minutes, whereas the second towards an increased beta sheet content happened between 1 to 1200 minutes. Another study found the increase in β-sheet and β-turn content due to heat and acidic pH for and human serum albumin (HSA) [96]. It is therefore reasonable that once proteins are exposed to high shear, cavitation or air/liquid interfaces, they might undergo tertiary and/or secondary structure alterations due the rearrangement of amino

acids which in turn changes the CD Spectra. Hence, CD spectroscopy is a powerful offline method to determine structural alterations of proteins. However, when proteins are exposed to thermal, pH or mechanical stress the formation of soluble aggregates is reasonable. Here, depending on the aggregation mechanism, native or minutely structurally changed proteins attach to each other forming larger structures like dimers, trimers or multimers [86]. If the protein concentration raises as intended in crossflow filtration the formation of soluble aggregates is also reasonable [97]. Although, it is important to track the formation of soluble aggregates, CD is not able to detect those minor formations if the protein structure of a single protein inside the di-, tri-, or oligomer complex has a very similar structure to the monomer. This was for example shown for HSA were a concentration of over 0.66 g L^{-1} must be exceeded to affect the CD signal [98]. Since the content of such soluble aggregates is mostly below 1% a change in the CD signal is not to be expected.

An analytical method to overcome the limitation of undetectable soluble aggregates is size exclusion chromatography (SEC). With a high performance size exclusion chromatography media (HP-SEC) it is possible to precisely and reproducible separate soluble aggregates from monomer protein [99, 100]. Molecular separation by SEC is based on the molecular weight or more precisely the hydrodynamic radius given by the quaternary structure of the protein. Hence, the combination of CD and SEC is a powerful tool to describe soluble protein aggregation and structure alterations. However, insoluble aggregates cannot be reliably measured with these techniques. Due to the sedimentation of insoluble inhomogeneous aggregates a reliable detection might be very challenging by CD. Since insoluble aggregates are in the size range of several micrometer, in HP-SEC analyisis such large molecules are filtered by the column pre-filter to avoid clogging the column.

There are several different methods to characterize insoluble aggregates in solution. For example the use of dynamic light scattering (DLS) is possible. Here the Brownian motion is measured and correlated to the size of the observed molecules. The Brownian motion of a certain particle decreases with the size of the particle. To determine the size distribution of particles in solution an autocorrelation function is used to define the size distribution of the particles. However, DLS is limited to the sedimentation of the observed particles. Particles above 10 to 50 µm (depending on the density) are big enough to sediment with a higher velocity than the particles moving by Brownian motion. Therefore, size estimation by DLS becomes difficult [101, 102]. Microscopic

methods can also be used. Here the solution containing insoluble protein aggregates is transferred to a microscope slide and the size distribution is evaluated. However, the estimation of the size is often user dependent and the chance of particle destruction during sample handling is high. Another disadvantage of DLS and generally all offline size measurement techniques is that sampling must be accurately. The solution to be sampled must be carefully mixed to get a representative sample without shredding large size aggregates. To overcome such limitations different techniques were developed to monitor the insoluble particle distribution online. Here, focused beam reflectance measurement (FBRM) should be mentioned. FBRM measures online and in-time particle size distributions of any particle from 0.5 to 1000 µm. FBRM utilizes a highly precise chord length distribution measurement. A constantly rotating focused laser emits light into the sample solution. When particles pass by the window of the probe they reflect the light. A sensor detects the length of the particles by taking the rotational speed of the laser into account. The sum of all cord lengths is collected and a distribution displayed. Hence this technique is sensitive to both particle size and concentration while the change in the distribution is reported in real time without the need for sampling or sample preparation. However, no shape of the underlying structure is assumed but the technique can be applied at any process concentration. Hence due to the stated advantages FBRM is a suited technique to monitor insoluble particle formation in bioprocesses.

2 Objectives

The working hypothesis is that shear stress cannot be seen as driving force for protein aggregation in bioprocesses. Therefore, the objective of this work was to clearly separate the influence of shear stress from the effect of cavitation and air/liquid interfaces which occur at high shear rates and might have been misattributed to shear stress in the past. Further it should be clarified if cavitation is a real harm for proteins and to identify the aggregation pathway behind. In order to meet the objectives it was necessary to develop a suited methodology, which was not available.

Cavitation in pumps or pipes always occurs together with high shear. During cavitation, gas bubbles are formed and after the collapse of these gas bubbles, hydroxyl radicals are generated. In order to be able to cut up the different effect new methods had to be developed to study high isolated shear rates, air/ respectively vapor/liquid interfaces and effects of hydroxyl radicals independently.

In order to challenge the research question/hypothesis the objectives were further divided:

- Design of a suited experimental set up to test the effect of cavitation on protein aggregation/destruction.
- The effect of cavitation should be addressed with respect to vapor/liquid interfaces by bubble growth as well as hydroxyl radical formation by bubble collapse. Hence, different methods should be developed to separately address both phenomena. To identify hydroxyl radical formation an adequate dosimeter must be developed to specifically sense those radicals.
- Separation of the effect of cavitation and shear rates.
- Since high shear rates above 10^6 s^{-1} cannot be generated under laminar flow conditions, a simple direct calculation is impossible. To address shear rates above this threshold a computational fluid dynamic simulation should be set up.
- Validation of the simulation data with experimental data
- Development of analytical methods to measure protein aggregation
- To allow generalization, test cavitation with a high number of proteins at different pI/pH combinations and concentrations.

3 Results

The research work has been published in two scientific articles

*Publication I (*Duerkop M., Berger E., Dürauer A., Jungbauer A. ,**Influence of cavitation and high shear stress on HSA aggregation behavior.** Engineering in Life Science, Volume 18, Issue 3, March 2018, Pages 169-178)

A methodology was developed which was able to generate extraordinarily high shear rates and cavitation. While the creation of such high shear rates and cavitation would be feasible using an impeller, such a method would also lead to the entrapment of air. To exclude the additional effect of air/liquid interfaces, a closed setup was considered and a micro-orifice was selected. This micro-orifice was integrated into the flow path of an ÄKTA piston pump which was required to overcome the large pressure drop. Above a flowrate of 12 mL min^{-1} threshold, cavitation occurred. The measured flowrate for the occurrence of cavitation matched the calculated flowrate expected from the dimensionless cavitation number; it was below 0.5. The effect of high shear rates and on proteins was investigated with the model protein human serum albumin (HSA).

Additionally, the effect of hydroxyl radicals generated by ultra-sonication and Fenton's reaction was additionally analyzed. The generation rate of hydroxyl radicals was monitored with a terephthalic acid dosimeter. The amount of hydroxyl radicals generated by ultra-sonication and the micro-orifice was set to the same level. If hydroxyl radicals were responsible for protein aggregation under hydrodynamic cavitation, a similar aggregation behavior of HSA would be expected. However, no indication for protein aggregation was found in the ultra-sonication experiments, which is contrary to the significant aggregation that was found when using the micro-orifice. However, the amount of radicals generated by Fenton's reaction induced protein aggregation. Therefore, hydroxyl radical formation by hydrodynamic cavitation was evaluated not to be the driving force for cavitation associated protein aggregation. Hence another mechanism beside hydroxyl radical formation must be responsible for cavitation associated HSA aggregation.

To identify whether shear stress inside the orifice or the surface generated by vapor/liquid interfaces was responsible for protein aggregation, a flow restrictor was integrated into the setup downstream of the micro-orifice to suppress cavitation. With this modified setup it was possible

to solely address the effect of shear stress. However, any direct calculation of shear rates in tubular systems is based on laminar flow conditions. Under the flow conditions inside the micro-orifice, the Reynolds number indicated a turbulent regime. Thus, a CFD simulation of the orifice was set up and validated according to the experimental pressure drop and the minimal flow rate of cavitation occurrence. With the use of several CFD based virtual plane sections it was possible to calculate average shear rates for the entire micro-orifice. Extraordinarily high shear rates were found at the wall of the tube, while the center shear strain was still far above the shear rates expected in common bioprocesses. However, the mass transport of proteins in a tubular system close to the wall is rather low due to the reduced flow rate. An averaging function was developed which normalized the shear according to the mass flow. The resulting mass flow averaged average shear rates of 10^6 s^{-1} are far above any other shear rates reported in the literature. Since cavitation was suppressed, the protein was only exposed to high shear rates.

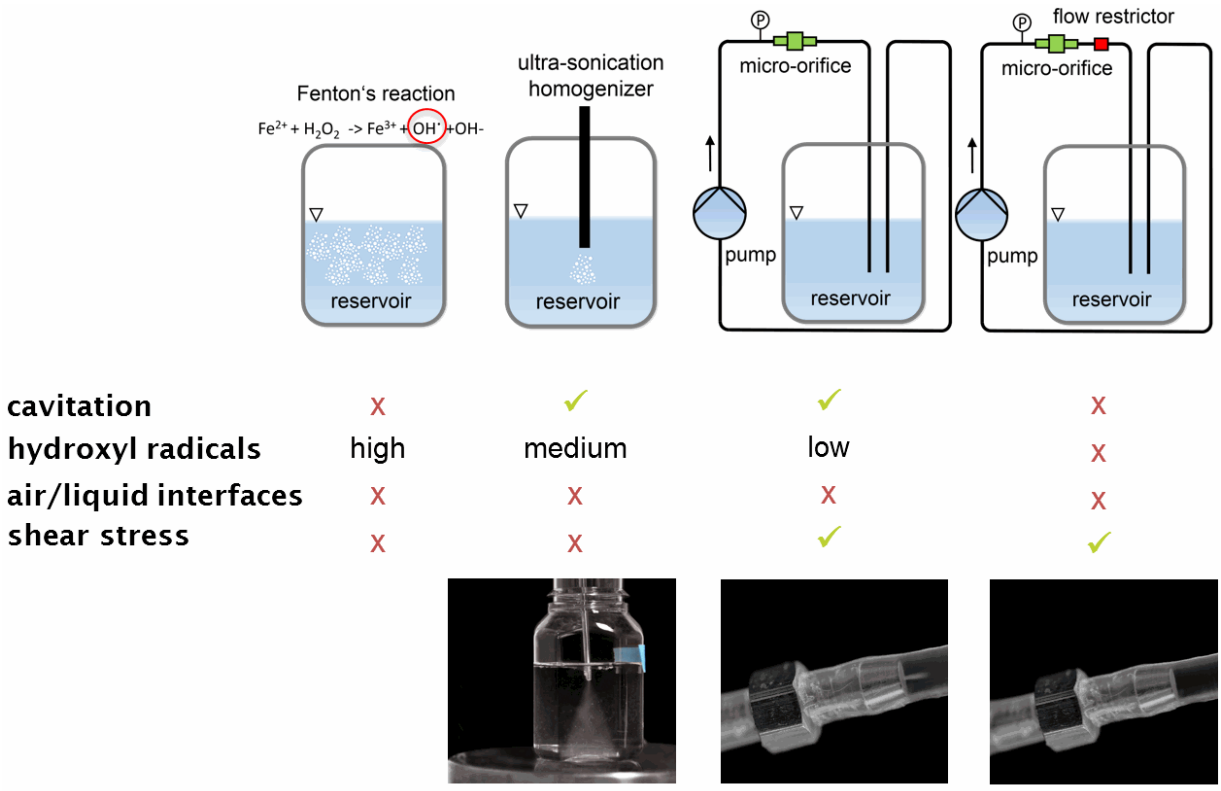

Figure 10: Four different methods used in publication I to evaluate the effect of cavitation, hydroxyl radicals and shear rates on HSA aggregation behavior. Different mechanical stresses are plotted against different stressing methods. Pictures at the bottom were taken while proteins were stressed. Cavitation can be seen in the ultra-sonication homogenizer and the micro-orifice experiment.

However, no indication for HSA aggregation under isolated shear conditions was found. Although extraordinarily high shear rates were described, no HSA aggregation occurred. Furthermore, the amount of hydroxyl radicals generated by hydrodynamic cavitation was evaluated to be too low protein aggregation. Hence the previously described aggregation can be solely attributed to the vapor/liquid interface generated by growing vapor cavities. To support the theory that vapor/liquid interfaces can be seen as the main driving force under cavitational flow further research with a larger set of proteins was suggested.

*Publication II (*Duerkop M., Berger E., Dürauer A., Jungbauer A. , **Impact of cavitation, high shear stress and air/liquid interfaces on protein aggregation.** Biotechnology Journal, 2018)

The research interest of publication II was to investigate if vapor/liquid interfaces are the driving force for protein aggregation under cavitational flow and secondly, if shear stress can generally be neglected as reason for aggregation mechanism when processing proteins. To arrive at such a general statement, it was required to test a large set of structurally different proteins. In publication I, the effect of cavitation was described solely on HSA. For this part of the project, nine different proteins were selected according to their secondary structure. Large β-structured antibodies as well as small α-helical dominated proteins were selected. One protein that consisted mostly of a random coiled structure was used to expand the range of proteins and allow generalization. To confirm that hydroxyl radicals generated by cavitation can be neglected as the source for protein aggregation the micro-orifice treatment developed for publication I was tested on this larger set of proteins. When cavitation was generated by the micro-orifice, GCSF and two additional proteins (HSA and Hemoglobin) exhibited a loss in monomeric concentration. The different behavior between ultra-sonication and micro-orifice treatment, as seen in publication I, indicated that although the hydroxyl radical formation was similar, the generated vapor/liquid interface of both methods was different. Since vapor/cavities generated by cavitation either grow under pressures conditions below the vapor pressure of the liquid or collapse under pressures above this threshold, such cavities are unstable. Hence, a precise and accurate measurement of a generated surface by cavitation is very difficult. Due to this fact, a foaming method was developed to generated air/liquid interfaces (Figure 11). This method utilized a free jet of protein solution penetrating the surface of the reservoir. Thereby generating a large amount of air/liquid interfaces leading to protein foam. With this method the effect of air/liquid interfaces could be compared to vapor/liquid interfaces from the cavitation experiment.

It was shown that the proteins being most sensitive to cavitation correlated with the aggregation rate in the foaming experiment. This indicated that vapor/liquid interfaces under cavitational flow are in fact as critical as air/liquid interfaces. Since all proteins showed aggregation towards air/liquid interfaces it we suggested that all of the tested proteins would show cavitational induced protein aggregation under prolonged conditions.

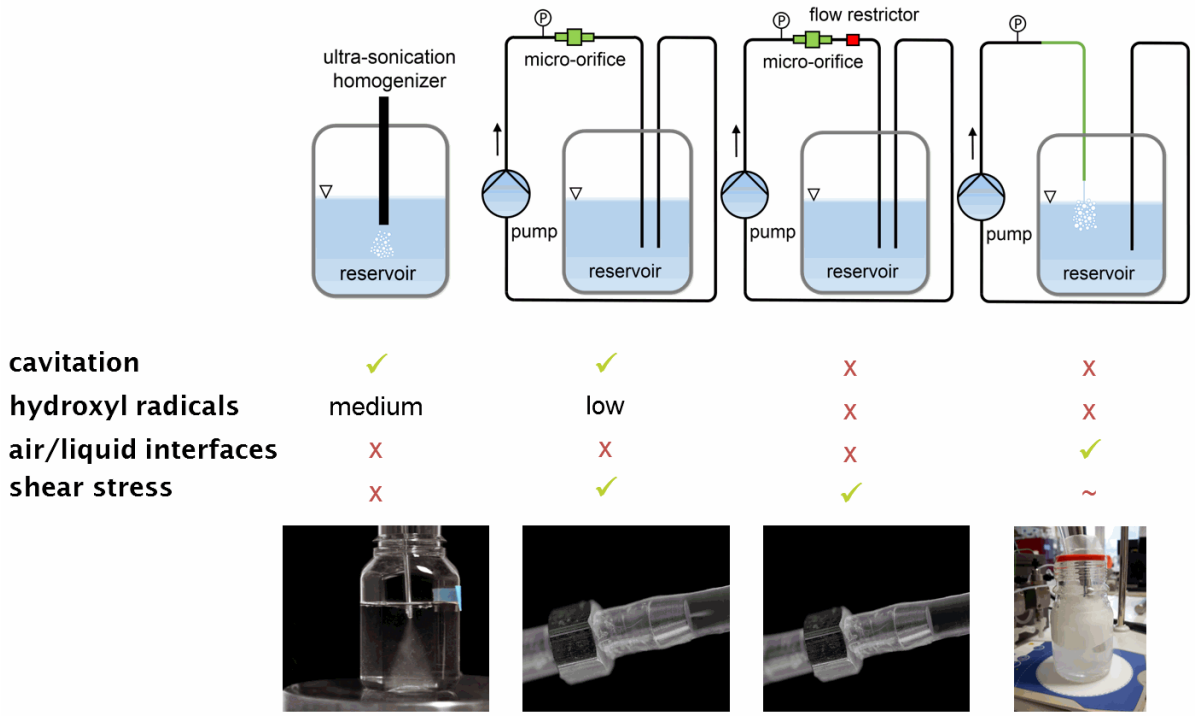

Figure 11: Four different methods used in publication II to evaluate the effect of cavitation, shear rates, air/liquid interfaces on the aggregation behavior of nine different proteins. Different mechanical stresses are plotted against different stressing methods

The aggregation mechanism of the proteins towards cavitation was also addressed with this research. CD spectroscopy revealed no structural alteration of the protein, remaining in the supernatant after cavitational treatment. The CD signal of the stressed solution did not shift indicating that the aggregation occurred instantly. To identify what happened to the protein being lost by protein stressing experiments, FBRM measurements were established. It was found that the cavitation produced insoluble aggregates in the µm scale. Together with the CD spectroscopy findings, it was suggested that protein aggregation occurred instantly upon contact to vapor/liquid interfaces.

The impact of cavitation under increased protein concentrations was also subject of this study. It was found that protein aggregation decreased with increasing protein concentration. This circumstance was explained due to the limited vapor/liquid interface provided by cavitation. At higher protein concentration these surfaces are saturated with protein very quickly. The higher the tested protein concentration, the lower the relative protein loss. This findings suggests that cavitation is most likely overlooked in bioprocesses at high protein concentrations. However, due

to the fact that protein aggregates serve as seeds for larger aggregation, addressing cavitation is crucial when designing bioprocesses.

Further the impact of pH/pI ratio was investigated with this research. The closer HSA or GCSF were to their isoelectric point while under stress, the higher the level of aggregation. This was explained due to the lower charge of the protein resulting in increased protein affinity to hydrophobic surfaces.

When stressing GCSF with the micro-orifice in the presence of surfactant, the aggregation dramatically dropped. The surface shielding effect of surfactants were identified as explanations for the reduced aggregation of GCSF. It could be concluded that surfactant reduces cavitational damage. Further, the impact of cavitational damage close to the pI of the proteins was highest. The aggregation behavior of proteins towards air/liquid interfaces was similar to cavitation. Finally, it was shown that the cavitational induced aggregation occurred instantly proofed that the vapor/liquid interfaces were responsible for aggregation and not hydroxyl radicals as often believed [67, 68]. Therefore, this research is a turning point in the literature.

Although all nine proteins were expected to show increased aggregation behavior under prolonged cavitation conditions, a scientific correlation between the different aggregation behaviors was not clearly found. It was not possible to correlate the different aggregation behavior with differential scanning calorimeter data. The protein with the highest stability in cavitation experiments (alpha-lactalbumin) showed lowest temperature stability while HSA, which aggregated under cavitational flow, showed highest stability in DSC. Additionally, the reduction of surface tension by the protein itself was addressed. GCSF reduced the surface tension of the buffer the most while showing highest aggregation tendency under cavitational flow. When surfactant was added, the aggregation behavior was reduced but the surface tension was even lower. Hence, the different surface tensions seen by different proteins was also not the reason for the different behaviors.

Cavitation was also suppressed using the method described in publication I. Although the shear rates experienced by the proteins were higher than reported elsewhere, not a single protein showed increased aggregation behavior compared to the control experiment. It could additionally be shown that high dimensionless shear cannot be seen as a critical process parameter, contrary to the scientific literature [28, 29, 103].

However, it was still unclear which level of shear rates would be required to unfold a certain protein. Hence, a simple model was derived within this work to answer at which level proteins will start to aggregate under isolated shear conditions (Figure 12).

$$\tau = \gamma\mu \; [Pa]$$
$$A = \frac{1}{2}\pi d^2 \; [m^2]$$
$$\mathrm{F} = \tau A \; [kg\, m\, s^{-2}]$$

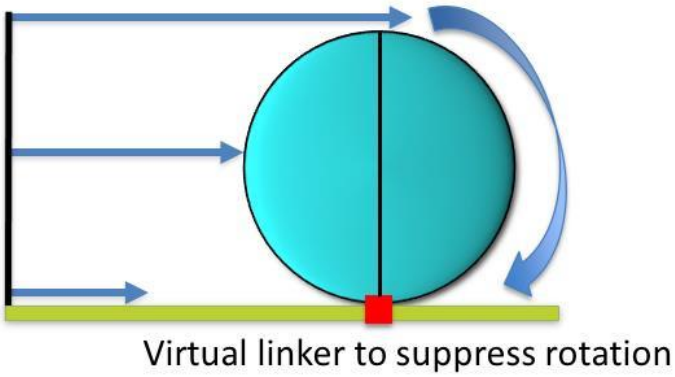

Figure 12: A protein in a shear gradient attached to the wall. The possible rotation of the protein is suppressed by the linker. Calculation of shear force (F), using the shear stress(τ) and the surface area on which the force acts (A).

A protein was virtually attached to the wall of a tube. This suppresses the rotational energy uptake of the protein. Therefore, the whole energy is used for stretching of the protein. The required shear rates to aggregate average sized proteins would be in the range of 10^9 s^{-1} which is far above any possible bioprocess operation. Further, it was calculated that the driving force for shear induced aggregation is more dependent on the size of the protein than the amount of shear. For Proteins in the size range of an antibody, one order of magnitude higher shear rates than reported by this work would at least be required. When looking at bigger structures such as plasmids or cells the shear rates achieved here could be sufficient to destroy these structures. However, with this work it was clearly proven that isolated shear rates independent of the incubation time cannot be seen as a critical process parameter for bioprocesses.

In summary, it can be stated that the objectives of the thesis were met:

- Different methods were developed to independently describe the effect of shear stress, cavitation and air/liquid interfaces.
- Within this work the effect of hydrodynamic cavitation generated by a micro-orifice on proteins was described for the very first time.
- The required concentration for hydroxyl radical associated protein aggregation was addressed within this work. A dosimeter methodology was developed to specifically measure hydroxyl radicals from solution. It was found that the generation rate of those radicals by hydrodynamic cavitation was not high enough to cause protein aggregation.
- The driving force for cavitation associated protein aggregation was found to be the increase in surface area due to vapor bubble growth. The surface and protein aggregation properties of such vapor/liquid interfaces were found to be similar to air/liquid interfaces. Hence cavitation was identified as potential risk for processing proteins. To measure those alterations HP-SEC, CD and FBRM measurements were established.
- The effect of shear stress was independently and carefully addressed with this work. A CFD Simulation of the micro-orifice was developed and validated. The simulation revealed that although the micro-orifice generated the highest ever reported shear rates, those share rates were still not high enough to lead to aggregation of even a single protein tested. Hence shear stress should not be regarded as a critical process parameter for proteins anymore.

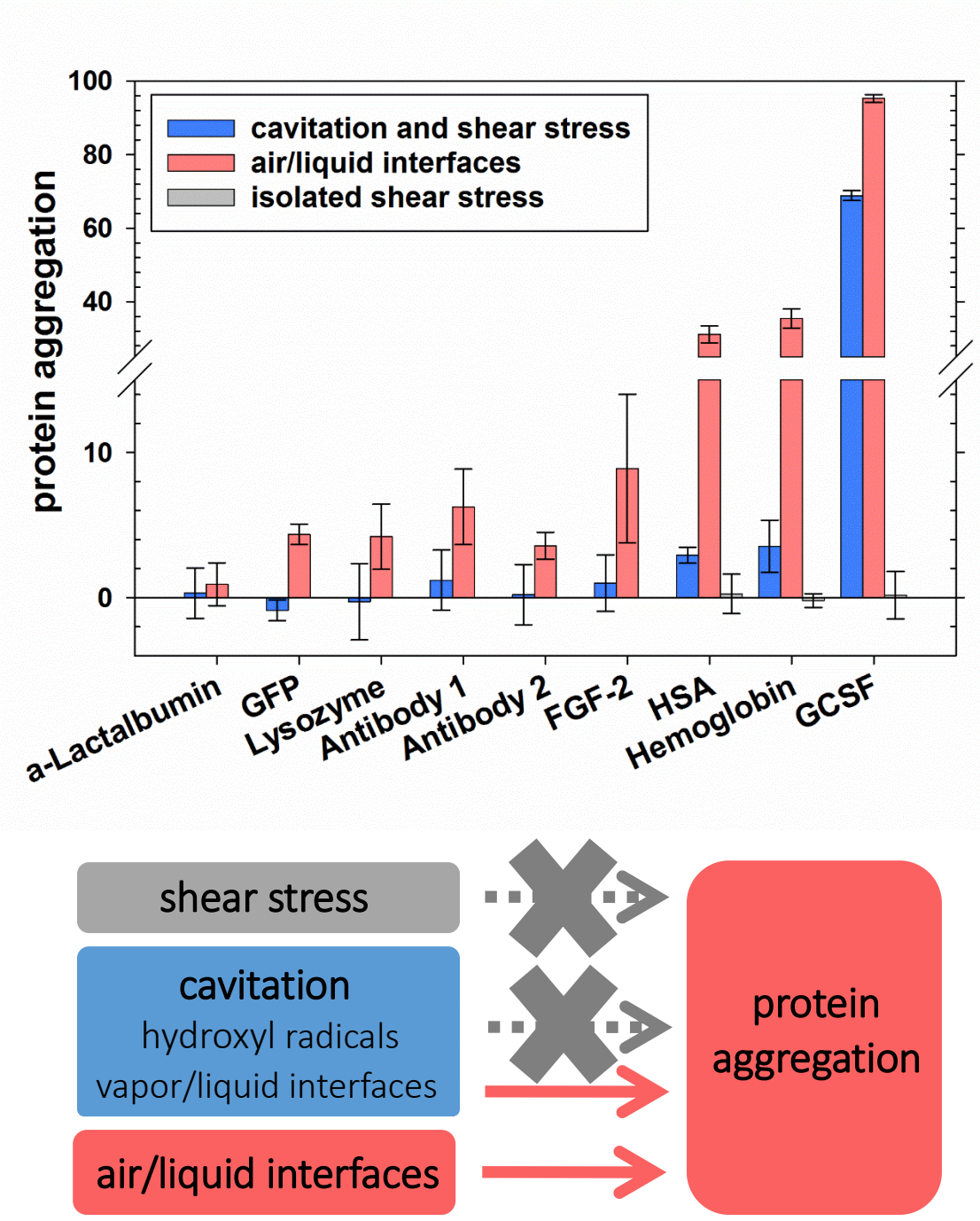

Figure 13: Graphical summary *of the thesis. Top: Different stress methods tested with each protein. Bottom: Identification of possible aggregation pathways.*

4 Outlook

With this work the myth of shear associated protein aggregation was finally busted. However, owing to the simple setup the effect of isolated shear can be analyzed to stress larger structures such as plasmid-DNA or even microbial and mammalian cells. Due to the low required volume and simple micro-orifice this method can be used in almost any lab, if an adequate pump is available. A large pharmaceutical company is currently establishing the within this work established micro-orifice treatment for stability testing of larger biological structures.

Furthermore, the effect of cavitation can be analyzed on any kind of protein or biological sample at low concentrations. Since vapor/liquid interfaces were found to be comparable to air/liquid interfaces the described cavitation method can build in to test proteins which are extremely sensitive to air/liquid interfaces like GCSF. With a stochastic, empirical, or chimeric protein mutation approach, the stability of such proteins can be increased and the new protein iteratively tested. Furthermore, the correlation between cavitation associated protein aggregation and protein structural properties causing this behavior should be solved.

5 List of Publications

I Duerkop M., Berger E., Dürauer A., Jungbauer A. ,**Influence of cavitation and high shear stress on HSA aggregation behavior.** Engineering in Life Science, Volume 18, Issue 3, March 2018, Pages 169-178

II Duerkop M., Berger E., Dürauer A., Jungbauer A., **Impact of cavitation, high shear stress and air/liquid interfaces on protein aggregation.** Biotechnology Journal, 2018

Contribution to the publications:

In publication I, Mark Duerkop developed the methodology to differentiate between the effects of cavitation and shear, designed and validated a CFD simulation, developed the dosimeter for hydroxyl radical measurement and wrote the manuscript.

In publication II, Mark Duerkop developed the methodology to compare vapor/liquid interfaces generated by cavitation with air/liquid interfaces. He developed both a CD structure determination and insoluble particle measurement protocol. Further he tested a large set of proteins on all the previously described methods. Finally Mark Duerkop wrote the manuscript.

6 Abbreviations

CCP	critical control parameter
CD	circular dichroism
CFD	computational fluid dynamic
Da	Dalton (g/mol)
DLS	dynamic light scattering
DMSO	dimethyl sulfoxide
FBRM	focused beam reflectance measurement
HP-SEC	high performance size exclusion chromatography
HSA	human serum albumin
hTPA	hydroxyl Terephthalic acid
SEC	size exclusion chromatography
TPA	Terephthalic acid

7 Symbols

ρ	density [kg m^{-3}]
t	incubation time [s]
p	local pressure [Pa]
$\boldsymbol{\gamma}$	shear rate [s^{-1}]
R	gas constant [8.314 kg m^2 s^{-2} K^{-1} mol^{-1}]
V	velocity [m s^{-1}]
μ	viscosity [Pa s]

8 List of figures

Figure 1: Top selling drugs of 2015 and 2016 in billion US Dollar. Recombinant obtained drugs are opaque while chemically produced compounds are transparently colored [3]. 2
Figure 2: Schematic description of a possible bioprocess which includes the production of the biopharmaceutical with a host inside a bioreactor and the followed separation and purification [15]. 3
Figure 3: Schematic diagram of a mechanical unfolding experiment and the force-extension profile for different unfolding states. Protein binding (1), linearization of the protein (2), unfolding of a single domain (3), unfolding of all domains (4). With the force (F) and the elongation distance (D) given for each step in the insert [25]. 7
Figure 4: Schematic drawing of a tube with a laminar flow profile. Shear rates can be calculated for each velocity layer. An antibody is schematically drawn into the shear field (purple). 9
Figure 5: Flow profiles in a tube: laminar flow (blue), transition (orange), turbulent flow (red) .10
Figure 6: Schematic description of an CFD simulation for the description of velocity inside a tube. A cubic mesh was chosen to describe the velocity profile. 12
Figure 7: Schematic drawing of the occurrence of cavitation generated by an orifice inside a tube. A steep increase in velocity leads to a decrease in local pressure below the vapor pressure. 14
Figure 8: Expected effect of cavitation on proteins.....14
Figure 9: Reaction of terephthalic acid with hydroxyl radicals to form hydroxyl terephthalic acid. 16
Figure 10: Four different methods used in publication I to evaluate the effect of cavitation, hydroxyl radicals and shear rates on HSA aggregation behavior. Different mechanical stresses are plotted against different stressing methods. Pictures at the bottom were taken while proteins were stressed. Cavitation can be seen in the ultra-sonication homogenizer and the micro-orifice experiment. 23
Figure 11: Four different methods used in publication II to evaluate the effect of cavitation, shear rates, air/liquid interfaces on the aggregation behavior of nine different proteins. Different mechanical stresses are plotted against different stressing methods 26
Figure 12: A protein in a shear gradient attached to the wall. The possible rotation of the protein is suppressed by the linker. Calculation of shear force (F), using the shear stress(τ) and the surface area on which the force acts (A). 28

Figure 13: Graphical summary *of the thesis. Identification of possible aggregation pathways.* 30

9 References

1. Sanchez-Garcia, L., et al., *Recombinant pharmaceuticals from microbial cells: A 2015 update.* Microbial Cell Factories, 2016. **15**(1).
2. Overton, T.W., *Recombinant protein production in bacterial hosts.* Drug Discovery Today, 2014. **19**(5): p. 590-601.
3. Philippidis, A. *The Top 15 Best-Selling Drugs of 2016* 2017 [cited 2017; Available from: http://www.genengnews.com/the-lists/the-top-15-best-selling-drugs-of-2016/77900868.
4. Aggarwal, S.R., *What's fueling the biotech engine-2012 to 2013.* Nature Biotechnology, 2014. **32**(1): p. 32-39.
5. Bunnage, M.E., *Getting pharmaceutical R&D back on target.* Nature Chemical Biology, 2011. **7**(6): p. 335-339.
6. Dimasi, J.A. and H.G. Grabowski, *The cost of biopharmaceutical R&D: Is biotech different?* Managerial and Decision Economics, 2007. **28**(4-5): p. 469-479.
7. Walsh, G., *Biopharmaceutical benchmarks 2014.* Nature Biotechnology, 2014. **32**(10): p. 992-1000.
8. Belsey, M.J., et al., *Biosimilars: Initial excitement gives way to reality.* Nature Reviews Drug Discovery, 2006. **5**(7): p. 535-536.
9. Burki, T.K., *First biosimilar drug approved in the USA.* The Lancet. Oncology, 2015. **16**(4): p. e161.
10. Norman, P., *Humira: the impending patent battles over adalimumab biosimilars.* Pharmaceutical patent analyst, 2016. **5**(3): p. 141-145.
11. Rathore, A.S. and H. Winkle, *Quality by design for biopharmaceuticals.* Nature Biotechnology, 2009. **27**(1): p. 26-34.
12. WHO, *Guidelines on the quality, safety, and efficacy of biotherapeutic protein products prepared by recombinant DNA technology*, 2013, WHO Press, World Health Organization, 20 Avenue Appia, 1211 Geneva 27, Switzerland. p. 91.
13. Azevedo, A.M., et al., *Chromatography-free recovery of biopharmaceuticals through aqueous two-phase processing.* Trends in Biotechnology, 2009. **27**(4): p. 240-247.
14. Rathore, A.S. and G. Kapoor, *Application of process analytical technology for downstream purification of biotherapeutics.* Journal of Chemical Technology and Biotechnology, 2015. **90**(2): p. 228-236.
15. Jozala, A.F., et al., *Biopharmaceuticals from microorganisms: from production to purification.* Brazilian Journal of Microbiology, 2016. **47**: p. 51-63.
16. Chou, K.C. and Y.D. Cai, *Predicting protein quaternary structure by pseudo amino acid composition.* Proteins: Structure, Function and Genetics, 2003. **53**(2): p. 282-289.
17. Rathore, N. and R.S. Rajan, *Current perspectives on stability of protein drug products during formulation, fill and finish operations.* Biotechnology Progress, 2008. **24**(3): p. 504-514.
18. Lins, L. and R. Brasseur, *The hydrophobic effect in protein folding.* FASEB Journal, 1995. **9**(7): p. 535-540.
19. Rosenberg, A.S., D. Verthelyi, and B.W. Cherney, *Managing uncertainty: A perspective on risk pertaining to product quality attributes as they bear on immunogenicity of therapeutic proteins.* Journal of Pharmaceutical Sciences, 2012. **101**(10): p. 3560-3567.
20. Ibarra-Molero, B., et al., *Thermal versus guanidine-induced unfolding of ubiquitin. An analysis in terms of the contributions from charge-charge interactions to protein stability.* Biochemistry, 1999. **38**(25): p. 8138-8149.

21. Luisi, D.L. and D.P. Raleigh, *pH-dependent interactions and the stability and folding kinetics of the N-terminal domain of L9. Electrostatic interactions are only weakly formed in the transition state for folding.* Journal of Molecular Biology, 2000. **299**(4): p. 1091-1100.
22. Li, H., et al., *Atomic force microscopy reveals the mechanical design of a modular protein.* Proceedings of the National Academy of Sciences of the United States of America, 2000. **97**(12): p. 6527-6531.
23. Forman, J.R., et al., *The remarkable mechanical strength of polycystin-1 supports a direct role in mechanotransduction.* Journal of Molecular Biology, 2005. **349**(4): p. 861-871.
24. Ng, S.P., et al., *Designing an extracellular matrix protein with enhanced mechanical stability.* Proceedings of the National Academy of Sciences of the United States of America, 2007. **104**(23): p. 9633-9637.
25. Brockwell, D.J., *Probing the mechanical stability of proteins using the atomic force microscope.* Biochemical Society Transactions, 2007. **35**(6): p. 1564-1568.
26. Hann, E., et al., *The effect of protein complexation on the mechanical stability of Im9.* Biophysical Journal, 2007. **92**(9): p. L79-L81.
27. Best, R.B., et al., *Force mode atomic force microscopy as a tool for protein folding studies.* Analytica Chimica Acta, 2003. **479**(1): p. 87-105.
28. Charm, S.E. and B.L. Wong, *Shear effects on enzymes.* Enzyme and Microbial Technology, 1981. **3**(2): p. 111-118.
29. Charm, S.E. and C.J. Lai, *Comparison of ultrafiltration systems for concentration of biologicals.* Biotechnology and Bioengineering, 1971. **13**(2): p. 185-202.
30. Tirrell, M. and S. Middleman, *Shear modification of enzyme kinetics.* Biotechnology and Bioengineering, 1975. **17**(2): p. 299-303.
31. Thomas, C.R., A.W. Nienow, and P. Dunnill, *Action of shear on enzymes: Studies with alcohol dehydrogenase.* Biotechnology and Bioengineering, 1979. **21**(12): p. 2263-2278.
32. Thomas, C.R. and P. Dunnill, *Action of shear on enzymes: Studies with catalase and urease.* Biotechnology and Bioengineering, 1979. **21**(12): p. 2279-2302.
33. Virkar, P.D., et al., *Studies of the effect of shear on globular proteins: Extension to high shear fields and to pumps.* Biotechnology and Bioengineering, 1981. **23**(2): p. 425-429.
34. Jaspe, J. and S.J. Hagen, *Do protein molecules unfold in a simple shear flow?* Biophysical Journal, 2006. **91**(9): p. 3415-3424.
35. Bee, J.S., et al., *Response of a concentrated monoclonal antibody formulation to high shear.* Biotechnology and Bioengineering, 2009. **103**(5): p. 936-943.
36. Gooch, J.W., *Hagen-Poiseuille Equation*, in *Encyclopedic Dictionary of Polymers*, J.W. Gooch, Editor. 2011, Springer New York: New York, NY. p. 355-355.
37. Ng, S.P., et al., *Mechanical Unfolding of TNfn3: The Unfolding Pathway of a fnIII Domain Probed by Protein Engineering, AFM and MD Simulation.* Journal of Molecular Biology, 2005. **350**(4): p. 776-789.
38. Puchner, E.M. and H.E. Gaub, *Force and function: probing proteins with AFM-based force spectroscopy.* Current Opinion in Structural Biology, 2009. **19**(5): p. 605-614.
39. Horejs, C., et al., *Single-molecule force spectroscopy reveals the individual mechanical unfolding pathways of a surface layer protein.* Journal of Biological Chemistry, 2011. **286**(31): p. 27416-27424.
40. Wilkes, J.O., *Fluid Mechanics for Chemical Engineers with Microfluidics and CFD*. 2006: Pearson Education.
41. Fromm, J.E. and F.H. Harlow, *Numerical solution of the problem of vortex street development.* Physics of Fluids, 1963. **6**(7): p. 975-982.
42. Harlow, F.H. and J.E. Welch, *Numerical calculation of time-dependent viscous incompressible flow of fluid with free surface.* Physics of Fluids, 1965. **8**(12): p. 2182-2189.
43. Harlow, F.H., J.P. Shannon, and J. Eddie Welch, *Liquid waves by computer.* Science, 1965. **149**(3688): p. 1092-1093.

44. Harlow, F.H. and J.P. Shannon, *Distortion of a splashing liquid drop.* Science, 1967. **157**(3788): p. 547-550.
45. Coleman, H.W. and F. Stem, *Uncertainties and CFD code validation.* Journal of Fluids Engineering, Transactions of the ASME, 1997. **119**(4): p. 795-803.
46. Stern, F., et al., *Comprehensive approach to verification and validation of CFD simulations—Part 1: Methodology and procedures.* Journal of Fluids Engineering, Transactions of the ASME, 2001. **123**(4): p. 793-802.
47. Hanjalić, K. and B.E. Launder, *A Reynolds stress model of turbulence and its application to thin shear flows.* Journal of Fluid Mechanics, 1972. **52**(4): p. 609-638.
48. Wassel, A.T. and I. Catton, *Calculation of turbulent boundary layers over flat plates with different phenomenological theories of turbulence and variable turbulent Prandtl number.* International Journal of Heat and Mass Transfer, 1973. **16**(8): p. 1547-1563.
49. Patankar, S.V., V.S. Pratap, and D.B. Spalding, *Prediction of turbulent flow in curved pipes.* Journal of Fluid Mechanics, 1975. **67**(3): p. 583-595.
50. Hawkes, E.R. and R.S. Cant, *Implications of a flame surface density approach to large eddy simulation of premixed turbulent combustion.* Combustion and Flame, 2001. **126**(3): p. 1617-1629.
51. Menter, F.R., M. Kuntz, and R. Bender. *A scale-adaptive simulation model for turbulent flow predictions*. in *41st Aerospace Sciences Meeting and Exhibit*. 2003.
52. Menter, F.R., *Review of the shear-stress transport turbulence model experience from an industrial perspective.* International Journal of Computational Fluid Dynamics, 2009. **23**(4): p. 305-316.
53. Deglon, D.A. and C.J. Meyer, *CFD modelling of stirred tanks: Numerical considerations.* Minerals Engineering, 2006. **19**(10): p. 1059-1068.
54. Lamb, W.S., *Cavitation and Aeration in Hydraulic Systems*. 1987: BHRA.
55. Suslick, K.S., *Sonochemistry.* Science, 1990. **247**(4949): p. 1439-1445.
56. Riesz, P. and T. Kondo, *Free radical formation induced by ultrasound and its biological implications.* Free Radical Biology and Medicine, 1992. **13**(3): p. 247-270.
57. Tomita, Y. and A. Shima, *Mechanisms of impulsive pressure generation and damage pit formation by bubble collapse.* Journal of Fluid Mechanics, 1986. **169**: p. 535-564.
58. Blake, J.R. and D.C. Gibson, *Cavitation Bubbles Near Boundaries*. Annual Review of Fluid Mechanics. Vol. 19. 1987. 99-123.
59. Franc, J.P. and J.M. Michel, *Fundamentals of Cavitation*. 2006: Springer Netherlands.
60. Stadtman, E.R., *Oxidation of free amino acids and amino acid residues in proteins by radiolysis and by metal-catalyzed reactions.* Annual Review of Biochemistry, 1993. **62**: p. 797-821.
61. Xu, G., K. Takamoto, and M.R. Chance, *Radiolytic Modification of Basic Amino Acid Residues in Peptides: Probes for Examining Protein-Protein Interactions.* Analytical chemistry, 2003. **75**(24): p. 6995-7007.
62. Rasheed, Z., M.W.A. Khan, and R. Ali, *Hydroxyl radical modification of human serum albumin generated cross reactive antibodies.* Autoimmunity, 2006. **39**(6): p. 479-488.
63. Takamoto, K. and M.R. Chance, *Radiolytic protein footprinting with mass spectrometry to probe the structure of macromolecular complexes*, in *Annual Review of Biophysics and Biomolecular Structure*2006. p. 251-276.
64. Wang, L. and M.R. Chance, *Structural mass spectrometry of proteins using hydroxyl radical based protein footprinting.* Analytical chemistry, 2011. **83**(19): p. 7234-7241.
65. Fenton, H.J.H., *LXXIII. - Oxidation of tartaric acid in presence of iron.* Journal of the Chemical Society, Transactions, 1894. **65**: p. 899-910.
66. Neyens, E. and J. Baeyens, *A review of classic Fenton's peroxidation as an advanced oxidation technique.* Journal of Hazardous Materials, 2003. **98**(1-3): p. 33-50.
67. Randolph, T.W., et al., *Do not drop: Mechanical shock in vials causes cavitation, protein aggregation, and particle formation.* Journal of Pharmaceutical Sciences, 2015. **104**(2): p. 602-611.

68. Torisu, T., et al., *Synergistic Effect of Cavitation and Agitation on Protein Aggregation.* Journal of Pharmaceutical Sciences, 2017. **106**(2): p. 521-529.
69. Weissler, A., H.W. Cooper, and S. Snyder, *Chemical effect of ultrasonic waves: Oxidation of potassium iodide solution by carbon tetrachloride.* Journal of the American Chemical Society, 1950. **72**(4): p. 1769-1775.
70. Lentz, Y.K., T.J. Anchordoquy, and C.S. Lengsfeld, *DNA acts as a nucleation site for transient cavitation in the ultrasonic nebulizer.* Journal of Pharmaceutical Sciences, 2006. **95**(3): p. 607-619.
71. Mimura, T., et al., *Hydroxyl radical scavenging effects of guaiacol used in traditional dental pulp sedation: Reaction kinetic study.* Biomedical Research, 2005. **26**(4): p. 139-145.
72. Purich, D., *The Inhibitor Index: A Desk Reference on Enzyme Inhibitors, Receptor Antagonists, Drugs, Toxins, Poisons, Biologics, and Therapeutic Leads*. 2017: CRC Press.
73. Singh, A., et al., *Involvement of singlet oxygen in biochemical systems.* Clinical Respiratory Physiology, 1981. **17**(Suppl.): p. 31-41.
74. Hyland, K. and C. Auclair, *The formation of superoxide radical anions by a reaction between O2, OH- and dimethyl sulfoxide.* Biochemical and Biophysical Research Communications, 1981. **102**(1): p. 531-537.
75. Santone, K.S., D.M. Kroschel, and G. Powis, *Enhanced formation of ethane and n-pentane by rat hepatocytes in the presence of dimethyl sulfoxide.* Biochemical Pharmacology, 1986. **35**(8): p. 1287-1292.
76. Floyd, R.A., C.A. Lewis, and P.K. Wong, *[27] High-Pressure Liquid Chromatography-Electrochemical Detection of Oxygen Free Radicals*, in *Methods in Enzymology*1984. p. 231-237.
77. Cleland, L.G., et al., *Plasma and synovial fluid gentisate in patients receiving salicylate therapy.* Journal of Rheumatology, 1985. **12**(1): p. 136-139.
78. Linxiang, L., et al., *An HPLC assay of hydroxyl radicals by the hydroxylation reaction of terephthalic acid.* Biomedical Chromatography, 2004. **18**(7): p. 470-474.
79. Mason, T.J., et al., *Dosimetry in sonochemistry: the use of aqueous terephthalate ion as a fluorescence monitor.* Ultrasonics - Sonochemistry, 1994. **1**(2): p. S91-S95.
80. Barreto, J.C., et al., *Terephthalic acid: A dosimeter for the detection of hydroxyl radicals in vitro.* Life Sciences, 1994. **56**(4): p. PL89-PL96.
81. Ishibashi, K.I., et al., *Detection of active oxidative species in TiO2 photocatalysis using the fluorescence technique.* Electrochemistry Communications, 2000. **2**(3): p. 207-210.
82. Barati, A.H., et al., *Free hydroxyl radical dosimetry by using 1 MHz low level ultrasound waves.* Iranian Journal of Radiation Research, 2006. **3**(4): p. 163-169.
83. Wang, W., S. Nema, and D. Teagarden, *Protein aggregation-Pathways and influencing factors.* International Journal of Pharmaceutics, 2010. **390**(2): p. 89-99.
84. Adam, N.K., *The physics and chemistry of surfaces*. 1952: Oxford University Press.
85. Cheesman, D.F. and J.T. Davies, *Physicochemical and Biological Aspects of Proteins at Interfaces*, in *Advances in Protein Chemistry*1954. p. 439-501.
86. Philo, J.S. and T. Arakawa, *Mechanisms of protein aggregation.* Current Pharmaceutical Biotechnology, 2009. **10**(4): p. 348-351.
87. Walsh, G. and B. Murphy, *Biopharmaceuticals, an Industrial Perspective*. 2013: Springer Netherlands.
88. Wang, W., Y.J. Wang, and D.Q. Wang, *Dual effects of Tween 80 on protein stability.* International Journal of Pharmaceutics, 2008. **347**(1-2): p. 31-38.
89. Mahler, H.C., et al., *Protein aggregation: Pathways, induction factors and analysis.* Journal of Pharmaceutical Sciences, 2009. **98**(9): p. 2909-2934.
90. Donaldson, T.L., E.F. Boonstra, and J.M. Hammond, *Kinetics of protein denaturation at gas-liquid interfaces.* Journal of Colloid And Interface Science, 1980. **74**(2): p. 441-450.
91. Narendranathan, T.J. and P. Dunnill, *The effect of shear on globular proteins during ultrafiltration: Studies of alcohol dehydrogenase.* Biotechnology and Bioengineering, 1982. **24**(9): p. 2103-2107.

92. Iwai, Y. and S. Li, *Cavitation erosion in waters having different surface tensions.* Wear, 2003. **254**(1-2): p. 1-9.
93. Sunde, M. and C.C.F. Blake, *From the globular to the fibrous state: Protein structure and structural conversion in amyloid formation.* Quarterly Reviews of Biophysics, 1998. **31**(1): p. 1-39.
94. Kelly, J.W., *The alternative conformations of amyloidogenic proteins and their multi-step assembly pathways.* Current Opinion in Structural Biology, 1998. **8**(1): p. 101-106.
95. Sethuraman, A., et al., *Protein unfolding at interfaces: Slow dynamics of α-helix to β-sheet transition.* Proteins: Structure, Function and Genetics, 2004. **56**(4): p. 669-678.
96. Thakur, R., et al., *Interaction of different prototropic species of an anticancer drug ellipticine with HSA and IgG proteins: multispectroscopic and molecular modeling studies.* Physical Chemistry Chemical Physics, 2015. **17**(26): p. 16937-16946.
97. Rosenberg, E., et al., *Ultrafiltration concentration of monoclonal antibody solutions: Development of an optimized method minimizing aggregation.* Journal of Membrane Science, 2009. **342**(1-2): p. 50-59.
98. Bhattacharya, A., et al., *Concentration-dependent reversible self-oligomerization of serum albumins through intermolecular β-sheet formation.* Langmuir, 2014. **30**(49): p. 14894-14904.
99. Chou, D.K., et al., *Effects of Tween 20® and Tween 80® on the stability of Albutropin during agitation.* Journal of Pharmaceutical Sciences, 2005. **94**(6): p. 1368-1381.
100. Arosio, P., et al., *Aggregation stability of a monoclonal antibody during downstream processing.* Pharmaceutical Research, 2011. **28**(8): p. 1884-1894.
101. Wang, W. and C.J. Roberts, *Aggregation of Therapeutic Proteins*. 2010: Wiley.
102. Van de Voorde, M., M. Werner, and H.J.Ã. Fecht, *The Nano-Micro Interface: Bridging the Micro and Nano Worlds*. 2015: Wiley.
103. Charm, S.E. and B.L. Wong, *Enzyme inactivation with shearing.* Biotechnology and Bioengineering, 1970. **12**(6): p. 1103-1109.

10 Publications

Engineering in Life Sciences

Eng. Life Sci. **2017**, *00*, 1–10 www.els-journal.com

Mark Duerkop[1]
Eva Berger[1]
Astrid Dürauer[1,2]
Alois Jungbauer[1,2]

[1]Austrian Centre of Industrial Biotechnology, Continuous Integrated Manufacturing, Vienna, Austria

[2]University of Natural Resources and Life Sciences, Department of Biotechnology, Vienna, Austria

Research Article

Influence of cavitation and high shear stress on HSA aggregation behavior

Neither the influence of high shear rates nor the impact of cavitation on protein aggregation is fully understood. The effect of cavitation bubble collapse-derived hydroxyl radicals on the aggregation behavior of human serum albumin (HSA) was investigated. Radicals were generated by pumping through a micro-orifice, ultra-sonication, or chemically by Fenton's reaction. The amount of radicals produced by the two mechanical methods (0.12 and 11.25 nmol/(L min)) was not enough to change the protein integrity. In contrast, Fenton's reaction resulted in 382 nmol/(L min) of radicals, inducing protein aggregation. However, the micro-orifice promoted the formation of soluble dimeric HSA aggregates. A validated computational fluid dynamic model of the orifice revealed a maximum and average shear rate on the order of 10^8 s^{-1} and 1.2×10^6 s^{-1}, respectively. Although these values are among the highest ever reported in the literature, dimer formation did not occur when we used the same flow rate but suppressed cavitation. Therefore, aggregation is most likely caused by the increased surface area due to cavitation-mediated bubble growth, not by hydroxyl radical release or shear stress as often reported.

Keywords: Downstream processing / Protein aggregation / Protein denaturation / Protein purification / Unfolding

Additional supporting information may be found in the online version of this article at the publisher's web-site

Received: April 11, 2017; *revised:* October 4, 2017; *accepted:* November 2, 2017

DOI: 10.1002/elsc.201700079

1 Introduction

Irreversible mechanical stretching of proteins due to shear stress and the resulting aggregation behavior is unclear in the literature. From the early stages of bioprocess engineering until now, mechanical stress has been thought to be a real harm in processing proteins [1–4]. However, more recent studies [5, 6] have not supported these assumptions, and some studies have attributed protein aggregation during processing to conformational changes in the protein at the air-liquid interface rather than to shear stress [7, 8]. It has been hypothesized that, at really high shear rates, the effect of cavitation may be overlooked and the possible effect misattributed to shear stress [9, 10]. In bioprocesses, protein solutions are often pumped through narrow orifices (e.g., high pressure homogenizers, valves, or gear pumps). As a result of the velocity increase in these gaps, the local pressure decreases as described by the Bernoulli equation Eq. (1), where v is velocity, p the hydrostatic pressure, and ρ the density of the liquid.

$$p + \frac{\rho}{2} v^2 = const. \quad (1)$$

Cavitation occurs when the local static pressure falls below the vapor pressure of the liquid, resulting in the liquid boiling at ambient temperatures. When the pressure increases downstream of the orifice, these vapor cavities are unstable and collapse under high pressure and temperature [11], resulting in the formation of hydroxyl radicals [12]. The destructive nature of these radicals generated by X-ray radiolysis of water or Fenton's reaction on certain amino acid side chains was reported previously [13–16]. The Fenton reaction is induced when ferrous iron (Fe(II)) is present together with hydrogen peroxide at low pH [17]. When studying the influence of hydroxyl radicals on proteins, Fenton's reaction can be used as a positive control due to the high radical generation rate.

An alternative source of hydroxyl radicals is ultra-sonication [12]. In this method, ultrasound waves are transmitted through the medium, compressing and stretching the molecular spacing

Correspondence: Professor Alois Jungbauer (alois.jungbauer@boku.ac.at), University of Natural Resources and Life Sciences, Department of Biotechnology, Muthgasse 18, 1190, Vienna, Austria

Abbreviations: CFD, Computational fluid dynamics; **HSA**, Human serum albumin; **hTPA**, Hydroxyterephthalic acid; **SEC**, Size exclusion chromatography; **TPA**, Terephthalic acid; **VOF**, Volume of fluid

of the medium. Thus, the average distance between the molecules varies as they oscillate about their mean position. When the distance between water molecules is extremely large, the local pressure undercuts the vapor pressure of the liquid and cavitation occurs [18]. Hydroxyl radicals occurring from ultra-sonication were already associated with DNA degradation [19].

Cavitation can be detected and quantified in biopharmaceutical processes by the well-established terephthalic acid (TPA) dosimeter [20, 21]. Generated hydroxyl radicals react with TPA, forming hydroxyl terephthalic acid (hTPA), a stable fluorescence-active, heat-resistant [22] chemical. We applied this technique to compare cavitation intensity between an ultrasonic homogenizer, a micro-orifice, and Fenton's reaction.

In fluid dynamics, the dimensionless cavitation number (Ca) is used to predict cavitation Eq. (2). The equation relates the local static pressure in a liquid (p) to the vapor pressure of the liquid (p_v), the density (ρ), and the flow velocity (v). Below 0.2 cavitation can be expected [23].

$$Ca = \frac{2\,(p - p_v)}{\rho * v^2} \tag{2}$$

According to this engineering correlation, a micro-orifice and flow conditions were selected to achieve velocities high enough to generate cavitation [24]. We also wanted to describe the shear rate inside the micro-orifice. For laminar flow, the maximum shear rate near the wall can be calculated using a stress approximation Eq. (3) [25], where Q is the volumetric flowrate, r is the radius of the tube, and y is the shear rate.

$$\gamma = \frac{4Q}{\pi r^3} \tag{3}$$

However, this equation is only valid when calculating maximum wall shear stress in laminar flow with a single velocity component parallel to the wall. Reynolds equation Eq. (4) is used to evaluate whether laminar flow is present, where ρ is the density of the liquid, v the linear flow velocity, d the diameter of the tube, and μ the dynamic viscosity.

$$Re = \frac{\rho v d}{\mu} \tag{4}$$

We show that laminar flow conditions were not present for our desired flow rates. Thus, a validated computational fluid dynamics (CFD) simulation was set up to reliably calculate an average shear rate for the whole micro-orifice cross-section.

The aim of the present study was to evaluate whether hydroxyl radicals generated by cavitation resulting from a micro-orifice are a possible source of protein aggregation. The radical generation rate was compared to that of ultra-sonication and Fenton's reaction. In addition, the influence of extremely high shear rates with and without cavitation on HSA aggregation behavior was studied.

2 Materials and methods

2.1 Protein standard

We selected HSA as the model protein due to its ability to form soluble aggregates in buffered solutions. It was purchased as highly pure lyophilized powder (A3782, Sigma-Aldrich, St. Louis, MO, USA). We prepared 0.25 mg/mL HSA in 10 mM sodium phosphate and 5 mM sodium chloride (pH 6.5) as standards. Standards were 0.2 μm filtrated and degassed with sterile rapid flow units (566-0020, Thermo Fisher Waltham, MA, USA). Every experiment was carried out in triplicate.

2.2 Size exclusion chromatography

The soluble aggregate content and concentrations of HSA samples were analyzed by high performance size exclusion chromatography. The runs were performed on an Agilent 1290 LC system (Santa Clara, CA, USA). We used a TSKgel G3000SWXL column (5 μm, 7.8 mm id x 300 mm + 6 mm id x 40 mm guard) from Tosoh (Shiba, Minato-Ku, Tokyo, Japan). Phosphate running buffer (13 g/L KH_2PO_4, 9.4 g/L K_2HPO_4, 14.61 g/L sodium chloride pH 6.5) was used at a flow rate of 0.4 mL/min. Protein samples were filtered using a 0.2 μm filter and 20 μl directly injected without any dilution.

2.3 Terephthalic acid dosimeter

TPA was purchased from Sigma-Aldrich (185361) and used as a 30 mM stock solution in 0.2 M NaOH adjusted to pH 6.5 or 9 with phosphoric acid. To establish the relationship between fluorescence signal and hydroxyl radicals, hTPA was purchased from Sigma-Aldrich (752525) and three independent dilution series prepared. For each dilution, 10 mg of hTPA was dissolved in 100 g of 0.2 M NaOH previously adjusted to pH 6.5 using phosphoric acid. The resulting 549 μM hTPA solution was diluted 1:10 twice, followed by dilution 1:3 six times. Finally, the fluorescence signal was measured for the last five dilutions.

2.4 Fluorescence measurements

To evaluate different cavitation intensities with the TPA dosimeter, we used an Infinite® 200 PRO fluorescence detector (TECAN, Maennedorf, Zuerich, Switzerland). Triplicate 150 μL aliquots of each sample were measured in a Nunclon Delta Black 96 Microwell plate (137101, ThermoFisher) at excitation and emission wavelengths of 315 and 425 nm, respectively. The electrical gain was adjusted to 150 to easily compare results between different plates.

2.5 Fenton's reaction

For Fenton's reaction, we mixed 1 mL of 0.12 M TPA in 0.25 M NaOH, 1 mL of 0.5 M phosphate buffer (pH 9.0; pH 3.0 for protein experiments), and 1 mL of 8 mM iron(II)chloride-tetrahydrate in a 5 mL Eppendorf tube. To initiate the reaction, we added 1 mL of 4% hydrogen peroxide (v/v). For protein aggregation experiments, the TPA solution was replaced with 1 mg/mL HSA in 0.3 M phosphate (pH 9.0 or 3.0).

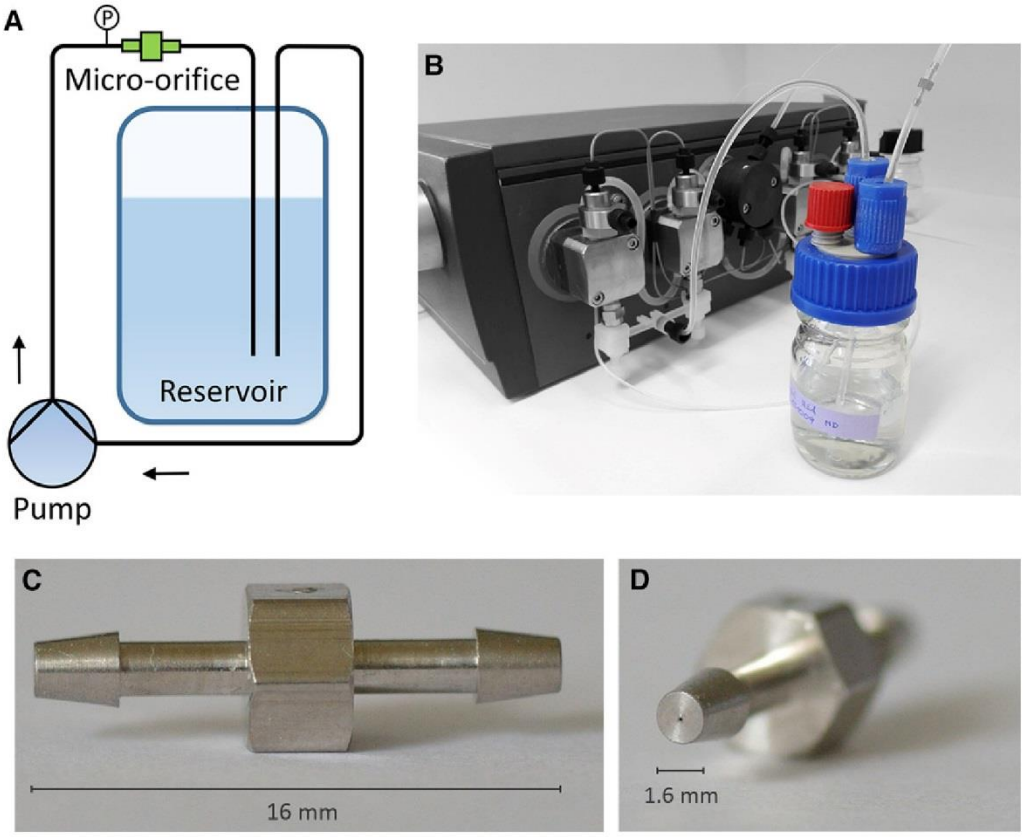

Figure 1. The protein stressing setup with the integrated micro-orifice. (A) Schematic drawing. (B) Photograph. The micro-orifice is located at the top right. (C) side view onto the orifice. (D) Front view of the flow reduction.

2.6 Ultra-sonication

A UP100H ultra-sonic homogenizer (Hilscher, Teltow, Brandenburg, Germany) with an MS3 sonotrode was used at 60% intensity in continuous mode to generate cavitation. Sample solutions (60 mL) were sonicated in a jacketed 100 mL glass beaker constantly cooled to 25°C by a F12-ED circulator (Julabo, Seelbach, Baden-Wuerttemberg, Germany) connected with silicon tubes.

2.7 Micro-orifice

T-4-SS micro-orifices (Fig. 1) were purchased from O'Keefe Controls Co. (Monroe, CT, USA). These devices were delivered with a barb connector on each side, which allowed an easy connection to 1/16'' tubes. The diameter reduction to 99 μm generated a back pressure of up to 30 bar at a flow rate of 26 mL/min. To ensure a continuous flow rate with the described requirements, we integrated the micro-orifice into the flow path of an ÄKTA P-901 piston pump (GE Healthcare, Chicago, IL, USA) (Fig. 1). At different flow rates through the micro-orifice, 60 mL of protein or TPA solution was recirculated for 90 and 1440 min. To evaluate the influence of the pump on protein aggregation the micro-orifice was replaced by a 2 m 0.75 μm id tube. Hence, the effect of the pump can be subtracted from the combined effect pump and orifice. To suppress cavitation we increased the back-pressure behind the micro-orifice with a 31.5 cm tube 0.25 mm id PEEK tube (1/16 '' od) (GE) glued into the tube exiting the micro-orifice (1/16 '' id).

2.8 Computational fluid dynamic simulation

To simulate the flow inside the micro-orifice and calculate an average shear rate over the flow reduction, a CFD simulation was set up using the computer program Star-CCM+® (CD-adapco, Melville, NY, USA). The geometry of the orifice was obtained from a technical drawing by the manufacturer. The inlet diameter through the barb connector was set to 1.2 mm. A continuous conical narrowing from 1.2 mm to 99 μm was adjusted in 0.25-mm increments. The orifice length itself was set to 0.33 mm. After the reduction, the diameter instantly expanded to the diameter of the connected transparent Fluoroethenepropene tube (1/16'', which is equal to 1.59 mm). We chose a three-dimensional, steady, Eulerian multiphase including volume of fluid (VOF) and cavitation-segregated flow, realized K-Epsilon turbulence with Reynolds averaged Navier-Stokes model. The minimum allowable wall distance and reference pressure were set to 1.0×10^{-9}m and 1013 mbar, respectively. We picked a cubic mesh to better resolve the contribution of both liquid and vapor in each cell derived from the VOF model. Therefore, we focused on reducing the cell size in the critical regions, including the orifice reduction or the free jet region, after the device.

3 Results and discussion

3.1 Selection of a micro-orifice

We compared different methods to study the effect of hydroxyl radicals on protein aggregation behavior. We used Fenton's reaction for a high radical generation rate per time, ultra-sonication as a well-established method for the generation of detectable amounts of radicals [18, 26, 27], and a micro-orifice with an unknown generation rate. A stirring device to simulate protein mixing processes at high revolution rates was also taken into account but considered to not be feasible due to the resulting vortex and air entrapment in the protein solution. Using a micro-orifice integrated into a pumping flow path overcomes the issue of air inclusion due to the closed system. In addition, this setup mimics the conditions downstream of a high pressure homogenizer quite well, or the slit between the rotor and the wall of a fast rotating gear pump. We used the dimensionless cavitation number (Ca) to roughly predict the required flow. Estimating a downstream pressure of 106.3 kPa, assuming an orifice diameter of 100 μm, vapor pressure of water at 20°C of 2338 Pa, and a density of water of 998 kg/m^3, a linear flow rate of 33 ms^{-1} (15.6 mL/min) was required to be below the cavitation number threshold of 0.2, ensuring the occurrence of cavitation [23]. Thus, the T-4-SS micro-orifices with a nominal diameter of 99 μm was suitable for generating cavitation with an ÄKTA system pump. We further increased the flow rate up to 56.3 m/s (26 mL/min) to increase the cavitation strength.

3.2 CFD simulation of shear rates

The prevailing flow inside a tube or orifice can be estimated by the Reynolds number Eq. (4). A simple calculation of shear rate is only possible when the flow is laminar [28–30]. Assuming a liquid density of 998 kg/m^3, a linear velocity of 56.3 m/s, a micro-orifice diameter of 9.9 × 10^{-5} m, and a dynamic viscosity of 8.9 × 10^{-4} Pa, the resulting Reynolds number was 6250, indicating turbulent flow. Additionally, the occurrence of a defined vena contracta complicates the flow profile, requiring a numerical solution by CFD [31]. To simplify the complex time- and location-dependent turbulent flow, we used a steady simulation approach that averaged the turbulence over time. The CFD simulation was validated by comparing the simulated and experimentally determined pressure drops at several different flow rates (Fig. 2). The accuracy of the pump was evaluated with ±1.3% in the range of 8 to 30 mL/min. We accurately predicted the pressure drop with the CFD simulation. Although our simulations underestimated the measured pressure drop by 4% at 26 mL/min and overestimated the pressure by 9% at 8 mL/min, we were able to precisely predict the minimum flow rate for cavitation (online supporting data Table 1). We observed both an increase in fluorescence signal when using the TPA dosimeter and the occurrence of noise produced by the implosion of vapor cavities. The implemented cavitation model predicted a realistic number of cells with vapor content at the corresponding flow rates in the CFD simulation, concluding that cavitation was occurring. However, at a flow rate of 11 mL/min, the simulation

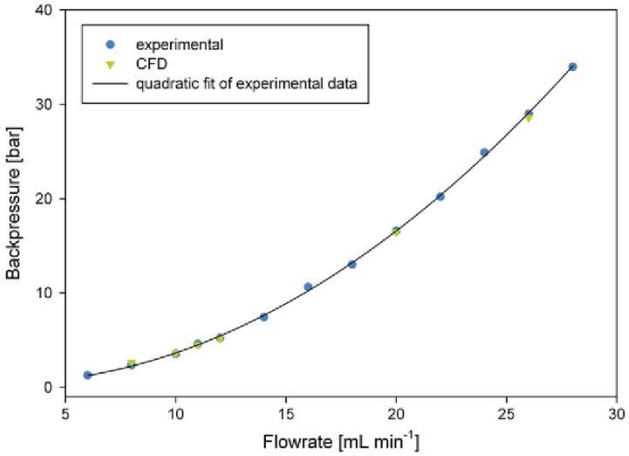

Figure 2. Pressure curve for the micro-orifice integrated into the ÄKTA flow path and CFD calculation at six different flow rates. Experimentally measured data (blue) and a quadratic fit of the data (black) are shown. Simulation data are in green.

demonstrated some cells with vapor content, but we did not notice any noise or increase in hTPA signal. Either the fluorescence assay was not sensitive enough to detect this minor cavitation level, or the simulation simply overestimated the reality. As the simulation matched our experiments very well, we generated 110 cross-sections through the whole orifice reduction (every 3.2 μm) *in silico* to estimate shear rates.

A plane section is a virtual two-dimensional space located inside the geometry used to display physical values, such as pressure or velocity, for all of the cells it contains (Fig. 3). For the calculation of shear rates, we wrote a user script in Star CCM+ that derived the velocity vector perpendicular to the wall of each cell to the next cell located closer to the center of the reduction according to Eq. (5), where $\dot{\gamma}$ is the shear rate, Δv the velocity difference between two cells, and h the distance between these cells.

$$\dot{\gamma} = \frac{\Delta v}{h} \tag{5}$$

We showed at the beginning of the vena contracta that the maximum obtained wall shear rate was in the order of 10^8 s^{-1} (Fig. 3). Although studies on high shear rate-dependent aggregation have been reported [5, 9, 32–35], the values from our simulation exceed these values by a factor of at least 10. In addition, the maximum shear rate was 22-times higher than one would expect from the laminar flow profile at the wall (4.5 × 10^6 s^{-1}), which further indicates the importance of a validated CFD simulation. However, the mass flow rate at the wall and, thus, the amount of proteins sensing this extremely high shear stress is rather low. Therefore, a mass flow-averaged shear rate over the whole orifice reduction was required. We additionally picked the velocity and density profiles of each cell, allowing us to calculate the average shear rate ($\dot{\gamma}$) Eq. (6) by taking into account the overall mass flow from all sections and cells ($\dot{M}_i$) the shear rate contribution (γ_i), and the mass flow of each individual cell, given by the velocity (v_i), density (ρ_i), and cell size (A_i).

$$\dot{\gamma} = \frac{1}{\sum_i \dot{M}_i} \sum_i v_i \rho_i A_i \gamma_i \tag{6}$$

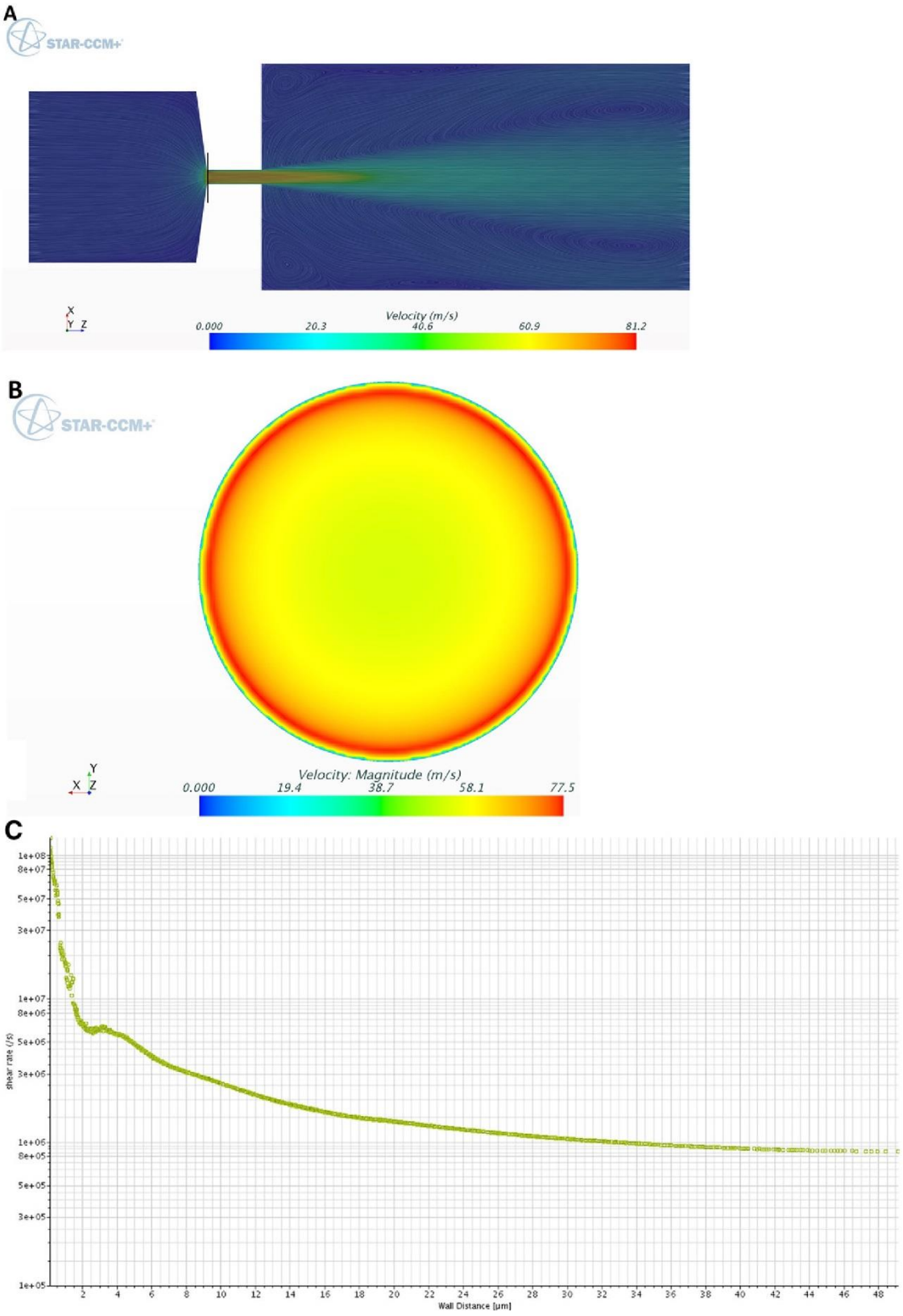

Figure 3. Velocity and shear profiles indicated by plane section through the micro-orifice. (A) Color represents the flow velocity, whereas the lines give information about the direction. (B) Plane section indicated by the black line in (A). (C) Shear rates across the plane section in (B) from the wall to the center.

This calculation enabled a detailed average description of the shear rate inside the micro-orifice, which was not possible with ordinary theoretical assumptions due to the focusing effect of the vena contracta and the resulting complex velocity profile [31]. However, we calculated an extremely high average shear rate of 1.2×10^6 s^{-1}. We obtained 5×10^6 s^{-1} when averaging the shear rate for all of the cells of the 110 cross-sections without taking into account the reduced mass flow rate at the wall. Hence, the mass flow averaged calculation provides a more realistic picture because the averaged shear rate would have been overestimated by a factor of 4. As we used a static simulation, the local shear rates could even be higher due to fluctuations in the turbulence, whereas our steady simulation averaged velocity and shear rates over time.

3.3 Suppressing cavitation with a flow restrictor

To separate the influence of cavitation from the high demonstrated shear rates, we suppressed cavitation by increasing the downstream pressure of the orifice with a flow restrictor. We used a 31.5 cm Teflon tube with a diameter of 0.25 mm, increased the downstream pressure to 21 bar. The resulting cavitation number was 1.3 and no increase in fluorescence signal was obtained after 24 hours of pumping with TPA solution. We performed another CFD simulation and obtained an average shear rate of 1.6×10^6 s^{-1}. The 33% increase in the average shear rate can be explained by the higher mass flow rate near the wall because no gas phase is transported.

3.4 Calibration of hydroxyl radical formation with hTPA

To investigate hydroxyl radical-mediated protein aggregation by cavitation, we correlated the arising fluorescence signals of the micro-orifice, the ultra-sonication homogenizer and Fenton's reaction with hydroxyl radical concentrations by analyzing the reactant of the TPA reaction, hTPA. We obtained a linear correlation for the stock solution and found that a gain of one fluorescence unit corresponded to 59.3 ± 3.8 pmol/L hydroxyl radicals.

3.5 Hydroxyl radical formation by micro-orifice and ultra-sonication treatment

Hydroxyl radical generation by the ultra-sonication sonotrode and the micro-orifice was tested with the TPA dosimeter after 60 and 1440 min, respectively. With both devices, we visually detected cavitation (Fig. 4) by the characteristic bubble formation at the exit of the orifice or the apex of the ultra-sonication tip. The micro-orifice and ultra-sonic homogenizer generated 2.09 and 189.7 fluorescence counts per minute. With the micro-orifice, the flow rate determined the cavitation intensity, whereas the time constant and power input were relevant for the ultra-sonic homogenizer. The oscillating tip of the ultra-sonic homogenizer resulted in a 90-times higher signal due to the high local energy input [36]. Converting the fluorescence signals to moles of hydroxyl radicals using the calibration curve, we found that 0.124 nmol/(L min) was generated by the micro-orifice, whereas the ultra-sonication sonotrode was capable of generating 11.25 nmol/(L min) which is in good agreement with expectations from the literature [37]. We expected that the same amount of hydroxyl radicals will result in similar levels of protein aggregation. To investigate hydroxyl radical-mediated HSA aggregation, we picked an incubation time of 1 and 90 min for the ultra-sonic homogenizer and micro-orifice, respectively.

3.6 Hydroxyl radical formation by Fenton's reaction

To investigate the influence of high concentrations of hydroxyl radicals on protein aggregation, we used Fenton's reaction as an additional radical source. Fe(II) reacted with hydrogen peroxide to form ferric iron (Fe(III)), one hydroxyl radical, and one hydroxide ion [38]. To measure hydroxyl radical formation with TPA, the pH was set to 9 to prevent TPA precipitation. In addition, the catalytic back reaction of Fe(III) to Fe(II) was prevented due to the high pH, resulting in the formation of insoluble iron(III) hydroxide (K_{sp} 2.7×10^{-39} mol^4/L^4 [39]). Therefore, hydroxyl radicals were the only radical species, which was necessary to avoid misinterpreting the results. Although Fenton's reaction is normally conducted at pH 3, some researchers have shown that an even faster hydroxyl radical release occurs at pH 9 [40]. After initiation of the reaction, we measured the fluorescence signal at 10, 30, and 60 min. The fluorescence signal did not change after 10 min, indicating that the reaction was over after a few minutes. A total of 381.56 nmol/(L min) hydroxyl radicals were formed by this reaction, which was 34-times higher than ultra-sonication and 3067-times higher than with the micro-orifice (Table 1). The reaction might have been over after several seconds but sample mixing and repeated plate reader analysis required several minutes, hence the generation rate per minute was probably even higher.

3.7 Protein stress

The HSA solution was stressed by the micro-orifice, ultra-sonication, and hydroxyl radicals generated by Fenton's reaction. We used a low protein concentration of 0.25 g/l in all experiments. With this concentration structural analytics like HP-SEC are less error prone because no dilutions have to be done which decreases sample to sample deviations. Further, in case dilutions are done it is well know that a protein could refold and then we could make a false conclusion. Therefore, a direct

Table 1. Comparison of hydroxyl radical formation by different methods

Treatment	nmol/(L min)	Proportion
Pumping + micro-orifice	0.12 ± 0.01	
Ultra-sonic homogenizer	11.25 ± 1.68	90
Fenton's reaction, pH 9	381.56 ± 81.25	34/3067

Data are presented as mean ± SD. The proportion between different treatments also indicated.

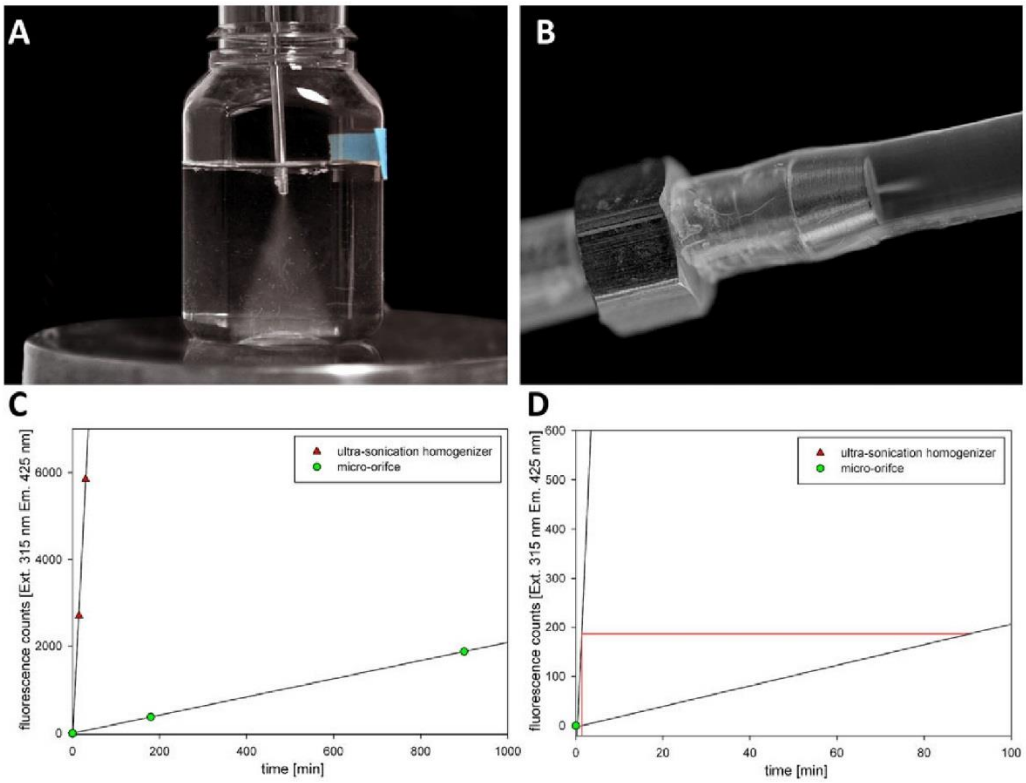

Figure 4. Visualization of cavitation. (A) Ultra-sonication. (B) micro-orifice. (C) Generation of hydroxyl radicals measured as fluorescence counts by the terephthalic acid dosimeter. Data are presented as the means of three experiments ± SD which is within the color marking. (D) Zoomed in view of (C) to calculate time when the same amount of radicals is generated by the different methods.

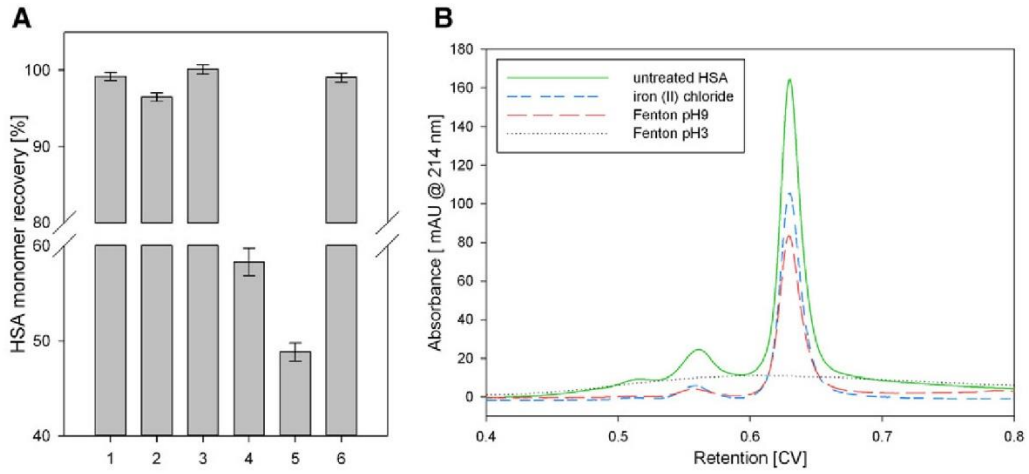

Figure 5. (A) HSA recovery of soluble HSA monomer before and after different treatments. 1: pumping (control); 2: pumping through the micro-orifice; 3: ultra-sonication; 4: iron(II)chloride at pH 9; 5: Fenton's reaction at pH 9; 6: suppressed cavitation. Error bars represent the standard deviation of three independent experiments. (B) SEC chromatograms of different HSA samples. Untreated HSA (green) was compared to an HSA solution containing iron(II)chloride (blue), HSA treated with Fenton's reaction at pH 9 (red), and Fenton's reaction at pH 3 (black dotted).

injections is less critical regarding interpretation. The concentration of HSA monomers in the supernatant did not change with ultra-sonication (Fig. 5). Treatment with the micro-orifice reduced the HSA monomers by 3.3 ± 0.3 %, and the dimeric form increased by the same amount (Fig. 6). Although both systems generated the same amount of radicals, the aggregation behavior was different. We also increased the incubation time for the ultra-sonication homogenizer to 30 min. After 30 min the hydroxyl radical concentration was similar to the Fenton's reaction after 1 min but we did not find increased HSA

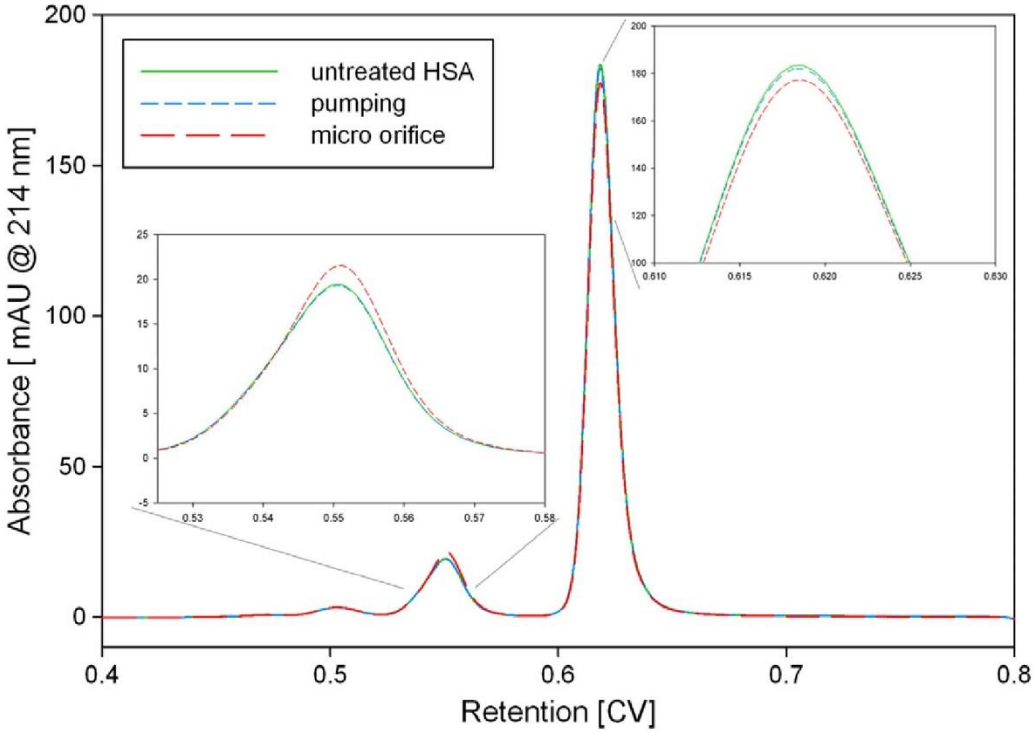

Figure 6. HP-SEC samples of HSA treated with the micro-orifice. Untreated HSA (green) was compared to an experiment with (red) and without the micro-orifice (blue). The decrease in monomeric HSA and the increase in dimeric HSA by the micro-orifice treatment is visible.

aggregation. The Intensity of hydroxyl radicals per time is most reasonable not high enough. However, we also processed a HSA sample with the ultra-sonication homogenizer for 1 h. After this time we could notice increased aggregation. Although we used a circulation bath to cool the sample, the homogenizer produced a lot of heat. We measured the tip temperature after 1 h and obtained 58°C. Therefore, aggregation in samples treated longer than 30 min with this specific setup is most likely generated by the hot sonication tip and not related to cavitation. In contrast, Fenton's reaction at pH 9 resulted in 9.5 % ± 1.6 % protein aggregation (Fig. 5). However, at alkaline pH we also lose a certain amount of HSA due to co-precipitation with iron hydroxide [41, 42]. We showed that this effect occurred without the addition of hydrogen peroxide at pH 9; thus, under the prevailing buffer conditions, oxidation of Fe(II) to Fe(III) occurs spontaneously. We lost 41.7 ± 2.1% of the HSA due to this treatment, which is more than the amount obtained from the effect of hydroxyl radicals. However, when adding hydrogen peroxide to the protein solution, the additional 9.5% protein loss was most likely due to the fast release of hydroxyl radicals in Fenton's reaction. Although a maximum of 2 mM iron was available in the reaction solution, the spontaneous oxidation of Fe(II) to Fe(III) without peroxide [43] may explain the rather low generation rate of 3.82 μmol/L after 10 min. We also performed Fenton's reaction at pH 3, which resulted in total protein aggregation without any undesired iron hydroxide (Fig. 5). Unfortunately, we were not able to measure hydroxyl radical formation due to the insolubility of TPA at acidic pH. We assume that the amount of hydroxyl radicals generated by cavitation is most reasonable not high enough to cause relevant protein aggregation. Although the generation of hydroxyl radicals by cavitation is evident it is unclear if these radicals are the driving force for protein aggregation or DNA fragmentation [12]. Protein aggregation by cavitation was already described for an antibody and recombinant human growth hormone (rhGH) [44]. No chemical modifications was found for the antibody while the data for rhGH was inconsistent. Recent research on cavitation did also not find radial associated oxidation of an antibody by cavitation events [45]. However, in both studies protein aggregation could be noticed, which indicates that the driving force behind cavitation induced aggregation is more reasonable the generated surface area and not hydroxyl radicals. Additionally the described aggregation could be suppressed with surfactant. Hence we suggest that the aggregation mechanism towards air/liquid interfaces by shaking and cavitation is similar. Further, we could suppress cavitation inside the micro-orifice by inserting a flow restrictor downstream of the micro-orifice, which allowed us to investigate the influence of isolated high shear rates on protein aggregation (Fig. 5). No additional HSA dimers were formed and the monomer content did not change. Therefore, the described generation of dimers obtained by the micro-orifice was most likely due to the additional surface area generated by the device. We observed that, although the cavitation intensity was higher for the ultra-sonic homogenizer, the stability of vapor cavities was higher with the micro-orifice; several bubbles were still visible several centimeters downstream from the orifice. Although the protein solution was degassed, the described stabilization of vapor cavities downstream of the orifice was most likely due to the protein. Thus, the aggregating effect of cavitation is likely less correlated with hydroxyl radical intensity, but rather with the surface area and stability of vapor cavities. Mechanical stress in form of extensional flow was recently proposed as

mechanism for aggregation [4]. However, the most relevant control experiment has not been conducted, namely the influence of the plunger. Protein aggregation in those experiments most reasonable occured due to the friction between the plunger and the wall. In our experiments the impact of the shear, cavitation, friction between the piston and sealing, and particle formation by abrasion by the position of the pumps was corrected in order to be able to observe the impact of the orifice. Although we did not calculate the extensional flow strain due to the higher velocity gradient it is above the described value. Hence, we think that neither shear nor extensional force is able to unfold proteins under isolated conditions. On the other side we came to the conclusion that the increase in vapor/liquid interfaces generated by cavitation is a reasonable mechanism for aggregation. However, for future work the focus should be set to analyze cavitation mediated protein aggregation with additional methods. Dynamic light scattering analysis could be used to track insoluble particle formation while circular dichroism could be used to get a better insight into secondary structural alterations.

4 Concluding remarks

In the present study, we demonstrated that HSA did not aggregate due to cavitation-mediated hydroxyl radicals, as insufficient radicals were generated. Although hydroxyl radicals belong to the most aggressive radical species, even the high energy input of the ultra-sonic homogenizer did not have a high enough generation rate to alter HSA aggregation level. However, a change in HSA aggregation behavior was observed when pumping through the micro-orifice. Due to our validated CFD simulation, we calculated an average shear rate and stress of 1.2×10^6 s^{-1} and 1200 Pa, respectively. Although the shear stress applied to the proteins was higher than reported elsewhere in the literature, when cavitation was suppressed and the pumping rate the same, HSA aggregation did not occur. We conclude that the impact of isolated shear conditions on protein integrity is low. Nevertheless, we observed HSA aggregation when cavitation occurred. Therefore, the increased surface area due to cavitation bubble growth was identified to be responsible for aggregation. Our future work will evaluate the effect of cavitation on the behavior of structurally different proteins at different concentrations. Further, we want to compare protein aggregation behavior during cavitation with air/liquid interfaces and address the aggregation mechanism.

Practical application

The influence of high shear rates and cavitation on the aggregation/destruction of proteins is not fully understood. We developed a methodology to mimic both cavitation and extremely high shear rates to investigate protein behavior. The method is able to discriminate the effects of both mechanical shear stress and cavitation and will serve as a tool for root cause analysis when proteins aggregate during bioprocessing, as well as to predict if a protein is resistant to cavitation and shear stress.

This work was supported by the Federal Ministry of Science, Research and Economy (BMWFW), the Federal Ministry of Traffic, Innovation and Technology (bmvit), the Styrian Business Promotion Agency SFG, the Standortagentur Tirol, the Government of Lower Austria, and ZIT - Technology Agency of the City of Vienna through the COMET Funding Program managed by the Austrian Research Promotion Agency FFG.

The authors have declared no conflict of interest.

Nomenclature

A [m^2]	area of a certain mesh face front
Ca [-]	dimensionless cavitation number
d [m]	diameter of a tube
h [h]	distance between two mesh cells
$\dot{M}$ [kg/s]	mass flow average
p [kg/(m s^2)]	local pressure
p_v [kg/(m s^2)]	vapor pressure of a liquid
Q [m^3/s)]	volumetric flow rate
r [m]	radius of a tube
Re [-]	Reynolds number
v [m/s]	velocity

Greek symbols

ρ [kg/m^3]	density
γ [s^{-1}]	shear rate
μ [kg/(m s)]	dynamic viscosity

5 References

[1] Charm, S. E., Wong, B. L., Enzyme inactivation with shearing. *Biotechnol. Bioeng.* 1970, *12*, 1103–1109.
[2] Tirrell, M., Middleman, S., Shear modification of enzyme kinetics. *Biotechnol. Bioeng.* 1975, *17*, 299–303.
[3] Charm, S. E., Wong, B. L., Shear effects on enzymes. *Enzyme Microb. Technol.* 1981, *3*, 111–118.
[4] Dobson, J., Kumar, A., Willis, L. F., Tuma, R. et al., Inducing protein aggregation by extensional flow. *PNAS* 2017, *114*, 4673–4678.
[5] Jaspe, J., Hagen, S. J., Do protein molecules unfold in a simple shear flow? *Biophys. J.* 2006, *91*, 3415–3424.
[6] Harrington, T. J., Gainer, J. L., Kirwan, D. J., Effects of fluid shear on immobilized enzyme kinetics. *Enzyme Microb. Technol.* 1991, *13*, 610–616.
[7] Donaldson, T. L., Boonstra, E. F., Hammond, J. M., Kinetics of protein denaturation at gas-liquid interfaces. *J. Colloid Interface Sci.* 1980, *74*, 441–450.
[8] Narendranathan, T. J., Dunnill, P., The effect of shear on globular proteins during ultrafiltration: studies of alcohol dehydrogenase. *Biotechnol. Bioeng.* 1982, *24*, 2103–2107.
[9] Bee, J. S., Stevenson, J. L., Mehta, B., Svitel, J. et al., Response of a concentrated monoclonal antibody formulation to high shear. *Biotechnol. Bioeng.* 2009, *103*, 936–943.

[10] Nayak, A., Colandene, J., Bradford, V., Perkins, M., Characterization of subvisible particle formation during the filling pump operation of a monoclonal antibody solution. *J. Pharm. Sci.* 2011, *100*, 4198–4204.
[11] Suslick, K. S., Sonochemistry. *Science* 1990, *247*, 1439–1445.
[12] Riesz, P., Kondo, T., Free radical formation induced by ultrasound and its biological implications. *Free Radic. Biol. Med.* 1992, *13*, 247–270.
[13] Takamoto, K., Chance, M. R., Radiolytic protein footprinting with mass spectrometry to probe the structure of macromolecular complexes, *Annu. Rev. Biophys. Biomol. Struct.* 2006, *35*, 251–276.
[14] Xu, G., Takamoto, K., Chance, M. R., Radiolytic modification of basic amino acid residues in peptides: probes for examining protein-protein interactions. *Anal. Chem.* 2003, *75*, 6995–7007.
[15] Stadtman, E. R., Oxidation of free amino acids and amino acid residues in proteins by radiolysis and by metal-catalyzed reactions. *Annu. Rev. Biochem.* 1993, *62*, 797–821.
[16] Wang, L., Chance, M. R., Structural mass spectrometry of proteins using hydroxyl radical based protein footprinting. *Anal. Chem.* 2011, *83*, 7234–7241.
[17] Fenton, H. J. H., LXXIII. - Oxidation of tartaric acid in presence of iron. *J. Chem. Soc. Trans.* 1894, *65*, 899–910.
[18] Weissler, A., Cooper, H. W., Snyder, S., Chemical effect of ultrasonic waves: oxidation of potassium iodide solution by carbon tetrachloride. *J. Am. Chem. Soc.* 1950, *72*, 1769–1775.
[19] Lentz, Y. K., Anchordoquy, T. J., Lengsfeld, C. S., DNA acts as a nucleation site for transient cavitation in the ultrasonic nebulizer. *J. Pharm. Sci.* 2006, *95*, 607–619.
[20] Villeneuve, L., Alberti, L., Steghens, J. P., Lancelin, J. M. et al., Assay of hydroxyl radicals generated by focused ultrasound. *Ultrason. Sonochem.* 2009, *16*, 339–344.
[21] Barreto, J. C., Smith, G. S., Strobel, N. H. P., McQuillin, P. A. et al., Terephthalic acid: a dosimeter for the detection of hydroxyl radicals in vitro. *Life Sci.* 1994, *56*, PL89–PL96.
[22] Linxiang, L., Abe, Y., Nagasawa, Y., Kudo, R. et al., An HPLC assay of hydroxyl radicals by the hydroxylation reaction of terephthalic acid. *Biomed. Chromatogr.* 2004, *18*, 470–474.
[23] Lamb, W. S., *Cavitation and Aeration in Hydraulic Systems*, BHRA, Cranfield, Bedford, England, 1987.
[24] Testud, P., Moussou, P., Hirschberg, A., Aurégan, Y., Noise generated by cavitating single-hole and multi-hole orifices in a water pipe. *J. Fluids Struct.* 2007, *23*, 163–189.
[25] Gooch, J. W., Hagen-Poiseuille Equation, in: Gooch, J. W. (Ed.), *Encyclopedic Dictionary of Polymers*, Springer New York, New York, NY 2011, pp. 355–355.
[26] Hoffmann, M. R., Hua, I., Höchemer, R., Application of ultrasonic irradiation for the degradation of chemical contaminants in water. *Ultrason. Sonochem.* 1996, *3*, S163–S172.
[27] Naffrechoux, E., Chanoux, S., Petrier, C., Suptil, J., Sonochemical and photochemical oxidation of organic matter. *Ultrason. Sonochem.* 2000, *7*, 255–259.
[28] Hammond, T. G., Hammond, J. M., Optimized suspension culture: the rotating-wall vessel. *Am. J. Physiol.* 2001, *281*, F12–F25.
[29] Bird, R. B., Stewart, W. E., Lightfoot, E. N., *Transport Phenomena* 2nd ed., John Wiley & Sons, New York, New York, 2002.
[30] Brückl, L., Schröder, T., Scheler, S., Hahn, R. et al., The Effect of shear on the structural conformation of rhGH and IgG1 in free solution. *J. Pharm. Sci.* 2016, *105*, 1810–1818.
[31] Thompson, B. R., Maynes, D., Webb, B. W., Characterization of the hydrodynamically developing flow in a microtube using MTV. *J. Fluids Engineer. Transact. ASME* 2005, *127*, 1003–1012.
[32] Maa, Y. F., Hsu, C. C., Protein denaturation by combined effect of shear and air-liquid interface. *Biotechnol. Bioeng.* 1997, *54*, 503–512.
[33] Wieland, D. C. F., Garamus, V. M., Zander, T., Krywka, C. et al., Studying solutions at high shear rates: a dedicated microfluidics setup. *J. Synchrotron Radiat.* 2016, *23*, 480–486.
[34] Thomas, C. R., Dunnill, P., Action of shear on enzymes: Studies with catalase and urease. *Biotechnol. Bioeng.* 1979, *21*, 2279–2302.
[35] Virkar, P. D., Narendranathan, T. J., Hoare, M., Dunnill, P., Studies of the effect of shear on globular proteins: extension to high shear fields and to pumps. *Biotechnol. Bioeng.* 1981, *23*, 425–429.
[36] Dhanalakshmi, N. P., Nagarajan, R., Ultrasonic intensification of the chemical degradation of methyl violet: an experimental study. *Internat. J. Chem. Mol. Nucl. Mater. Metallurg. Engineer.* 2011, *5*, 6.
[37] Juretic, H., Montalbo-Lomboy, M., Van Leeuwen, J., Cooper, W. J. et al., Hydroxyl radical formation in batch and continuous flow ultrasonic systems. *Ultrason. Sonochem.* 2015, *22*, 600–606.
[38] Neyens, E., Baeyens, J., A review of classic Fenton's peroxidation as an advanced oxidation technique. *J. Hazard. Mater.* 2003, *98*, 33–50.
[39] Lide, D. R., *Handbook of Chemistry and Physics* 65th ed., CRC Press, Boca Raton, FL, 1984 2312.
[40] Jung, Y. S., Lim, W. T., Park, J. Y., Kim, Y. H., Effect of pH on Fenton and Fenton-like oxidation. *Environ. Technol.* 2009, *30*, 183–190.
[41] Haase, C., Stieler, J. T., Arendt, T., Holzer, M., Pseudophosphorylation of tau protein alters its ability for self-aggregation. *J. Neurochem.* 2004, *88*, 1509–1520.
[42] Yamamoto, A., Shin, R. W., Hasegawa, K., Naiki, H. et al., Iron (III) induces aggregation of hyperphosphorylated τ and its reduction to iron (II) reverses the aggregation: Implications in the formation of neurofibrillary tangles of Alzheimer's disease. *J. Neurochem.* 2002, *82*, 1137–1147.
[43] Stumm, W., Lee, G. F., The chemistry of aqueous iron. *Schweizerische Zeitschrift für Hydrologie* 1960, *22*, 295–319.
[44] Randolph, T. W., Schiltz, E., Sederstrom, D., Steinmann, D. et al., Do not drop: Mechanical shock in vials causes cavitation, protein aggregation, and particle formation. *J. Pharm. Sci.* 2015, *104*, 602–611.
[45] Torisu, T., Maruno, T., Hamaji, Y., Ohkubo, T. et al., Synergistic effect of cavitation and agitation on protein aggregation. *J. Pharm. Sci.* 2017, *106*, 521–529.

Online supporting data:

Table 1: Comparison of cavitation detection from experiment and simulation.

Detection method		Flow rate, mL min^{-1}							
		8	9	10	11*	12	16	20	26
Experimental	Noise	no	no	no	no	**yes**	**yes**	**yes**	**yes**
	TPA	no	no	no	no	**yes**	**yes**	**yes**	**yes**
CFD model		no	n.d.	no	**yes/no**	**yes**	**n.d.**	**yes**	**yes**

*Several cells at the beginning of the reduction contained a small amount of vapor. n.d., not determined.

RESEARCH ARTICLE

Protein Aggregation

Biotechnology Journal

www.biotechnology-journal.com

Impact of Cavitation, High Shear Stress and Air/Liquid Interfaces on Protein Aggregation

*Mark Duerkop, Eva Berger, Astrid Dürauer, and Alois Jungbauer**

The reported impact of shear stress on protein aggregation has been contradictory. At high shear rates, the occurrence of cavitation or entrapment of air is reasonable and their effects possibly misattributed to shear stress. Nine different proteins (α-lactalbumin, two antibodies, fibroblast growth factor 2, granulocyte colony stimulating factor [GCSF], green fluorescence protein [GFP], hemoglobin, human serum albumin, and lysozyme) are tested for their aggregation behavior on vapor/liquid interfaces generated by cavitation and compared it to the isolated effects of high shear stress and air/liquid interfaces generated by foaming. Cavitation induced the aggregation of GCSF by +68.9%, hemoglobin +4%, and human serum albumin +2.9%, compared to a control, whereas the other proteins do not aggregate. The protein aggregation behaviors of the different proteins at air/liquid interfaces are similar to cavitation, but the effect is more pronounced. Air-liquid interface induced the aggregation of GCSF by +94.5%, hemoglobin +35.5%, and human serum albumin (HSA) +31.1%. The results indicate that the sensitivity of a certain protein toward cavitation is very similar to air/liquid-induced aggregation. Hence, hydroxyl radicals cannot be seen as the driving force for protein aggregation when cavitation occurs. Further, high shear rates of up to $10^8\ s^{-1}$ do not affect any of the tested proteins. Therefore, also within this study generated extremely high isolated shear rates cannot be considered to harm structural integrity when processing proteins.

1. Introduction

Today the impact of hydrodynamic flow phenomena especially shear stress regarding protein unfolding is still a controversial debate. Charm and Wong[1] reported enzyme inactivation of catalase and fibrinogen at shear rates of $1155\ s^{-1}$, whereas Tirrell and Middleman[2] reported urease inactivation already at shear rates of $50\ s^{-1}$. In contrast to these results, Thomas and Dunnill[3] did not find shear-induced damage studying catalase and urease, even at shear rates up to $10^6\ s^{-1}$. Similar to these results, horse cytochrome c could not be inactivated at shear rates of $2 \times 10^5\ s^{-1}$[4] and aggregation was not observed in a concentrated antibody solution at shear rates of $2.5 \times 10^5\ s^{-1}$.[5] In contrast, the aggregation of BSA, β2-microglobulin, and GCSF induced by extensional flow was described recently.[6] Extensional forces act solely in the flow direction. Hence the debate continues if elongational forces beside shear rates can unfold proteins.

In general, the shear rate (γ) in a certain region is calculated by the fluid velocity gradient perpendicular to the flow direction (v_z) $\gamma = dv_z/dx$, whereas the shear stress (τ) is dependent on the described shear rate and viscosity (μ) $\tau = \gamma\mu$. The force applied to a certain protein is the product of both the shear stress and the area of the protein (A) on which this pressure acts, $F = \tau A$.[7] The force required to unfold proteins as measured with atomic force microscopy seems to be between below 20 to 220 pN for α-helical and β-sheet dominated proteins.[8]

The force applied by shear or extensional flow irreversibly stretches proteins, but the unanswered question that remains is at which shear rate the irreversible process starts. Bee, Stevenson, Mehta, Svitel, Pollastrini, Platz, Freund, Carpenter, and Randolph[5] calculated the required shear rate to unfold an antibody with a force of 150 pN in a 3 mPas solution as $5 \times 10^7\ s^{-1}$, whereas Jaspe and Hagen[4] developed a bead-based model that predicted the shear rate required to unfold a 100 amino acid protein in water to be $10^7\ s^{-1}$. Because such extraordinary high shear rates were not reported the enhanced air/liquid interfaces in reactors or rheometer experiments may explain the described protein aggregation and not shear stress.[9,10]

Furthermore, at extremely high shear rates, cavitation may occur and the effect of this phenomenon may be misattributed to shear stress.[5,11] Cavitation occurs when the local static pressure in a liquid falls below the vapor pressure of the liquid, forming vapor filled cavities. These cavities are stable as long as the local pressure remains below the vapor pressure. When the local pressure recovers, these bubbles collapse leading to enormous

M. Duerkop, E. Berger, Dr. A. Dürauer, Prof. A. Jungbauer
Austrian Centre of Industrial Biotechnology
1190 Vienna, Austria
E-mail: alois.jungbauer@boku.ac.at

Dr. A. Dürauer, Prof. A. Jungbauer
University of Natural Resources and Life Sciences
Muthgasse 18, 1190 Vienna, Austria

The ORCID identification number(s) for the author(s) of this article can be found under https://doi.org/10.1002/biot.201800062.

DOI: 10.1002/biot.201800062

pressure and temperature spikes [12], forming microjets and hydroxyl radicals.[13] Due to the destructive nature of these microjets, cavitation is a real harm for solid materials. In bioprocesses, the occurrence of cavitation is reasonable in valves and pumps or at the tip of high revolving impellers. If protein interaction with vapor/liquid interfaces results in the same protein aggregation behavior as described for air/liquid interface, preventing cavitation in bioprocesses is crucial. In a previous study we showed that the influence of cavitation derived from a micro-orifice reduced the monomeric content of human serum albumin (HSA) and enhanced dimeric HSA,[14] whereas isolated shear rates of up to $10^8\ s^{-1}$ had no influence on HSA aggregation behavior. Furthermore, we hypothesized that the main driving force for protein aggregation when cavitation occurs is most likely the increased vapor/liquid interface due to cavitation bubble formation and not the hydroxyl radical formation obtained from bubble collapse as previously described.[15]

The aim of the present study was to compare the effect of cavitation with the effect of air/liquid interfaces to clearly identify the protein aggregation mechanism of cavitation. Therefore, we used a large set of proteins and a wide range of concentrations. We developed a simple foaming methodology to investigate the influence of air/liquid interfaces on the protein aggregation of the same proteins. Thus, we were able to compare the influence of vapor/liquid interfaces produced by cavitation with foaming-associated air/liquid interfaces. When we used a flow restrictor to suppress cavitation, shear rates were similar, and we could describe the effect of extremely high isolated shear rates on different proteins.

2. Experimental Section

2.1. Protein Standards

We used two IgG1 antibodies (antibody1 and 2) supplied as clarified supernatants, the target and manufacturer of which cannot be disclosed. Homogenized FGF-2 *Escherichia coli* supernatant was provided by Gerald Striedner, and a highly pure GFP solution (>99.5%) was obtained from Rainer Hahn (both from the Department of Biotechnology, University of Natural Resources and Life Sciences, Vienna, Austria). The antibodies and FGF-2 were purified by MabSelect SuRe and Heparin Sepharose 6 Fast Flow, respectively (GE Healthcare, Chicago, IL, USA). The fractions from the elution peaks were pooled from 50% peak maximum to 50% peak maximum for both the antibody and FGF-2 runs to obtain highly pure fractions. The two antibody pools were then neutralized. We obtained GCSF (purity >99.5%) as a gift from a donor who wishes to remain anonymous. We used Slide-A-Lyzer™ dialysis cassettes (3.5K MWCO, 30 mL; ThermoFisher Waltham, Massachusetts, USA) to change the buffer of the antibodies, FGF-2, and GCSF to the final buffer (10 mM sodium phosphate and 5 mM sodium chloride). The pH of the FGF-2 buffer was set to 8.5, antibody1 was diluted in pH 6.5, antibody2 in pH 6.0, and GCSF in pH 5.5. We incubated the dialyses cassettes in 500 mL of the buffer at 4 °C for 18 h, replacing the buffer after 3 and 15 h. The dialyzed protein solution was then loaded onto HP-SEC to analyze the content and purity. Finally, the protein solutions were diluted with the final buffer to a protein concentration of $0.25\ mg\ mL^{-1}$. Lyophilized Hemoglobin (H2500), α-lactalbumin (L6010), HSA (A3782), and lysozyme (L6876) were purchased from Sigma–Aldrich (St. Louis, MO, USA). A total of 0.25 mg mL^{-1} of each protein was dissolved separately in dialysis buffer (pH 6.5). Hemoglobin was prepared at pH 6. We also gravimetrically prepared HSA standards of 0.08, 0.8, 2.5, 8.0, and $25\ mg\ mL^{-1}$ in the described buffer at pH 6.5. We also addressed aggregation tendency under different pH conditions. Therefore, we separately prepared $1.0\ mg\ mL^{-1}$ protein standards of HSA and antibody2 in 1 mM phosphate buffer (pH 6). For the experiments, we diluted these standards 1:4 in 10 mM phosphate, 5 mM sodium chloride at varying pH. For HSA, the buffer had a pH of 5.2, 5.7, 6.2, 6.7, and 7.4, and for antibody2 the pH was 5.8, 6.4, 6.9, and 7.4. A 10 mM citrate buffer with 5 mM sodium chloride was prepared for the experiments with GCSF (pH 4.0, 4.7, 5.4, and 6.0) and α-lactalbumin (pH 4.3, 4.9, 5.5, and 6.1). To minimize process time-dependent protein aggregation, the preparation and stressing of protein solutions, SEC, and CD were all carried out on the same working day.

2.2. Size Exclusion Chromatography

Size exclusion analysis was performed on an Agilent 1290 LC system (Santa Clara, California, USA). We used a TSKgel G3000SWXL column (5 µm, $7.8 \times 300\ mm + 6 \times 40\ mm$ guard) from Tosoh (Shiba, Minato-Ku, Tokyo, Japan). We used phosphate running buffer ($13\ g\ L^{-1}$ KH2PO4, $9.4\ g\ L^{-1}$ K2HPO4, $14.61\ g\ L^{-1}$ sodium chloride) at a flow rate of $0.4\ mL\ min^{-1}$. The pH of the running buffer was adjusted to the pH of the buffer of the protein to be analyzed, ranging from 5.5 for GCSF to 7.5 for FGF-2. We used pH 7.5 instead of 8.5 for FGF-2 due to the limited pH stability of this resin. The protein samples were filtered through a 0.2 µm filter and 20 µL directly injected without any dilution. For HSA samples with higher protein concentrations, the injection volume was reduced to avoid detector saturation.

2.3. Circular Dichroism

We used a Chirascan (Photophysics Limited, Leatherhead, Surrey, United Kingdom) CD spectrometer to analyze the secondary structure of different proteins by far-UV spectroscopy. The instrument was flushed with nitrogen at a flow rate of $6\ L\ min^{-1}$. We measured between 180 and 260 nm using a 1 mm path length, 1 nm spectral bandwidth, step size of 1 nm, and step time of 10 s with undiluted, filtered (0.2 µm) protein samples at $0.25\ mg\ mL^{-1}$. After recording a protein spectrum, it was baseline corrected to the corresponding buffer.

2.4. Micro-Orifice

T-4-SS micro-orifices were purchased from O'Keefe Controls Co. (Monroe, Connecticut, USA). These devices were delivered with a barb connector on each side, allowing easy connection to tubes with an inner diameter of 1/16″. To provide a flow rate of $26\ mL\ min^{-1}$ at high backpressures of up to 30 bar, we integrated

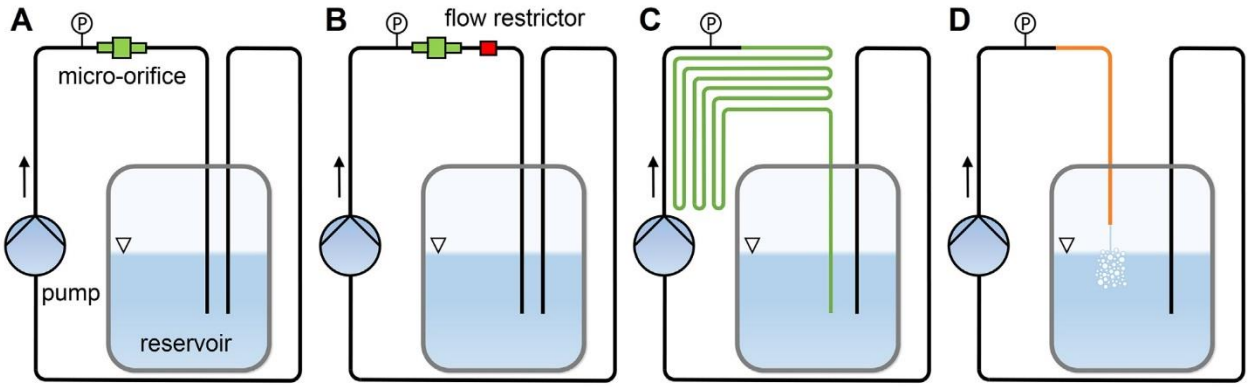

Figure 1. Different protein stressing setups. A) With a 100 mL reservoir, ÄKTA P-901 pump, pressure sensor, and micro-orifice to generate cavitation and high shear stress. B) Same setup with an integrated flow restrictor to suppress cavitation but maintain shear stress. C) With a 2 m tube (green) for the generation of high dimensionless shear. D) With a PEEK tube (orange) ending above the protein solution surface to generate protein foam.

the micro-orifice into the flow path of an ÄKTA P-901 piston pump (GE Healthcare, Chicago, Illinois, USA) (**Figure 1**A). As a negative control of cavitation, we replaced the micro-orifice with a 2-m, 0.75-mm inner diameter (ID) tube. A total of 62 mL of each protein solution was placed in a 100 mL bottle (Duran, Wertheim, Germany). The solution was pumped in a loop for 2 min at 10 mL min^{-1} while the bottle was gently shaken to obtain a homogenous starting sample. After sampling 2 mL, the remaining solution was pumped in a loop for 90 min at 26 mL min^{-1} through the micro-orifice or the 0.75-µm ID tube. In another experiment, we suppressed cavitation inside the micro-orifice by increasing the backpressure behind the device (Figure 1B). Therefore, we glued a 31.5-cm, 0.25-mm ID PEEK tube (1/16″ outer diameter) (GE) into the tube exiting the micro-orifice (1/16″ ID). Every protein stressing and corresponding control experiment was carried out in triplicatesand duplicates, respectively.

2.5. Device for High Dimensionless Shear

To investigate the influence of high dimensionless shear on protein aggregation, we placed a 2-m, 0.25-mm ID PEEK tube (GE) behind the pump (Figure 1C). After sampling 2 mL as described above, the remaining 60 mL of protein solution was pumped through the tube in a loop for 195 min at 12 mL min^{-1}.

2.6. Foaming Device

To further investigate the influence of surface area on protein aggregation, we integrated a 30-cm, 0.25-mm ID PEEK tube (GE) into the ÄKTA flow path. A free jet was obtained by placing the end of the tube 5 cm above the surface of the reservoir (Figure 1D). As in the cavitation experiment, we prepared 62 mL and sampled it prior to stressing as described above. The remaining 60 mL of protein solution was pumped through the device in a loop for 90 min at 26 mL min^{-1}. The bottle was placed on a magnetic stirring device and the foam given 10 h to settle and dissolve into the solution while stirring constantly at 100 rpm.

3. Results and Discussion

3.1. Protein Aggregation Induced by the Piston Pump

Our research covered a wide range of proteins with varying composition to test on shear stress, cavitation, and air/liquid interfaces. We selected different structural proteins like HSA due to its ability to naturally form soluble oligomers[16] and a fibroblast growth factor 2 (FGF-2) mutant with its unique random coiled structure. We used highly pharmaceutically relevant proteins, including two different recombinant antibodies and GCSF which is prone to spontaneous aggregation under physiological conditions.[17] We also selected lysozyme and calcium-depleted α-lactalbumin, two structurally homologous proteins with different chemical stabilities,[18] green fluorescence protein (GFP), and hemoglobin to expand the range of proteins and allow generalization.

To investigate the effect of shear, cavitation, and foaming, the proteins solutions were cycled 39 times in four different stress devices (Figure 1) using a piston pump. In order to avoid misinterpretation due to the effects caused by the pump itself, the proteins were cycled without these devices and used as a control. For α-lactalbumin, the loss in monomeric protein was not detectable (100.9 ± 1.1% recoveries) when stressing the proteins without the micro-orifice. For HSA and GFP, we measured 98.5 ± 0.2% and 98.5 ± 0.4% recoveries. For lysozyme, hemoglobin, and antibody1, the recoveries were 98.5 ± 1.5%, 96.3 ± 0.9%, and 96.3 ± 1.5%, respectively. The lowest recoveries were found for GCSF (95.9 ± 0.8%), FGF-2 (95.7 ± 1.8%), and antibody2 (94.7 ± 0.1%). The reported aggregation is caused by the piston pumps. Subvisible particles formed between the seal and pump piston, reduced the amount of soluble protein.[11,19] Although the loss of monomeric antibody2 was rather high (5.3%), the cycle number must be taken into account. In 39 cycles the theoretical protein loss after each circulation is 0.14%,

which is hardly detectable by any analytical method. However it is very important to address pump induced protein aggregation to avoid misinterpretation of the data. Dobson, Kumar, Willis, Tuma, Higazi, Turner, Lowe, Ashcroft, Radford, Kapur, and Brockwell[6] addressed the impact of extensional flow on protein aggregation but did not investigate the impact of the plunger used for pumping. Hence it is not clear if the described aggregation behavior was solely associated with extensional flow. As seen from the data above, without control experiments the effect of shear stress, cavitation, and foaming would be tremendously overestimated for all the tested proteins.

3.2. Protein Aggregation Induced by the Micro Orifice

When we investigated the effect of cavitation and high shear rates generated by the micro-orifice on all of the proteins, the aggregation behavior varied strongly with the protein species (**Figure 2**). The aggregation tendency was strongest with GCSF. The soluble concentration of GCSF was reduced by $68.9 \pm 1.4\%$ compared to the pumping control experiment. Further, 2% of the remaining GCSF supernatant after the micro-orifice treatment was found as soluble aggregates which was not present in the control experiment. We also tracked the particle size distribution for GCSF with and without the integrated micro-orifice; the additional loss of 68.9% is most likely insoluble aggregates as described with FBRM (SI Appendix, Figure SF1). We could show that for GCSF the particle count of the pumping control experiment after 39 circulations was only 20 while 840 particles were formed during the micro-orifice treatment. The major fraction of particles were in the range of 10–30 µm. The generation of cavitation bubbles and aggregate formation after passing the cavitation device was filmed (Video 1), and the slow disintegration of large GCSF aggregates after vapor cavities have collapsed can be seen clearly. Like shooting stars, protein aggregates formed at the liquid/vapor interface of the vapor cavities slowly disintegrate after the vapor cavities collapse. Although GCSF protein aggregation also occurs spontaneously when stored above pH 3.5,[20] the amount of GCSF aggregation due to the mechanical stress generated from the micro-orifice was enormous. According to Krishnan, Chi, Webb, Chang, Shan, Goldenberg, Manning, Randolph, and Carpenter,[17] the expected initial aggregation rate for GCSF at a concentration of $0.25\,g\,L^{-1}$ in PBS (pH 6.9) is $4.5 \times 10^{-9}\,mol\,L^{-1}\,h^{1}$. As expected from the literature, we did not observe any detectable amount of GCSF aggregation after 30 h storage at $0.25\,g\,L^{-1}$ in pH 5.5 at 20 °C. However, the aggregation rate after stressing GCSF with the micro-orifice was $6.0 \pm 0.1\,\mu mol\,L^{-1}\,h^{-1}$, which is 1340-times higher than the initial aggregation rate. We also repeated the micro-orifice cavitation experiment with GCSF and $0.5\,g\,L^{-1}$ Tween 80® and found the aggregation tendency of GCSF reduced from $68.9 \pm 1.4\%$ without surfactant to $2.2 \pm 0.8\%$.

Further, the concentration of hemoglobin and HSA was reduced by $4 \pm 1.1\%$ and $2.9 \pm 0.6\%$, respectively, when stressed with the micro-orifice. We found that 2.5% loss of HSA (out of the 2.9% loss) could be attributed to dimerization. For the other six proteins, we did not observe aggregation in the presence of cavitation and high shear. Furthermore, lysozyme activity assay did not show a loss of activity after the stress treatment (SI Appendix, Figure SF2).

3.3. Effect of Shear Stress with Suppressed Cavitation

To determine whether cavitation and/or shear rates were responsible for the aggregation of GCSF, hemoglobin, and HSA, we used a flow restrictor downstream of the orifice, which increased the backpressure. Therefore, cavitation was suppressed and the maximum and average shear rates were 10^8 and $1.6 \times 10^6\,s^{-1}$.[14] For all three proteins, aggregation was not increased under the isolated shear conditions (**Figure 3**). Although the applied shear rates were among the highest ever reported in the literature and GCSF is a very mechanically

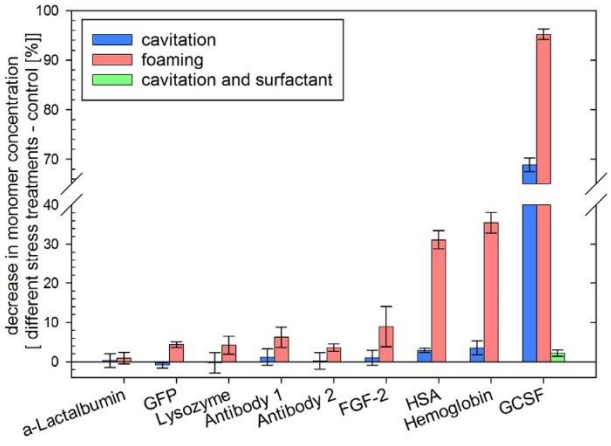

Figure 2. Comparison of protein aggregation from cavitation and foaming for nine different proteins. Data points represent the means of three experiments minus control ± SD.

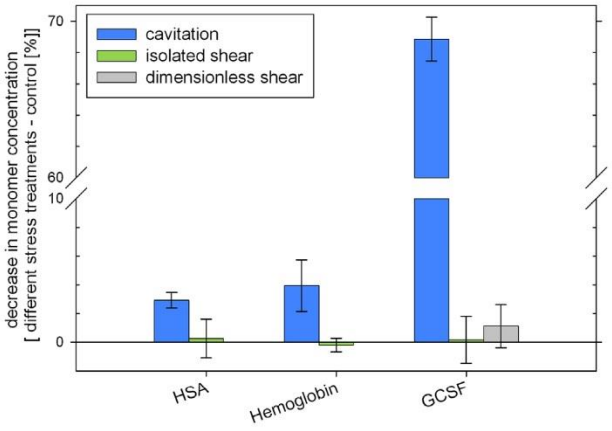

Figure 3. Comparison of protein aggregation behavior with three different treatments. Human serum albumin (HSA), hemoglobin, and granulocyte colony stimulating factor (GCSF) exhibited increased aggregation with cavitation (blue bars), whereas isolated shear (green) and dimensionless shear (gray) did not increase aggregation. Data points represent the means of three experiments minus control ± SD.

sensitive protein there was no additional aggregation due to shear stress. These shear rates used with this setup were 3–5 orders of magnitude higher than the shear rates expected in common bioprocesses, yet not a single protein exhibited increased aggregation. Due to the closed setup of our methodology, the influence of the air/liquid interfaces could be excluded. This is an advantage of this method compared to shear stress generated in a rheometer or a stirred tank, in which the generation of air bubbles cannot be excluded. These findings suggest that the aggregation of GCSF, HSA, and hemoglobin from the previous experiment being caused by cavitation rather than high shear stress.

3.4. Effect of High Dimensionless Shear on Protein Aggregation

The activity of several enzymes, such as rennet, catalase, and carboxypeptidase, was reduced when the product of the average shear rate and incubation time, also known as the Camp number, was $>10^4$.[21] When stressing proteins with the micro-orifice, the Camp number was only 9.4 for one circulation since the exposure time was only approximately 6 µs for each circulation. To evaluate whether high Camp numbers can indeed be a cause of protein aggregation, we pumped the sensitive GCSF protein through a 0.25-µm ID PEEK tube and calculated the average shear rate. In laminar flow regimes the maximum shear rate (γ)[7] at the wall can be estimated with Equation 1, where Q is the volumetric flow and r is the radius of the tube.

$$\gamma = \frac{4Q}{\pi r^3} \tag{1}$$

For the described setup the maximum shear was $1.3 \times 10^5\ s^{-1}$ while the average shear rate being two-thirds of the maximum shear rate which was $8.7 \times 10^4\ s^{-1}$.[4] With an average exposure time of 0.5 s a dimensionless shear of 4.3×10^4 was produced. Although the applied dimensionless shear was higher than the required 10^4, we did not observe GCSF aggregation (Figure 3). If all 39 circulations were considered the dimensionless shear was 1.7×10^6.

3.5. Why do Proteins Not Unfold Under Simple Shear Stress?

The shear force resulting from differences in local velocity are thought to be responsible for changes in a protein's secondary and/or tertiary structures, resulting in unfolding.[22] As the proteins are in free solution, a large amount of energy transferred by this velocity gradient is used to rotate the proteins and not only to stretch them. Harrington et al.[23] immobilized penicillinase and lactate dehydrogenase on the inner wall of a nylon tube and stressed these proteins with shear rates up to $10\,350\ s^{-1}$ without any loss in activity. Although this is not extraordinarily high compared to our work or other studies,[4,5,9,24] the applied shear force could not be transferred to rotate proteins; thus, the proteins sensed maximum shear rates at any time. However, as already described, the force required to unfold a protein was measured by atomic force microscopy to be near 20 and 220 pN for an alpha-helical and beta sheet dominated protein, respectively. The force applied to the proteins by the micro-orifice can be estimated by taking into account the shear stress and protein surface sensing this shear. However, it is difficult to estimate the proportion between rotation and elongation of a non-spherical protein, especially in the turbulent flow generated by the micro-orifice. To estimate the occurring force, we theoretically linked our proteins to the outer wall of the device to mimic the results of Harrington et al. Due to this virtual linker, the shear force at the wall is considered to act on half of the protein surface. Considering the GCSF protein as an aspherical particle with a hydrodynamic radius of 1.4 nm,[25] stressed by the micro-orifice at maximum ($10^8\ s^{-1}$) in a 1 mPas solution, we obtained a force of 1.24 pN. For an antibody with a hydrodynamic radius of 5 nm, the applied force would be 15.71 pN. If we apply the same methodology to the average shear rate and theoretically consistently prevent rotation, the average force in the device would be 0.02 and 0.25 pN for GCSF and an antibody, respectively. Without neglecting the rotational energy uptake, the force utilized for protein stretching would be even lower. Assuming that proteins in solution unfold between 20 and 220 pN, it is obvious that isolated shear rates cannot be harmful to average-sized proteins in common bioprocesses. However, resent research found BSA, β2-microglobulin, and GCSF aggregation at extensional strain rates in the order of $10^4\ s^{-1}$. Although the researcher reported protein aggregation, the control experiment evaluating the impact of the plunger itself was not carried out. A similar calculation to determine the prevailing force in extensional flow can be derived but the required flow will most likely never be achieved since laminar flow regime must prevail.

Generally, the most important characteristics determining whether shear or extensional forces are harmful is defined by the size of the target based on the quadratic relationship more than the amount of applied shear. For large molecules like von Willebrand factor or plasmid DNA,[26] the impact of high shear rates may be tremendous. However, for compact and non-sticky proteins we do not expect any negative impact of isolated shear in any common bioprocess.

3.6. Cavitation Induced Protein Aggregation at Different Concentrations

The impact of hydrodynamic cavitation at different protein concentrations has not been investigated thus far. For each concentration a control experiment without cavitation was carried out to exclude phenomena like oligomerization or nonspecific surface binding. Under cavitational flow we found a decrease in monomer content of 3.4% equal to $2.7\ mg\ L^{-1}$ at an initial HSA concentration of $0.08\ g\ L^{-1}$. The relative aggregation tendency decreased at higher concentrations and reached zero for the 8 and $25\ g\ L^{-1}$ experiments (**Figure 4**A). Thus, the relative aggregation tendency of the protein under cavitational flow was highest at low concentrations. Most reasonable vapor/liquid interphases generated by cavitation bubbles were already saturated with proteins, even at low protein concentrations.

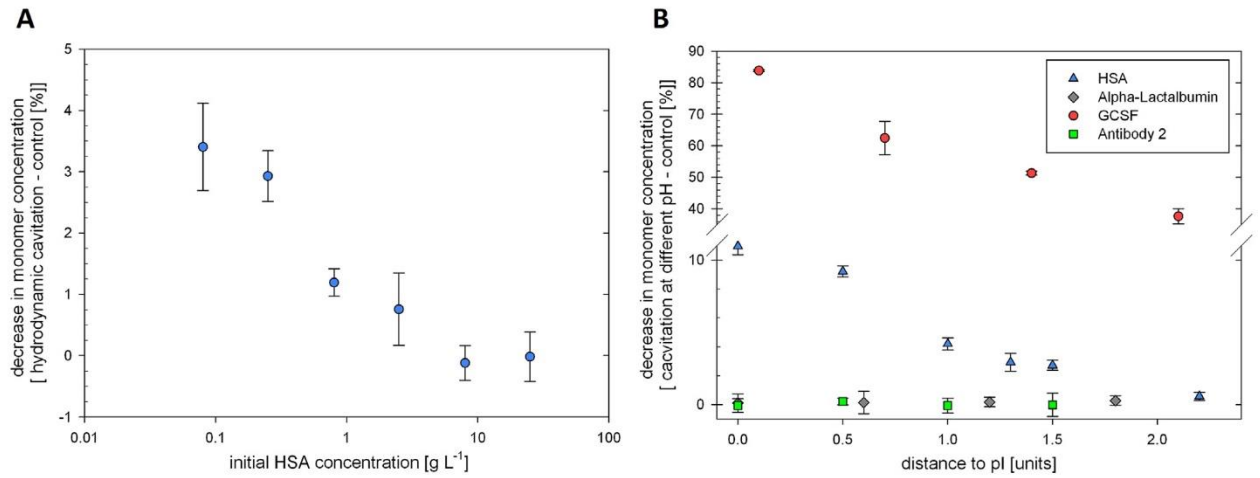

Figure 4. A) Human serum albumin concentration-dependent aggregation under cavitational flow. Data are presented as means of three experiments minus control ± SD. B) Impact of pH on protein aggregation in cavitational flow. Comparison of the behavior of cavitational insensitive antibody 2 (green) and alpha-lactalbumin (gray), and the sensitive proteins GCSF (red) and human serum albumin (HSA) (blue). Data points represent the means of three experiments minus control ± SD.

When the interphase was covered with protein, no further driving force was present at higher concentrations. If we assume that 2.7 mg L^{-1} is needed to cover the occurring surface with this specific setup, the remaining concentration of the initial 25 g L^{-1} after the treatment would be 24.9973 g L^{-1}. This difference can hardly be detected. We further found, that the amount of protein lost in the control experiment associated with the ÄKTA pump was 1.65 ± 0.9%, independent of the applied protein concentration. Therefore, the decrease in soluble HSA was most reasonably driven by the diffusion of protein solution into the sealing wash. Our results suggest that cavitation cavities are saturated with proteins already at low concentrations and the additional protein loss at higher concentration decreases. Hence, an increase in recovery at higher concentrations can only by explained by the constant surface area provided by cavitation. Our findings indicate that cavitation in a certain bioprocess at high protein concentrations is most likely overseen. According to Torisu, Maruno, Hamaji, Ohkubo, and Uchiyama[27] aggregates occurring from cavitation serve as a seeds for larger protein aggregates when further stress, like air/liquid interactions, occur. Therefore, addressing cavitation is crucial when designing bioprocesses.

3.7. pI/pH Ratio-dependent Protein Aggregation in Cavitational Flow

We initially considered that stressing should be performed at least 0.5–1.0 pH units away from the pI.[28] However, when cavitation occurs approaching a pH closer to the pI of a certain protein may drastically increase the aggregation if the vapor/liquid surface is responsible for aggregation and not hydroxyl radical formation. To address this, we tested the cavitation-sensitive proteins GCSF and HSA, as well as α-lactalbumin and antibody2 to determine whether a pH closer to the pI might also increase their aggregation tendency. We assumed a pI of 5.2 for HSA, 7.4 for antibody2, 6.1 for GCSF, and 4.5 for α-lactalbumin. Neither antibody2 nor α-lactalbumin aggregated at the pI (Figure 4B). Perhaps, the 5 mM of sodium chloride in the experimental buffer and the limited generated surface area already suppressed aggregation. However, GCSF and HSA exhibited increased aggregation. At pI (5.2), 11 ± 0.6% HSA was lost by cavitation compared to 2.9 ± 0.6% at a pH 6.5 and 0.6 ± 0.3% at pH 7.4, which is only 1/20 of the aggregation at the pI. A similar trend was observed for GCSF; at pH 4.0 the aggregation was 37.7 ± 2.4%, increasing to 83.9 ± 0.3% at pH 6.0. The finding also suggest the decrease in protein charge close to the pI triggers protein aggregation at the vapor/liquid interfaces of cavitation bubbles. However, due to the closed setup of our methodology and the defined amount of produced cavitation, it can be used to evaluate both the pH and vapor/liquid stability of a certain protein.

3.8. Comparison of Vapor/liquid and Air/liquid Interfaces

To compare the influence of vapor/liquid interfaces and air/liquid interfaces on protein aggregation behavior, we setup an experiment to generate protein foam. Protein species with a propensity to aggregate in the micro-orifice experiments had the greatest aggregation in the foaming experiment. The loss of monomeric GCSF was 94.5 ± 1.8% (Figure 2), hemoglobin 35.5 ± 2.6%, and HSA 31.1 ± 2.3%. For HSA 20.7 ± 1.6% of the monomer was converted to the dimeric form, whereas the other 10.4% was lost as insoluble aggregates as indicated by an increase in turbidity. Further, only little protein foam built up as the turbidity of the solution increased rapidly. Among all of the tested proteins, only α-Lactalbumin did not show increased aggregation upon contact to air/liquid interface. However, the absolute values obtained by the foaming experiment should not be overestimated because the generated air/liquid interface produced in the foaming experiment was much larger compared to the small vapor/liquid interface downstream of

the micro-orifice. Nevertheless, we assume an increase in aggregation for all the tested proteins with the exception of α-Lactalbumin under prolonged cavitation conditions.

3.9. Cavitation Induced Protein Aggregation Mechanism

Protein integrity was analyzed by SEC, which is a robust method that assesses the quaternary protein structure. However, slight changes in the structure which might have occurred due to hydroxyl radial modifications may not lead to a change in diffusivity because it is related to the cubic root of the size of the molecule and, thus, may not be detected. Therefore, we additionally analyzed secondary structure using far-UV CD (**Figure 5**) for the 0.25 g L^{-1} micro-orifice experiments. GCSF, hemoglobin, and HSA exhibited increased aggregation due to cavitation. We recorded the spectra before and after stress treatment. The spectra of the remaining protein in solution did not indicate any structural changes, which would appear as a shift in the curve pattern. As a result of the occurrence of insoluble aggregates, which were removed by the syringe filter before measurement by CD, only the absolute signal was reduced. Due to the lack of stable intermediate structures, protein aggregation generated by cavitation seems to occur spontaneously on the vapor/liquid interface. Similar to our results, instant aggregation behavior onto cavitation was recently suggested in a study were the combined effect of cavitation and shaking was analyzed.[27] No hydroxyl radial associated changes in the antibody structure could be measured with mass spectrometry.

In the experiment were Tween 80® was added to a GCSF solution cavitation associated aggregation could almost fully be suppressed. Tween shields proteins in solution from attaching to the interfaces and additionally reduces the surface tension.[5,29] It is also known that surfactant reduces the growth of cavitation bubbles leading to early break up of cavitation clusters.[30] Hence proteins have less time to attach to the bubble interfaces. Hence only 2.2% of GCSF was lost when cavitation occurred in the presence of Tween 80®.

We further tried to correlate aggregation behavior to intrinsic protein properties. We addressed thermal stability of the proteins by measuring unfolding temperatures with differential scanning calorimetry (SI Appendix, Figure SF4). α-lactalbumin showed the lowest temperature stability while HSA was found to be most

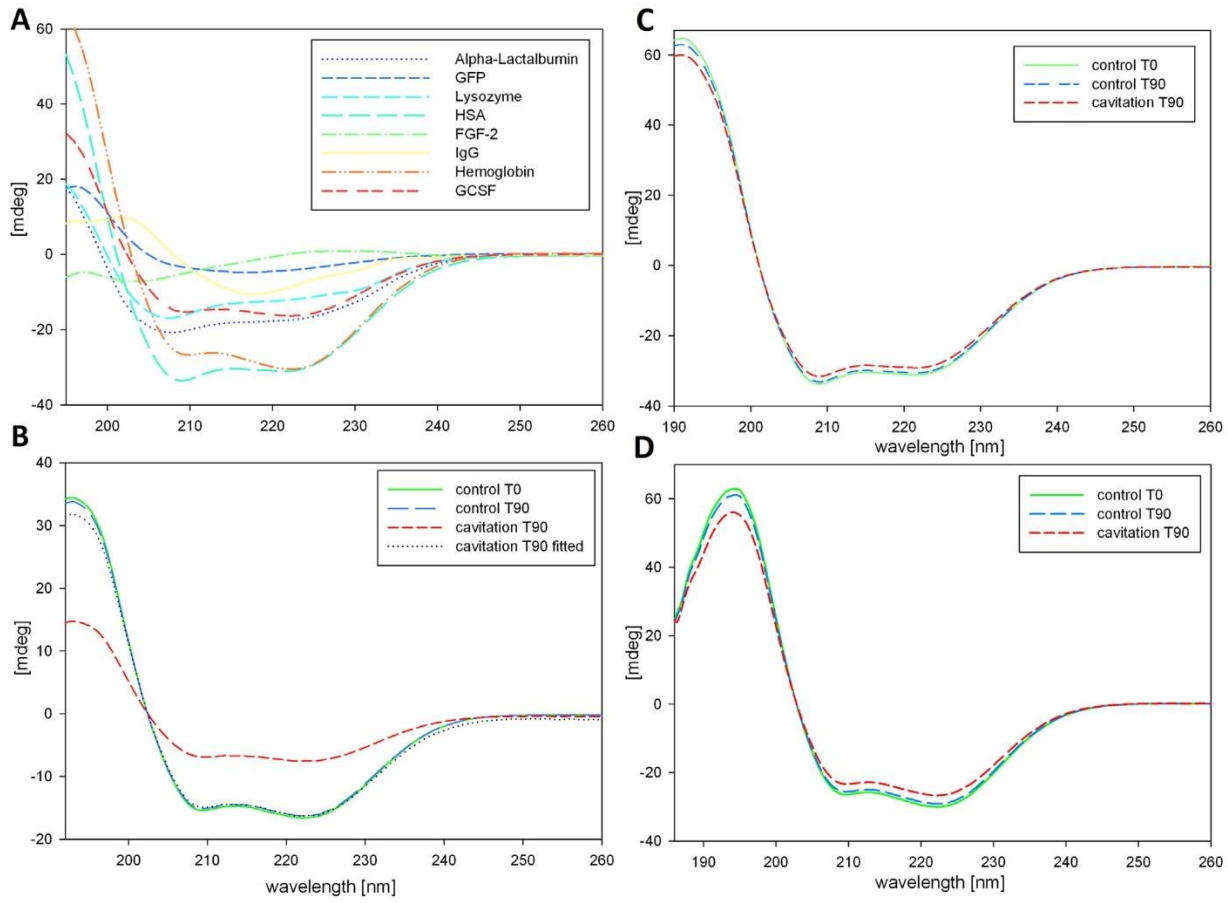

Figure 5. A) CD spectra of different proteins from 195 to 260 nm. Due to the structural similarity of both antibodies, only antibody 2 is shown. CD spectra before and after treatment for B) different GCSF samples. Here "T0 control" represents the sample before the control experiment, while "T90 control" and "T90 cavitation" represent sampling after the treatment. The fitted line (black dotted) represents the red line scaled up to the T0 control (green) at 215 nm. C)HSA, D) Hemoglobin.

stable of all tested proteins. Thus it was not possible to link thermodynamic stability of different protein species to mechanical unfolding induced by cavitation. It was also considered that the surface tension decrease due to the protein itself could explain the different behavior toward cavitation. However, no valid correlation between surface tension and protein aggregation could be drawn (SI Appendix, Figure SF5-6). Hence the intrinsic parameter for the different protein aggregation behavior should be subject of further studies, especially hydrophobic properties.

4. Conclusions

Three out of nine tested proteins were sensitive to the described cavitation method. Hemoglobin exhibited an increase in insoluble aggregates, whereas HSA and GCSF additionally exhibited an increase in soluble aggregates upon exposure to cavitation. The closer the pH of these protein solutions was to pI, the higher the tendency for aggregation when exposed to cavitation. However, when we suppressed cavitation in the presence of high shear rates, we did not observe aggregation of proteins sensitive to cavitation. Thus, extremely high shear rates associated with cavitation were not responsible for protein aggregation. Since a large set of proteins was tested, we hypothesize that the extremely high maximum and average shear rates of up to 10^8 and $1.6 \times 10^6\,s^{-1}$ should not be considered harmful for an average sized protein in common bioprocesses. However, the increase in vapor/liquid interface due to bubble growth generated by cavitation caused protein aggregation. The proteins that were sensitive to cavitation also exhibited the greatest aggregation in a foaming experiment in which a large air/liquid interface was built up. Therefore, we consider the impact of cavitation on protein aggregation to be similar to air/liquid-mediated protein aggregation. Thus, cavitation associated protein aggregation is driven by vapor/liquid interfaces and not by radicals as reported elsewhere. However, at high protein concentrations the effect of cavitation was lower. This behavior is most reasonable due to the fast protein saturation on the surface of vapor cavities. Based on our results, the occurrence of cavitation in gear pumps, pipe valves, or at stirrer blades should not be underestimated, whereas the effect of shear stress at levels found in common bioprocesses is not relevant for protein aggregation as long cavitation does not occur. The methods may also aid in developing new proteins with improved stability.

Abbreviations

CFD, Computational fluid dynamics; FBRM, Focus beam reflectance measurement; FGF-2, Fibroblast growth factor 2; GCSF, Granulocyte colony stimulating factor; HSA, Human serum albumin.

Suppoting Information

Supporting Information is available from the Wiley Online Library or from the author.

Acknowledgements

This work was supported by the Federal Ministry of Science, Research, and Economy (BMWFW), the Federal Ministry of Traffic, Innovation, and Technology (bmvit), the Styrian Business Promotion Agency SFG, the Standortagentur Tirol, the Government of Lower Austria, and Business Agency Vienna through the COMET-Funding Program managed by the Austrian Research Promotion Agency FFG.

Conflict of Interest

The authors declare no conflict of interest.

Nomenclature

$A\,[m^2]$ protein surface
$F\,[kg\ m\ s^{-2}]$ force acting on a protein
r [m] radius of a tube
$Q[m^3\ s^{-1}]$ volumetric flow rate
$v_z[m\ s^{-1}]$ velocity perpendicular to the wall

Greek Symbols

$\rho\,[kg\ m^{-3}]$ density
$\gamma[s^{-1}]$ shear rate
T[Pas] shear stress
$\mu\,[kg\ m^{-1}\ s\text{-}^{1}]$ dynamic viscosity

Keywords

bioprocess engineering, cavitation, downstream processing, industrial biotechnology, protein aggregation, protein purification, shear stress

Received: January 26, 2018
Revised: February 28, 2018
Published online:

[1] S. E. Charm, B. L. Wong, *Enzyme Microb. Technol.* **1981**, *3*, 111.
[2] M. Tirrell, S. Middleman, *Biotechnol. Bioeng.* **1975**, *17*, 299.
[3] C. R. Thomas, P. Dunnill, *Biotechnol. Bioeng.* **1979**, *21*, 2279.
[4] J. Jaspe, S. J. Hagen, *Biophys. J.* **2006**, *91*, 3415.
[5] J. S. Bee, J. L. Stevenson, B. Mehta, J. Svitel, J. Pollastrini, R. Platz, E. Freund, J. F. Carpenter, T. W. Randolph, *Biotechnol. Bioeng.* **2009**, *103*, 936.
[6] J. Dobson, A. Kumar, L. F. Willis, R. Tuma, D. R. Higazi, R. Turner, D. C. Lowe, A. E. Ashcroft, S. E. Radford, N. Kapur, D. J. Brockwell, *Proc. Natl. Acad. Sci. U. S. A.* **2017**, *114*, 4673.
[7] J. O. Wilkes, *Fluid Mechanics for Chemical Engineers With Microfluidics and CFD*, Prentice Hall, Upper Saddle River, NJ, USA **2006**.
[8] R. B. Best, D. J. Brockwell, J. L. Toca-Herrera, A. W. Blake, D. A. Smith, S. E. Radford, J. Clarke, *Anal. Chim. Acta* **2003**, *479*, 87; D. J. Brockwell, Biochem. Soc. Trans. **2007**, *35*, 1564; C. Horejs, R. Ristl, R. Tscheliessnig, U. B. Sleytr, D. Pum, *J. Biol. Chem.* **2011**, *286*, 27416.
[9] Y. F. Maa, C. C. Hsu, *Biotechnol. Bioeng.* **1997**, *54*, 503.

[10] M. Mohanty, R. S. Ghadge, N. S. Patil, S. B. Sawant, J. B. Joshi, A. V. Deshpande, *Chem. Eng. Sci*. **2001**, *56*, 3401; R. S. Ghadge, S. B. Sawant, J. B. *Joshi, Chem. Eng. Sci*. **2003**, *58*, 5125.
[11] A. Nayak, J. Colandene, V. Bradford, M. Perkins, *J. Pharm. Sci*. **2011**, *100*, 4198.
[12] K. S. Suslick, *Science* **1990**, *247*, 1439.
[13] P. Riesz, T. Kondo, *Free Radic. Biol. Med*. **1992**, *13*, 247.
[14] M. Duerkop, E. Berger, A. Duerauer, A. Jungbauer, *Eng. Life Sci. 18*, 169.
[15] T. W. Randolph, E. Schiltz, D. Sederstrom, D. Steinmann, O. Mozziconacci, C. Schöneich, E. Freund, M. S. Ricci, J. F. Carpenter, C. S. Lengsfeld, *J. Pharm. Sci*. **2015**, *104*, 602; M. W. Grinstaff, K. S. Suslick, *Proc. Nat. Acad. Sci. U. S. A*. **1991**, *88*, 7708.
[16] A. Bhattacharya, R. Prajapati, S. Chatterjee, T. K. Mukherjee, *Langmuir* **2014**, *30*, 14894; S. Skou, R. E. Gillilan, N. Ando, *Nat. Protoc*. **2014**, *9*, 1727.
[17] S. Krishnan, E. Y. Chi, J. N. Webb, B. S. Chang, D. Shan, M. Goldenberg, M. C. Manning, T. W. Randolph, J. F. Carpenter, *Biochemistry* **2002**, *41*, 6422.
[18] J. Y. Chang, L. Li, *FEBS Lett*. **2002**, *511*, 73.
[19] A. K. Tyagi, T. W. Randolph, A. Dong, K. M. Maloney, C. Hitscherich, Jr, J. F. Carpenter, *J. Pharm. Sci*. **2009**, *98*, 94.
[20] E. Y. Chi, S. Krishnan, B. S. Kendrick, B. S. Chang, J. F. Carpenter, T. W. Randolph, *Protein Sci*. **2003**, *12*, 903.
[21] S. E. Charm, B. L. Wong, *Biotechnol. Bioeng*. **1970**, *12*, 1103.
[22] C. R. Thomas, D. Geer, *Biotechnol. Lett*. **2011**, *33*, 443.
[23] T. J. Harrington, J. L. Gainer, D. J. Kirwan, *Enzyme Microb. Technol*. **1991**, *13*, 610.
[24] D. C. F. Wieland, V. M. Garamus, T. Zander, C. Krywka, M. Wang, A. Dedinaite, P. M. Claessonb, R. Willumeit-Römera, *J. Synchrotron Radiat*. **2016**, *23*, 480.
[25] A. Natalello, D. Ami, M. Collini, L. D'Alfonso, G. Chirico, G. Tonon, S. Scaramuzza, R. Schrepfer, S. M. Doglia, *PLoS ONE* **2012**, *7*.
[26] M. S. Levy, R. D. O'Kennedy, P. Ayazi-Shamlou, P. Dunnill, *Trends Biotechnol*. **2000**, *18*, 296.
[27] T. Torisu, T. Maruno, Y. Hamaji, T. Ohkubo, S. Uchiyama, *J. Pharm. Sci*. **2017**, *106*, 521.
[28] H. Ahmed, H. Ahmed, *Principles and Reactions of Protein Extraction, Purification, and Characterization*, CRC Press, Boca Raton, Florida **2004**; R. Pörtner, *Animal Cell Biotechnology: Methods and Protocols*, Humana Press, NY **2007**; A. Pandey, J. A. C. Teixeira, *Current Developments in Biotechnology and Bioengineering: Foundations of Biotechnology and Bioengineering*, Elsevier Science, Amsterdam, Netherlands **2016**.
[29] D. K. Chou, R. Krishnamurthy, T. W. Randolph, J. F. Carpenter, M. C. Manning, *J. Pharm. Sci*. **2005**, *94*, 1368.
[30] Y. Iwai, S. Li, *Wear* **2003**, *254*, 1.

5.1 Focus beam reflectance measurement

A G400 (Mettler Toledo, Columbus, Ohio, USA) focus beam reflectance measurement (FBRM) probe was used to analyze the particle size of insoluble aggregates. The probe was put into the 100 mL Duran bottle and the particle set tracked over 90 minutes of incubation. To ensure sustainable mixing near the probe window, we used a magnetic stirring device at 100 rpm. FBRM measurements of GSCF samples treated with and without the micro-orifice are shown in Supplementary Figure 1. The formation of insoluble aggregates is clearly visible by a steep increase in particles larger than 1 µm.

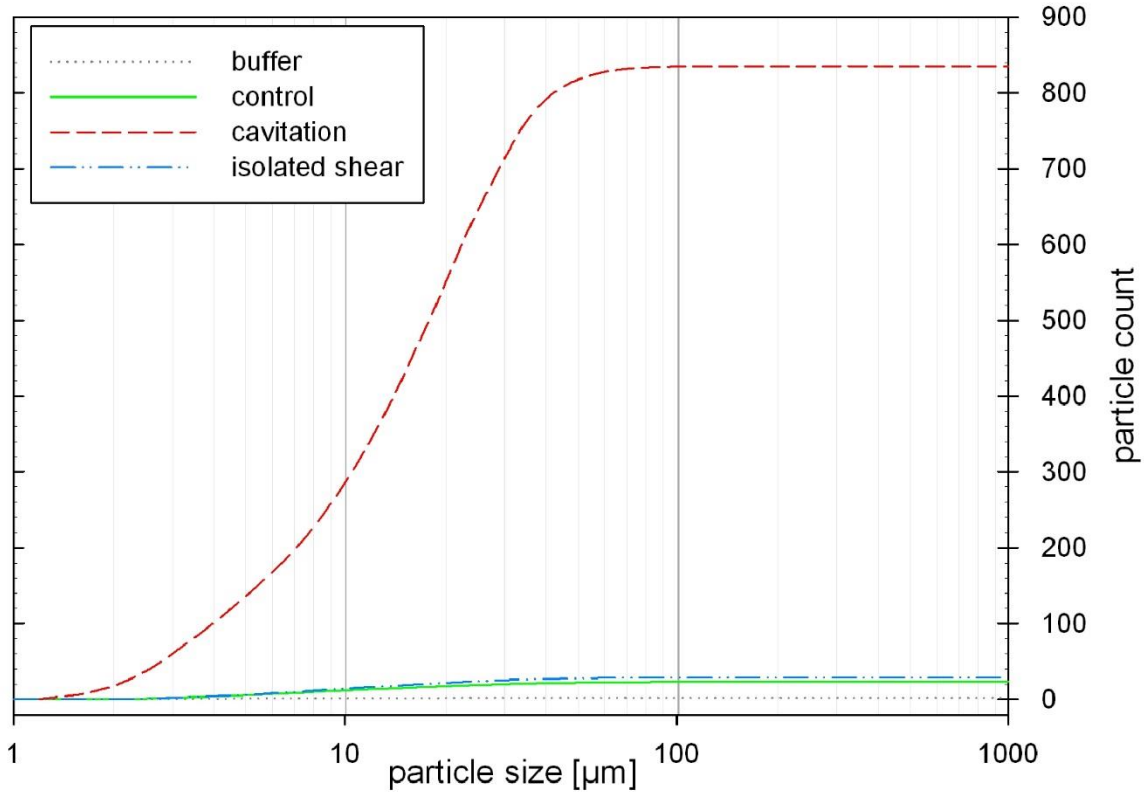

Supplementary Figure 1: GCSF particle distributions according to focus beam reflective measurement after 90 minutes of treatment. Particle formation obtained by cavitation (red) was different from the control (green) and isolated shear experiment (blue).

5.2 Lysozyme activity assay

A lysozyme activity assay was purchased from Sigma-Aldrich (LY0100-1KT). Samples were diluted as instructed by the manufacturer and the decrease in absorbance at 450 nm measured in a Cary 60 photometer (Agilent). It can be seen that the treatment of Lysozyme with the micro orifice did not reduce the activity of the enzyme.

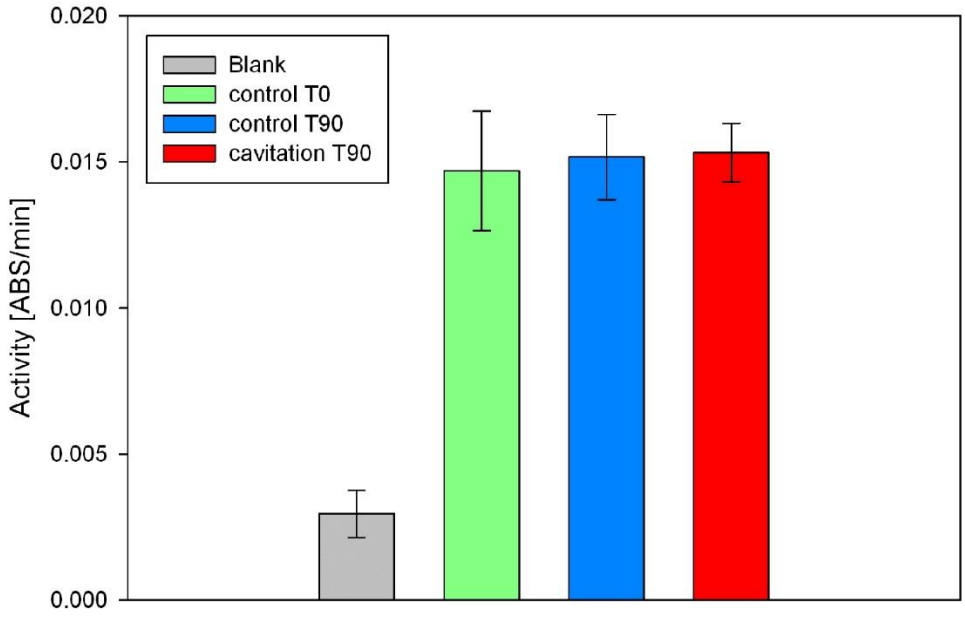

Supplementary Figure 2: Lysozyme activity assay. Data are presented as the means of three experiments ± SD.

5.3 Increasing cavitation strength by increasing the flow rate

It was shown that aggregation initiated by the micro-orifice was promoted by cavitation because isolated shear had no impact on any tested protein. However, cavitation intensity is flow rate-dependent. It increased with elevated flow rates, which was visually detectable (Video 2). Due to the altered formation rate of vapor cavities at higher flow rates, the vapor/liquid area sensed by proteins increased. In addition, the area in which these vapor cavities were stable increased due to a larger area in which the local pressure was below the vapor pressure. Thus, the additional surface area can be sensed by proteins before these cavities collapse. To analyze whether the increase in the vapor/liquid interface also increases GCSF aggregation, we varied the flow rate inside the micro-orifice but kept the number of cycles constant. At a flow rate of 8 mL min^{-1}, which is below the flow rate at which cavitation occurs , the aggregation rate after 39 cycles was similar to the control experiment without a micro-orifice at a flow rate of 26 mL min^{-1} (Supplementary Figure 3). In the absence of cavitation, only the already described pump-induced aggregation was noted. Beyond the micro-orifice cavitation threshold of 12 mL min^{-1}, GCSF aggregation increased with increasing flow rates. The amount of GCSF that aggregated after 39 cycles at the highest flow rate of 30 mL min^{-1} was 85.4 ± 1.6%.

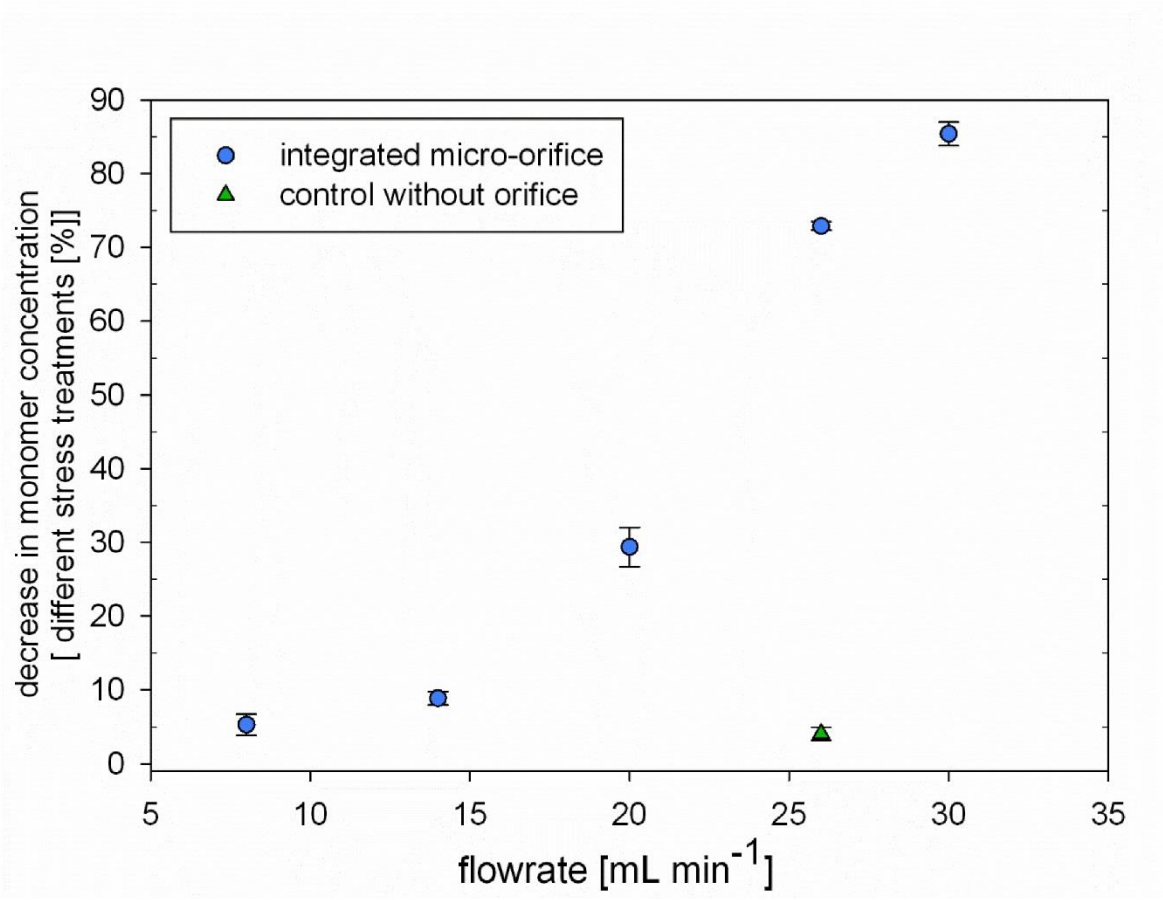

Supplementary Figure 3: Flow velocity-dependent GCSF aggregation. Increased aggregation at higher flow rates (blue) compared to a control experiment without cavitation (green). Data are presented as the means of three experiments ± SD

5.4 Differential scanning calorimetry (DSC)

Protein samples were prepared at a concentration of 1.0 mg/mL according to the method description (2.10 protein standards) in the corresponding buffer. Samples were loaded into the sample cell of a TA-Instruments (New Castle, DE,USA) Nano DSC instrument (model: 602000). Depending on the tested protein the reference cell was loaded with the corresponding buffer. Thermoscans of each protein were conducted as triplicates from 25 °C to 100 °C with a scan rate of 0.7 °C/min. The resulting thermogram data were analyzed using the TA Instrument s NanoAnalyse software. Between each run the system was flushed several times with water followed by the required buffer. When switching protein species an additional cleaning treatment with 0.5 M NaCl, 0.1 M acetic acid followed by water was performed to ensure total protein removal. The sample cell was incubated with the cleaning solution for 1h at 30°C, followed by flushing with 1 L of water.

It was shown that the lowest unfolding temperature was seen for α-lactalbumin which did not show protein aggregation neither in the cavitation nor in the foaming experiment. Contrary, HSA which was heavily prone to aggregation in both experiments showed highest temperature stability.

Hence, the results obtained by this method could not be correlated with the aggregation tendencies.

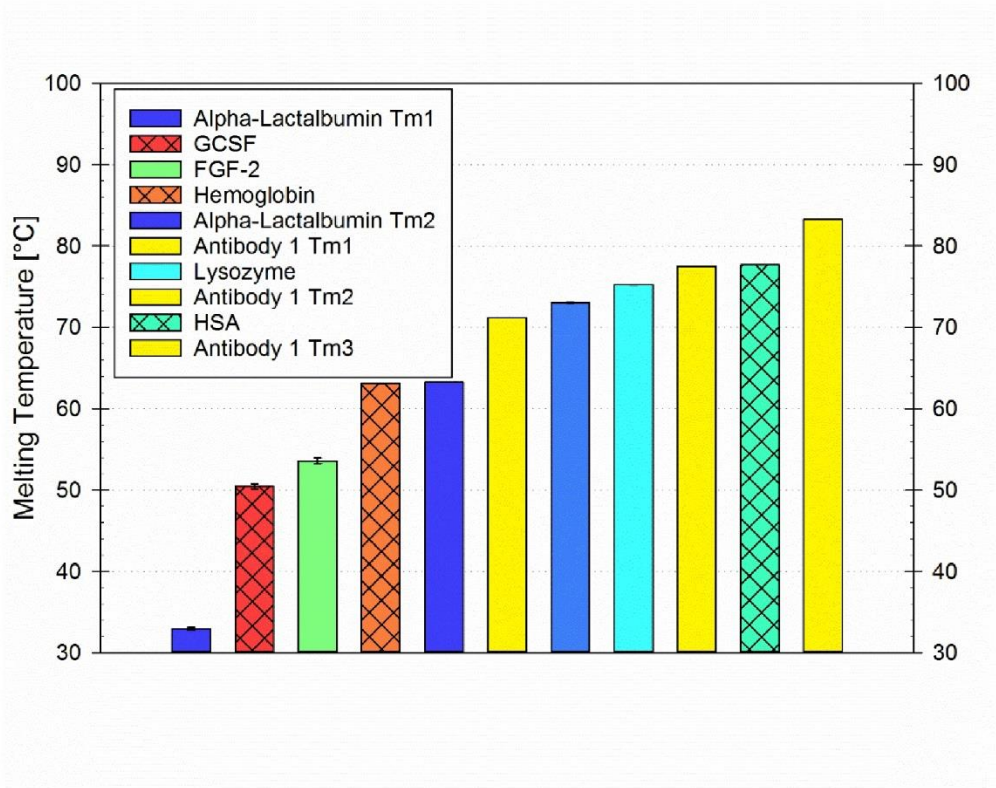

Supplementary Figure 4: DSC Data from all different protein species. Bars with a grid represent proteins being sensitive to cavitation. Data are presented as the means of three experiments ± SD.

5.5 Surface tension measurement

We additionally analyzed the differences in surface tension occurring from different protein species to evaluate if this correlates with protein aggregation behavior. Protein solutions were prepared according to the method description (2.1 protein standards) in the corresponding buffer. Samples were analyzed with a Krüss (Borsteler Chaussee 85,Hamburg, Germany) DSA30 contact angle goniometer.

Drops were generated with a 1.835 mm Syringe in hanging drop mode with a final drop size of 20 µL. The surface tension decrease was recorded for 5 minutes. Both the final surface tension as well as the first reaction constant k were plotted (Supplementary Figure 5 and 6). As a control both water and a 10 mM phosphate buffer pH 6.5 containing 5 mM NaCl were also analyzed in triplicates. Both water and the buffer delivered reasonable surface tensions with 72.1 ± 0.45 and 72.8 ± 0.32, respectively. GCSF and Hemoglobin showed highest aggregation behavior in the micro-orifice treatment although the generated the lowest surface tension. When GCSF was mixed with 0.5 mg/mL Tween ® the surface tension was lowest over all tested protein. However, since the aggregation behavior of GCSF with surfactant was found lower than without surfactant a correlation between protein intrinsic surface tension and cavitation associated protein aggregation is not reasonable. Also the formability, which can be described by the decrease in surface tension (k) could not be correlated to protein aggregation.

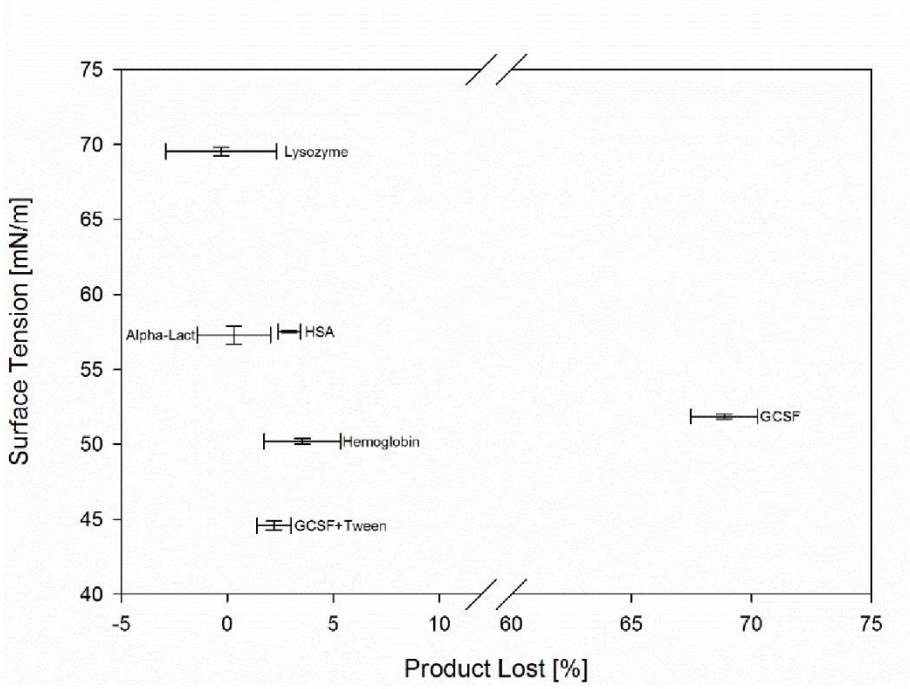

Supplementary Figure 5: Plot of surface tension against protein aggregation in the micro-orifice treatment. Data are presented as the means of three experiments ± SD.

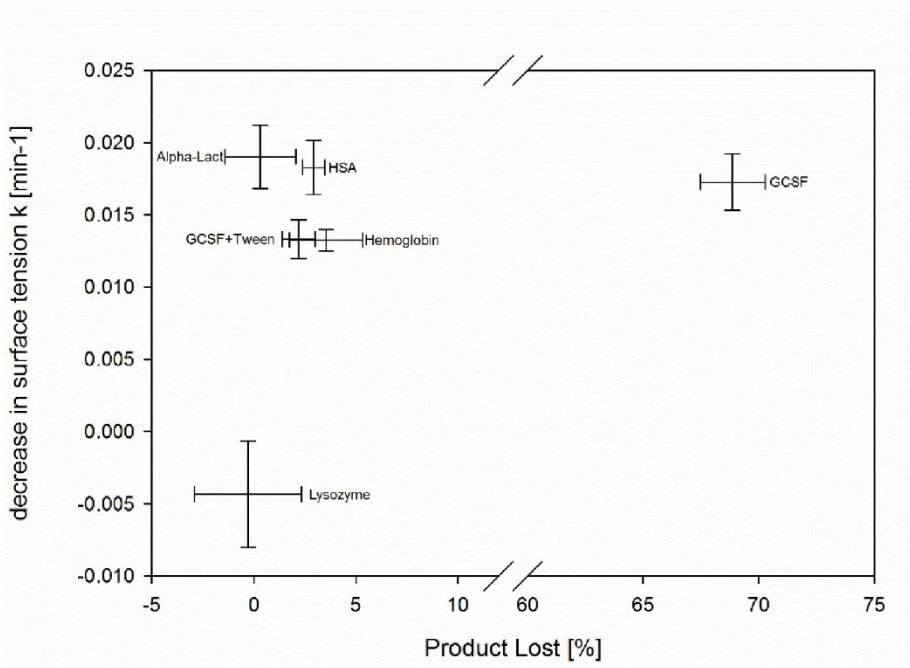

Supplementary Figure 6: Plot of decrease in surface tension against protein aggregation in the micro-orifice treatment. Data are presented as the means of three experiments ± SD.